Journal of Materials Chemistry A



REVIEW

View Article Online
View Journal



Cite this: DOI: 10.1039/d3ta06862e

Recent progress in perylene diimide supermolecule-based photocatalysts

Bin Yang,^a Liliang Lu,^a Shiyu Liu,^a Wenjin Cheng,^a Hao Liu,^a Chao Huang,^a Xintao Meng,^{*ab} Raul D. Rodriguez^{*c} and Xin Jia (1) **a

Perylene diimide supramolecular (PDIs) materials are promising candidates for harnessing sunlight to drive photocatalytic processes in environmental remediation and renewable energy production. However, the performance of pristine PDI photocatalysts is unsatisfactory. Consequently, extensive efforts are dedicated to enhancing the performance of this photocatalyst family, with many studies reported on the intrinsic structure regulation and heterojunction construction of PDI materials. This review focuses on recent advancements in these fields, including molecular structure design, enhancing crystallinity, regulating morphology, and constructing various heterojunctions. Additionally, this work highlights recent progress in their application in water splitting, degradation of pollutants, and other photocatalytic reactions. Challenges and future perspectives for exploring advanced PDI-based photocatalysts are thoroughly discussed and summarized.

Received 8th November 2023 Accepted 5th January 2024

DOI: 10.1039/d3ta06862e

rsc.li/materials-a

1. Introduction

The increasingly severe energy and environmental crisis make it necessary to develop theories and technologies for energy conversion and environmental remediation. Photocatalysis, an environment-friendly approach, offers great potential to achieve this aim by enabling the production of renewable energy and environmental remediation. In a photocatalytic process, a redox

reaction induced by photo-generated electrons and holes can be exploited in water splitting,² pollutant degradation,³ N₂ fixation,⁴ and CO₂ reduction.⁵ Over the past 47 years, a wide range of organic and inorganic photocatalysts has been designed, including metal oxides and sulfides, carbon nitrides, covalent organic frameworks, and metal–organic frameworks.⁶ However, their large-scale application is severely hindered by their low quantum efficiency. Therefore, developing efficient photocatalysts is crucial to drive the industrialization of photocatalysis.

All-organic n-type perylene diimide supramolecular (PDIs) materials are considered one of the most promising photocatalysts owing to their moderate bandgap, high molar extinction coefficient, abundant element resources, excellent photothermal stability, and easy preparation.⁷ Different from isolated perylene diimide molecules, PDI photocatalysts are

[°]Tomsk Polytechnic University, 30 Lenin Avenue, 634050 Tomsk, Russia. E-mail: raul@tpu.ru



Bin Yang

Dr. Bin Yang received his PhD in Chemical Engineering and Technology from Shihezi University, China, in 2022. Then he joined Shihezi University School of Chemistry and Chemical Engineering as an Associate Professor. His research interests include structural control of polymer-based photocatalytic materials and their applications in pollutant degradation and clean energy production.



Hao Liu

Hao Liu received his Bachelor's Degree in Chemical Engineering and Process in 2023. He is currently a Master's candidate. majoring in Chemical Engineering and Technology, at the School of Chemistry and Chem-Engineering, Shihezi ical University in China. His main research interests focus on the structural control of photocatalytic materials and their application pesticide degradation.

[&]quot;School of Chemistry and Chemical Engineering/State Key Laboratory Incubation Base for Green Processing of Chemical Engineering, Shihezi University, Shihezi, Xinjiang 832003, China. E-mail: 455894201@qq.com; jiaxin@shzu.edu.cn

^bResearch Institute of Farm Products Storage and Processing, Xinjiang Academy of Agricultural Sciences, Urumqi 830091, China

formed through the self-assembly of monomeric perylene diimide molecules, which are organized via non-covalent interactions such as hydrogen bonds, π - π stacking interaction, and van der Waals forces (Fig. 1a and b). To achieve excellent photocatalytic performance, researchers have recently focused on developing various PDI-based photocatalysts by regulating the intrinsic structure of PDI⁸ and constructing heterojunctions. Fig. 1c shows the growing research interest in PDI-based photocatalysts as reflected by the number of publications. However, certain limitations continue to hinder their photocatalytic performance. These drawbacks include a small specific surface area, limited exposure of active sites, poor crystallinity, unsatisfactory reduction potential and propensity for rapid recombination and short lifetime of photo-generated charges.

Several strategies are employed to address these crucial issues and boost the photocatalytic activity of PDIs, including molecular structure design, crystallinity improvement, and morphology control. Additionally, constructing heterojunctions by coupling PDIs with other functional semiconductors has also attracted significant attention owing to their remarkable effectiveness in improving their photocatalytic performance. Fig. 2 presents the classification of PDI-based heterojunctions based on different photo-generated charge transfer mechanisms between PDIs and the coupled semiconductor. The development of PDI-based heterojunctions shows great potential in overcoming the drawbacks of single photocatalysts. These heterojunctions can inherit the unique advantages of the individual semiconductors, such as extending the absorption range of visible light, suppressing the recombination of photo-generated charges, increasing the photo-corrosion stability, enhancing the oxidation and reduction potentials, and realizing spatial separation between the oxidation and reduction sites. Consequently, the photocatalytic performance of PDIs can be significatively enhanced through the formation of heterojunctions.



Chao Huang
based porous materials.

Chao Huang received his Bachelor's Degree in Chemical Engineering and Technology in 2020 and his Master's Degree in Chemical Engineering in 2023. He is currently a doctoral candidate, majoring in Chemical Engineering and Technology, at the School of Chemistry and Chemical Engineering, Shihezi University in China. His main research interests focus on the preparation and application of polyphenol-



Raul D. Rodriguez

Prof. Raul D. Rodriguez received his PhD in Physics and Chemistry of Nanomaterials in 2009 with the highest honors at the Institut des NanoSciences de Paris, Pierre et Marie Curie University, Paris, France. In 2011, he joined the DFG Research Unit Sensoric Microand Nano-Systems in the Semiconductor Physics group at TU Chemnitz, Germany. His experience includes implementing and developing novel methods

for nanoscale characterization. In 2017, he was appointed as a Full Professor at Tomsk Polytechnic University. His research focuses on flexible electronics, particularly novel plasmonic and 2D nanomaterials, for technological developments, including biomedicine, optoelectronics, energy, and safety applications.



Xintao Meng

Meng received Xintao Master's Degree from Xinjiang University, China, in 2013 and started working at the Institute of Agro-products Storage and Processing, Xinjiang Academy of Agricultural Sciences, in the same year and became an Associate Researcher in 2021. She is currently a doctoral candidate, majoring in Chemical Engineering and Technology at the School of Chemistry and Chem-Engineering, Shihezi ical

University, in China. Her main research interests include structural control of polymer-based photocatalytic materials and their applications in storing and keeping agricultural products fresh.



Xin Jia

Prof. Xin Jia obtained his PhD from Lanzhou University, China, in 2009. He began to work at Shihezi University in the same year and became a Full Professor in 2014. Now, he is the Vice Dean of the Graduate School. His research interests focus on the design and synthesis of functional polymers, material surface interface modification, and preparation and application of photocatalytic materials in agriculture. He has

published more than 100 papers as the first author or corresponding author.

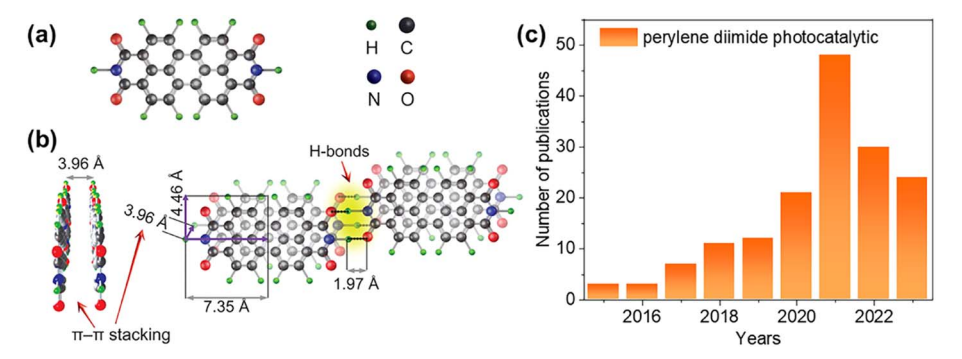


Fig. 1 (a) Schematic diagram of the perylene diimide molecule (a) and PDI assembly (b). 9 (c) Number of publications on PDI-based photocatalysts during the last decade (source: Web of Science; date: 8th Nov. 2023; keywords: perylene diimide photocatalytic).

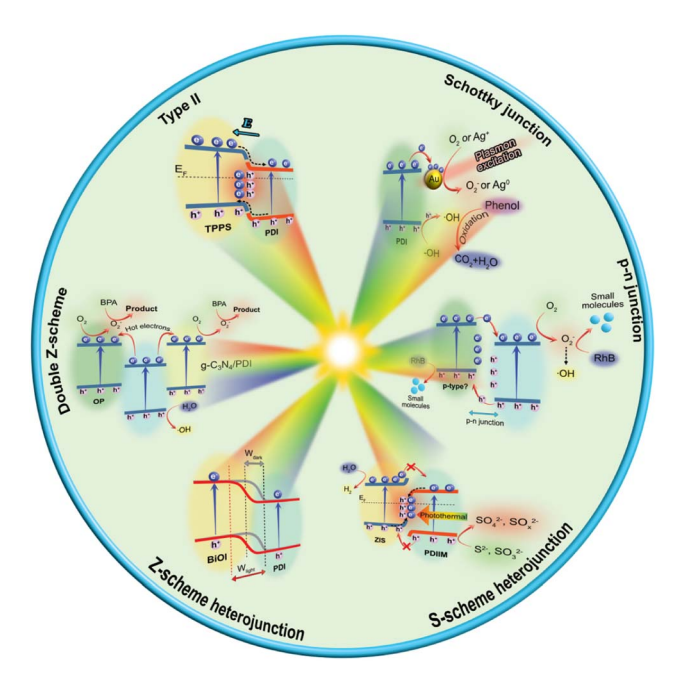


Fig. 2 Schematic diagrams of the typical PDI heterojunction. Double Z-type, 10 Schottky junction, 11 type-II, 12 S-scheme, 13 Z-scheme 14 and p-n junction.15

Herein, we comprehensively review the recent progress on PDI-based photocatalysts in the energy and environmental field. Firstly, the strategies for the modification of PDI photocatalysts are briefly summarized, including modifying their molecular structure, improving their crystallinity, and regulating their morphology. Secondly, the various PDI-based heterojunctions are reviewed, including the design principles of PDI/inorganic semiconductor, PDI/organic semiconductor, PDI/metal, and PDI/carbon material heterojunctions. Furthermore, the application of PDI-based heterojunctions in photocatalytic water splitting, pollutant degradation, N2 fixation, H2O2 production, CO2 reduction, and conversion of organic molecules are summarized. Finally, some concluding challenges and future perspectives for exploring advanced PDI-based heterojunctions are summarized. This review aims to provide valuable guidelines for the future development of highly active PDI-based

photocatalysts for the mitigation of environmental pollution and production of renewable energy.

Strategies for the modification of PDI-based photocatalysts

The investigation of highly active PDI-based photocatalysts plays a crucial role in improving the photocatalytic performance of PDI-based heterojunctions. In PDI-based heterojunctions, the characteristics of PDIs determine the type of heterojunction, the tightness and stability between interfaces, and the transport behavior of photo-generated charges, thereby significantly affecting their photocatalytic properties. Therefore, in this review, firstly, we discuss the various strategies for the modification of PDIs to enhance their characteristics.

Although PDI photocatalysts can independently complete the whole photocatalytic process, their photocatalytic performance is limited by three factors, as follows: (1) their high exciton binding energy and propensity for electron-hole pair recombination; (2) their relatively small specific surface area and limited active sites; (3) and their low crystallinity, narrow π delocalization channels, and disordered structure. In recent decades, numerous effective strategies have focused on addressing these issues through the modification of PDIs. These strategies include modification of their molecular structure, improving their crystallinity, and regulating their morphology. Here, we present a brief overview of the main modification strategies for enhancing PDI photocatalysts.

2.1 Modification of their molecular structure

PDIs are a class of compounds known as polycyclic aromatic hydrocarbons, which are characterized by a perylene core with imides at both ends. The conjugation between the electronefficient perylene core and the electron-withdrawing imide group facilitates efficient carrier migration. Typically, PDIs are synthesized through the condensation reaction between 3,4,9,10perylenetetracarboxylic dianhydride (PTCDA) and alkylamine or aniline under the protection of inert gas, using tetrahydrofuran, imidazole, quinoline, etc. as the solvent. Also, the substitution and modification of the chromophores (conjugated structures) are crucial for designing the molecular structure of PDIs, which

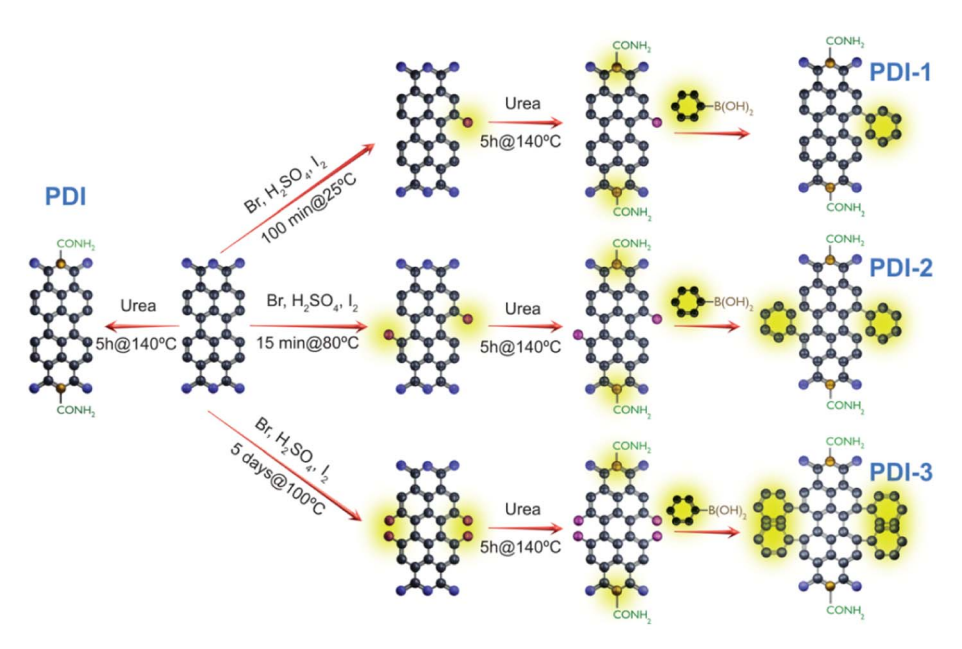


Fig. 3 Schematic illustration of the synthesis of PDI, PDI-1, PDI-2, and PDI-3. Reprinted with permission. 17 Copyright 2022, Wiley.

can significantly affect their electronic structure and redox capacity. For instance, Wang and co-workers17 synthesized a series of PDI polymers (Fig. 3), including PDI-1, PDI-2, and PDI-3, by introducing different amounts of phenyl groups at the bay position of PDI. The experimental results revealed that the oxygen (O2) production rate of the singly substituted PDI was the highest (2524.88 μ mol g⁻¹ h⁻¹) among the samples under visible light without any co-catalyst. This excellent performance can be attributed to its push-pull intramolecular charge transfer and high crystallinity, which significantly promoted the separation and transfer of photo-generated charges. As the number of substituents increased, the production rate of O2 decreased sharply, which was attributed to two factors. Firstly, the introduction of more groups at the bay position of the PDI structure reduced the local charge excitation of the PDI core, thereby hampering the production of O2. Secondly, increasing the number of electron donor substituents can seriously disrupt the crystallinity of the PDI polymers, leading to a decrease in the O₂ production rate. These findings highlight the crucial role of rational molecular structure modification to improve the O2 production performance of PDI polymers, mainly through the mono-substitution of electronic groups.

The modification of the molecular structure of perylene diimide also involves the design and substitution of auxochrome (side groups), which can significantly impact several factors. These factors include the redox ability, degree of planar conjugation of the monomer molecules, properties of the substituents, dipole moment of the monomer molecules, and intensity of the built-in electric field. For example, Kong *et al.*¹⁸ proposed the preparation of a non-covalent self-assembled phosphoric acid-substituted PDI (Fig. 4a). The photocatalytic activity was enhanced by replacing the terminal substituents with strong electron-withdrawing groups, leading to an improvement in both the separation of photoin-duced carriers and the spectral response range. In another study,

Zhu et al.¹⁹ synthesized a novel PDI photocatalyst modified with nicotinic acid (hp-PDIs-NA), which exhibited an ultra-thin hierarchical pore structure and bi-planar configuration (Fig. 4b). The results demonstrated that terminal substitution with aromatic compounds instead of aliphatic compounds is an important strategy for improving the performance of PDI photocatalysts.

2.2 Improvement in crystallinity

The enhancement of the crystallinity of PDIs in the process of assembling small molecules into PDIs via weak interactions is a crucial strategy for improving their photocatalytic performance, given that it can provide an "expressway" for the efficient movement of photo-generated carriers by strengthening the built-in electric field. The fabrication of a built-in electric field in PDIbased photocatalysts is evidenced to be a productive strategy to actuate the fast separation of photo-generated carriers and navigate their migration to the active sites for efficient redox reactions.20,21 For example, Zhu's group22 synthesized a highly crystalline PDI photocatalyst (PDI-NH) using the imidazole solvent method. This photocatalyst achieved a breakthrough O2 production rate (40.6 mmol g⁻¹ h⁻¹) and an apparent quantum yield (AQY) of 10.4%. The excellent performance was attributed to the well-constructed built-in electric field resulting from its high crystallinity, which effectively promoted the separation and migration of photo-generated charge carriers. Zhang et al.23 prepared PDI nanosheets with a high degree of crystallization (π conjugated-PDIs), which exhibited nearly 100% exposure of π conjugated planes. The preferential exposure of π -conjugated planes and the enhancement of the internal electric field contributed to the excellent photocatalytic activity of the π conjugated-PDIs, which was 8-17 times higher than that of previously reported PDI photocatalysts.

The formation process of PDIs mainly involves non-covalent bond interactions and π – π conjugated stacking (Fig. 1a).

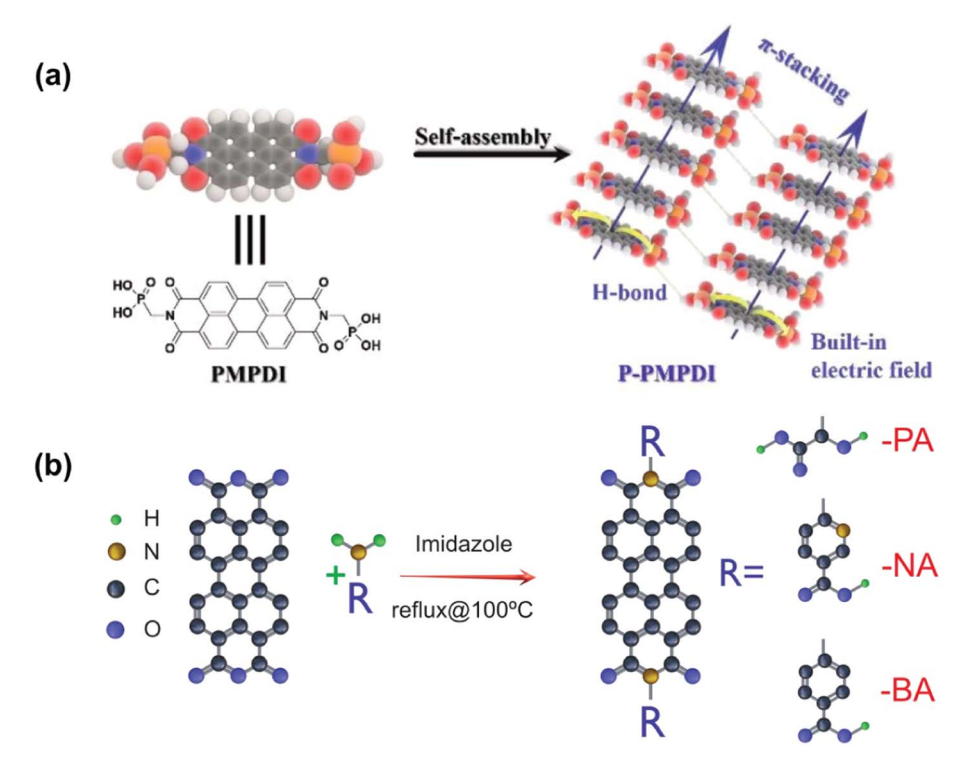


Fig. 4 (a) Schematic illustration of the synthesis of self-assembled phosphoric acid-substituted PDIs. Reprinted with permission.¹⁸ Copyright 2019, The Royal Society of Chemistry. (b) Method for the synthesis of PDI photocatalyst modified with nicotinic acid and reference catalyst. Reprinted with permission.¹⁹ Copyright 2022, Elsevier.

However, non-covalent bond interactions have limitations in improving their stability and charge transport. Thus, to address these shortcomings, the substitution of non-covalent bonds for covalent bonds has emerged as a suitable strategy. By introducing covalent bonds in PDIs, their corresponding visible light range can be expanded, dipole moment can be enhanced, bandgap position can be adjusted, and crystallinity improved. For instance, Zhu's group²⁴ successfully synthesized a highly crystalline PDI polymer photocatalyst (urea-PDI) by introducing covalent bonds to connect perylene diimide molecules (Fig. 5a). The urea-PDI photocatalyst exhibited excellent crystallinity and large molecular dipoles, which contributed to the generation of a built-in electric field, promoting the separation and transport of photo-generated carriers. In addition, they also prepared a conjugated triazine-perylene diimide (triazine-PDI) polymer photocatalyst with full spectrum photo-oxidative activity by combining cyanuric chloride with PDIs (Fig. 5b).25 Both theoretical analyses and experimental evidence showed that the highly-crystalline nature and strong π - π stacking of triazine-PDI generated a strong built-in electric field. This electric field provided efficient channels for the rapid transfer of photogenerated charges. As expected, the favorable structural characteristics, together with appropriate band energy levels contributed to the improvement in photocatalytic activity. Zhu's group¹⁵ further developed a PDI photocatalyst containing segregated π -conjugation units by inserting a non-conjugated ethylenediamine segment in the conjugated planes of 3,4,9,10-perylene tetracarboxylic anhydride (EDA-PTCDA)

through an acidizing solvent thermal approach (Fig. 5c). The difference in surface potential and excitation charge density confirmed the possible presence of a built-in electron trap effect in the unconjugated segment of EDA-PTCDA, resulting in a highly active EDA-PTDA/bacterial interface.

2.3 Regulation of morphology

Morphological regulation is one of the most effective strategies for enhancing the performance of PDI-based photocatalysts. By controlling the PDI morphology, various benefits can be achieved, including enhanced stability, increased specific surface area, exposure of more active sites, bandgap adjustment, and expanded absorption and utilization of visible light. For instance, Zhu's group9 employed a rapid and straightforward solution dispersion method to obtain a self-assembled PDI material with a distinctive willow leaf-like shape. This PDI photocatalyst, working under visible light without the need for a cocatalyst, exhibited an excellent performance in both photocatalytic pollutant degradation and O₂ evolution. The excellent photocatalytic activity was attributed to the overlapping orbital between the PDI molecular units and long-range conjugated π delocalization. Similarly, Zhang et al.26 synthesized a twodimensional ultrathin nanofiber by self-assembling carboxysubstituent PDIs through H-type π - π stacking and hydrogen bond interactions. The introduction of terminal carboxyl groups plays an important role in morphology control and stability. The resulting PDI nanofibers exhibited excellent migration efficiency of photo-generated charges and a large specific surface area,

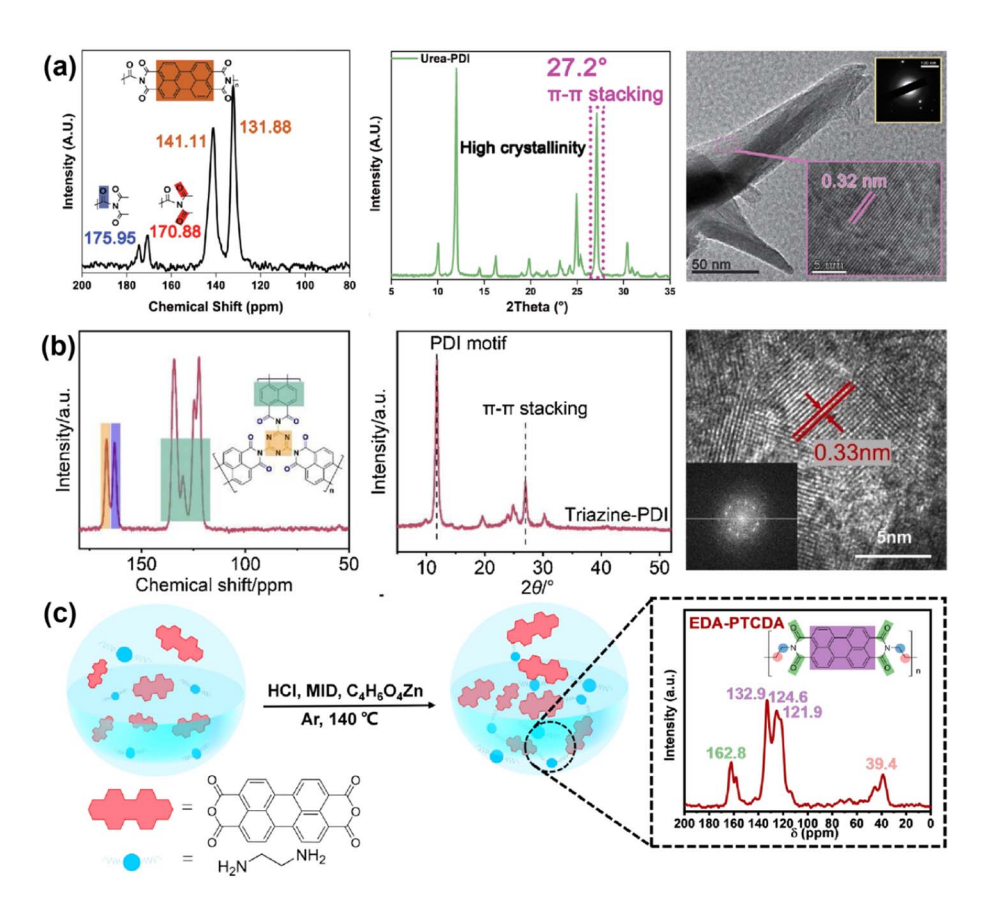


Fig. 5 (a) Solid ¹³CNMR spectrum, X-ray diffraction analysis, and HRTEM of urea-PDIs. Reprinted with permission.²⁴ Copyright 2020, Wiley. (b) Solid ¹³CNMR spectrum, X-ray diffraction analysis, and HRTEM of triazine-PDIs. Reprinted with permission.²⁵ Copyright 2021, Elsevier. (c) EDA-PTCDA synthetic procedure and solid-state ¹³C NMR spectrum. Reprinted with permission.¹⁶ Copyright 2023, Wiley.

enabling efficient organic pollutant degradation and water oxidation under visible light without the need for co-catalysts. However, the despite significant progress in controlling the morphology of PDIs, the current focus is on one-dimensional nanorods and nanofibers, and two-dimensional nanosheets. Thus, the further exploration of diverse PDI morphologies such as nanotubes, hollow nanospheres, and nanorods holds great potential for future advancements.

Despite the significant advancements in modifying single perylene diimide molecules, the photocatalytic activity of PDIs is still limited in several aspects. One crucial factor is the weak reduction potential of PDIs, which hampers their performance and application in photocatalytic reduction reactions such as H₂ evolution, N₂ fixation, and CO₂ reduction. In addition, the rapid recombination of photo-generated charges is still one of the most important obstacles limiting the photocatalytic activity of PDIs. These factors directly impede the industrial-scale application of PDI photocatalysts. Thus, finding new strategies to modify PDIs to obtain a better photocatalytic performance remains a formidable challenge.

PDI-based heterojunction

The narrow bandgap of photocatalysts can improve the efficient utilization of solar energy. However, it can also lead to the recombination of photo-generated charges. Alternatively, a wide bandgap not only helps suppress charge recombination but also ensures that photo-generated electrons and holes have strong oxidation or reduction abilities. However, an excessively wide bandgap limits the full-spectrum utilization of solar energy. Accordingly, the formation of a heterojunction can address the drawbacks caused by the "short barrel effect" of a single photocatalyst.27 The construction of a heterojunction creates a builtin electric field or diffusion electric field at the interface of two semiconductors, driving the migration and separation of photogenerated charges. This approach increases the lifetime of photo-generated charges and reduces their recombination. In addition, the construction of a heterojunction can also optimize the band positions and facilitate surface catalytic reactions. In recent years, the construction of PDI-based heterojunctions has attracted widespread attention due to their feasibility and effective energy conversion and environmental remediation, aiming to promote the photocatalytic activity of PDIs.

3.1 Design principles of PDI-based heterojunction

PDI-based heterojunctions usually consist of PDIs coupled with another component, which can be a semiconductor, ^{28,29} metal, ³⁰ carbon-based material, ^{31,32} or other materials. These heterojunctions exhibit efficient spatial separation across the interface, leading to the significant suppression of charge recombination. Moreover, the construction of PDI-based

heterojunctions incorporates the advantages of the second component, such as excellent light absorption, optimized bandgap, and enhanced surface catalytic reactions. Depending on the second component, PDI-based heterojunctions can be classified into the following systems: (1) PDI/inorganic semiconductor heterojunctions, such as PDI/metal oxide heterojunctions and PDI/metal sulfide heterojunctions; (2) PDI/ organic semiconductor heterojunction systems, such as PDI/ carbon nitride heterojunctions, PDI/metal-organic framework heterojunctions, PDI/covalent organic framework heterojunctions, and PDI/other supramolecular polymer heterojunctions; (3) PDI/metal heterojunctions and (4) PDI/carbonbased material heterojunctions. The latest important research progress on PDI-based heterojunctions is comprehensively summarized in the following section.

3.2 PDI/inorganic semiconductor heterojunctions

The widely used photocatalyst materials are primarily inorganic semiconductors due to their excellent photocatalytic activity, diversity, high crystallinity, and stable physicochemical properties. These materials include metal oxides, metal sulfides, and metal phosphides. Accordingly, recognizing the benefits of forming heterojunctions, researchers have combined various inorganic photocatalysts with PDIs to create heterojunction structures. The modification of PDIs with inorganic semiconductors has gained significant attention and warrants further exploration in this review. Therefore, in this section, we provide a detailed overview of the research progress on PDI/ inorganic semiconductor heterojunctions with the focus on PDI/metal oxide and PDI/metal sulfide systems.

3.2.1 Heterojunction between PDIs and metal oxide. Nanostructured metal oxide photocatalysts have controllable morphologies and structural characteristics, variable surface chemical properties, high surface area, specific crystalline properties, and rich availability. These features make them highly desirable materials for applications in renewable energy production and the degradation of environmental pollutants. However, the application of metal oxide photocatalysts in industry is significantly limited due to their low quantum yield, limited utilization of visible light, and rapid recombination of photo-generated charges. Thus, to improve the photocatalytic efficiency of metal oxide photocatalysts, two aspects need to be addressed, as follows: (1) promoting the efficient separation of photo-generated charges and (2) shifting their absorption spectrum towards longer wavelengths to extend their spectral response range. However, it is difficult to achieve both requirements in a single metal oxide. Consequently, the exploration of PDI/metal oxide heterojunctions, especially TiO2 and bismuth oxide, has attracted extensive research interest to overcome these limitations.

3.2.2 Heterojunction between PDIs and TiO₂. TiO₂ is one of the most studied metal oxides in photocatalysis because of its abundance, low cost, and biocompatibility. However, it has several issues that hinder its efficient photocatalytic activity, particularly low light absorption and separation of photogenerated charges, which are limited by its width bandgap of about 3 eV.33 Thus, extensive research has been conducted on PDI/TiO₂ heterojunctions to overcome these issues.^{34–36} For example, Zhu's group37 achieved a PDI/TiO2 photocatalyst by pH-induced polymerization (Fig. 6a-c). In this heterojunction, the one-dimensional PDI structure with short-range stacking patterns reduced the charge migration distance along the π - π stacking direction, thereby delaying the recombination of charges. Furthermore, TiO2, acting as an electron acceptor, facilitated efficient charge separation in the interface layer of the PDI shell through the C=O-Ti "bridge" electron channel. The synergy between PDIs and TiO₂ enhances the photocatalytic activity of the PDI/TiO2 photocatalyst for the degradation of pollutants under visible light, especially with the addition of EDTA. However, although the PDI/TiO2 heterojunction exhibited excellent photocatalytic properties under visible light, its performance under ultraviolet light remains limited, and further research in this area is needed. Thus, to address this, Zhu's group³⁸ constructed a semi-core-shell structure by coating a PDI self-assembly with TiO2 nanoparticles (Fig. 6d-f). This heterojunction system exhibited improved photocatalytic properties under ultraviolet light, visible light, and full spectrum light due to the synergistic effects between TiO2 and PDIs. The design of the PDI/TiO₂ heterojunction effectively overcomes the limitations of TiO2 in visible light photocatalysis and PDIs in ultraviolet light photocatalysis.

Morphology control is crucial in preventing the agglomeration of nanoparticles and maximizing the exposure of more active sites on the catalyst surface. In this case, the yolk-shell structure offers distinct advantages by providing an ideal platform for encapsulating ultrafine co-catalysts on both the inner porous shell and central core. This structure effectively shortens the charge transfer path and accelerates the separation of photo-generated charges. Thus, considering these advantages, Chen and co-workers39 developed SiO2@TiO2/PDI yolk-shell nanospheres (Fig. 7). These nanoparticles, with their unique yolk-shell structure and built-in electric field, demonstrated remarkable separation of photo-generated charges and multichannel migration, resulting in excellent activity for the degradation of phenol.

3.2.3 Heterojunction between PDIs and bismuth oxides. Bismuth oxide-based photocatalysts, as metal oxides, have attracted increasing attention due to their unique electronic and structural properties, which contribute to their excellent photocatalytic activity.40 However, despite the significant progress made in bismuth-based photocatalysts, they still suffer from drawbacks such as poor light absorption and stability. In this case, again, an effective approach to address these limitations is to make heterojunctions by combining PDIs with bismuth-based photocatalysts. Currently, several heterojunctions have been reported between PDIs and bismuth-based semiconductors, including PDIs/BiVO₄,41 PDIs/Bi₂W₂O₆,42,43 PDIs/Bi₂O₄, ⁴⁴ PDIs/BiOBr/Bi₄O₅Br₂, ⁴⁵ and PDIs/BiOX (X = Cl, Br, I).28,45,46 For example, Ji et al.47 developed a novel type II heterojunction of flaky-like BiOCl/PDIs by adjusting the selfassembly time of PDIs. Comparing the photocatalytic activity of the first self-assembled PDIs with BiOCl (BiO-Cl/PDIs-1) to the second self-assembly with PDI BiOCl (BiOCl/PDIs-2), it was



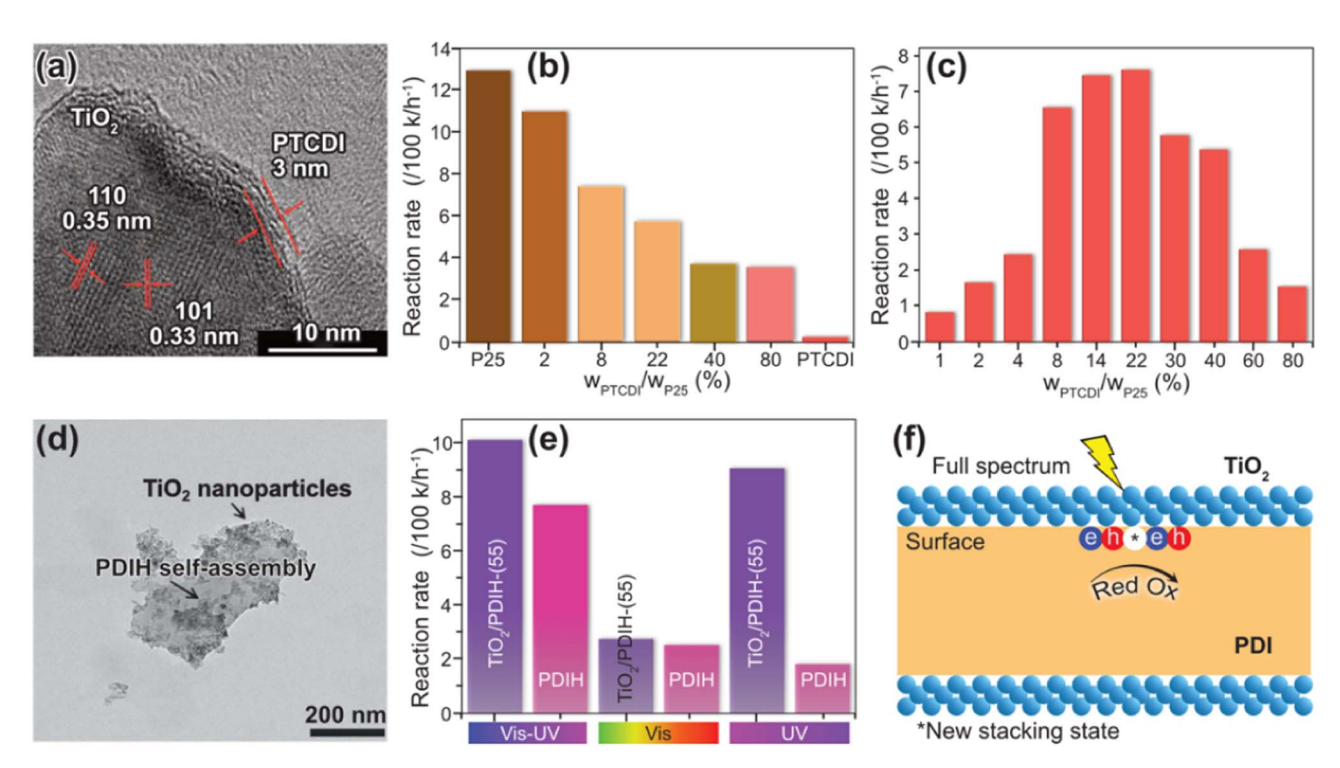


Fig. 6 (a) HRTEM image of PTCDI/P25 heterojunction. Photocatalytic degradation of MO over P25 and PTCDI/P25 under irradiation from (b) UV $(\lambda < 365 \text{ nm})$ and (c) visible light $(\lambda > 450 \text{ nm})$. Reprinted with permission.³⁷ Copyright 2016, the American Chemical Society. (d) HRTEM image of TiO₂/PDIH heterojunction. (e) Photocatalytic phenol degradation of pure PDIH and TiO₂/PDIH under irradiation from UV-visible, visible, and UV light. (f) Mechanism of photocatalytic reaction of TiO₂/PDIH. Reprinted with permission.³⁸ Copyright 2019, Wiley.

found that the latter showed a better performance for the degradation of cationic dyes. The improved photocatalytic activity of BiOCl/PDIs-2 can be attributed to its different exposed surfaces, narrower interplanar spacing, and stronger visible-light absorption. Furthermore, BiOCl/PDIs-2 possessed an optimized n-n heterojunction, resulting in tighter π - π stacking and enhanced migration of photo-generated carriers. In another study, Gao et al.28 successfully constructed a BiOCl/ PDI heterojunction with a full spectral response range (300 nm-750 nm). The anchoring of PDIs on the surface of rod-like BiOCl requires the formation of O-Bi bonds. Surface photovoltage experiments and DFT calculations confirmed the formation of a heterojunction, which extended the absorption range of visible light and significantly promoted the interfacial charge transfer. Compared to BiOCl and PDIs alone, BiOCl/ PDIs-2 showed 2.2-times and 1.6-times higher efficiency for the photocatalytic degradation of phenol. Zhu's group also conducted extensive research on bismuth-based heterojunctions. For instance, they synthesized a Bi₂WO₆/PDI heterojunction using a water bath heating method.42 The surface hybridization between the self-assembled PDIs and the band structure-matched Bi₂WO₆ facilitated the separation of photogenerated charges. The experimental results demonstrated that the main active species in the degradation process was the superoxide radical.

To investigate the role of the diffusion electric field in promoting the separation of photo-generated charges, Zhang and co-workers14 conducted a study on a PDI/BiOI

heterojunction prepared by in situ successive ion layer adsorption and reaction methods (Fig. 8a). This study demonstrated the local separation of photo-generated carriers on heterogeneous interfaces and the Z-scheme transfer mechanism (Fig. 8b-f) through Kelvin probe force microscopy, in situ irradiated XPS, and photo-deposition reactions. Both the experimental and DFT calculation results revealed that the electron density difference between PDIs and BiOI enabled a diffusioncontrolled charge separation process, which exceeded the built-in electric field across the heterogeneous interface. Remarkably, the PDI/BiOI heterojunction exhibited excellent photocatalytic activity, even under infrared light irradiation. These findings present a new blueprint for the development of advanced, stable, and cost-effective PDI/metal oxide heterojunction photocatalysts for solar hydrogen generation and environmental remediation.

3.2.4 Heterojunction between PDIs and other metal oxides. Besides TiO2 and bismuth oxide, other metal oxides have also been combined with PDIs to construct heterojunctions with enhanced photocatalytic efficiency, such as WO3,48 ZnSnO3,49 ZnFe₂O₄,⁵⁰ SnO₂,⁵¹ Zn_{0.5}Cd_{0.5}S,⁵² Ti₃C₂,⁵³ and Ag₃PO₄.⁵⁴ For instance, Yu et al. 55 applied a hydrothermal and recrystallization method to create an inorganic-organic hybrid Sn₃O₄/PDI heterojunction photocatalyst. In this system, PDIs self-assembled on Sn₃O₄ nanosheets, forming a "hook-and-loop" adhesive surface, which effectively traps bacteria through its large number of hydrogen bonds and π - π stacking interactions. Meanwhile, the formation of a heterojunction enabled full-

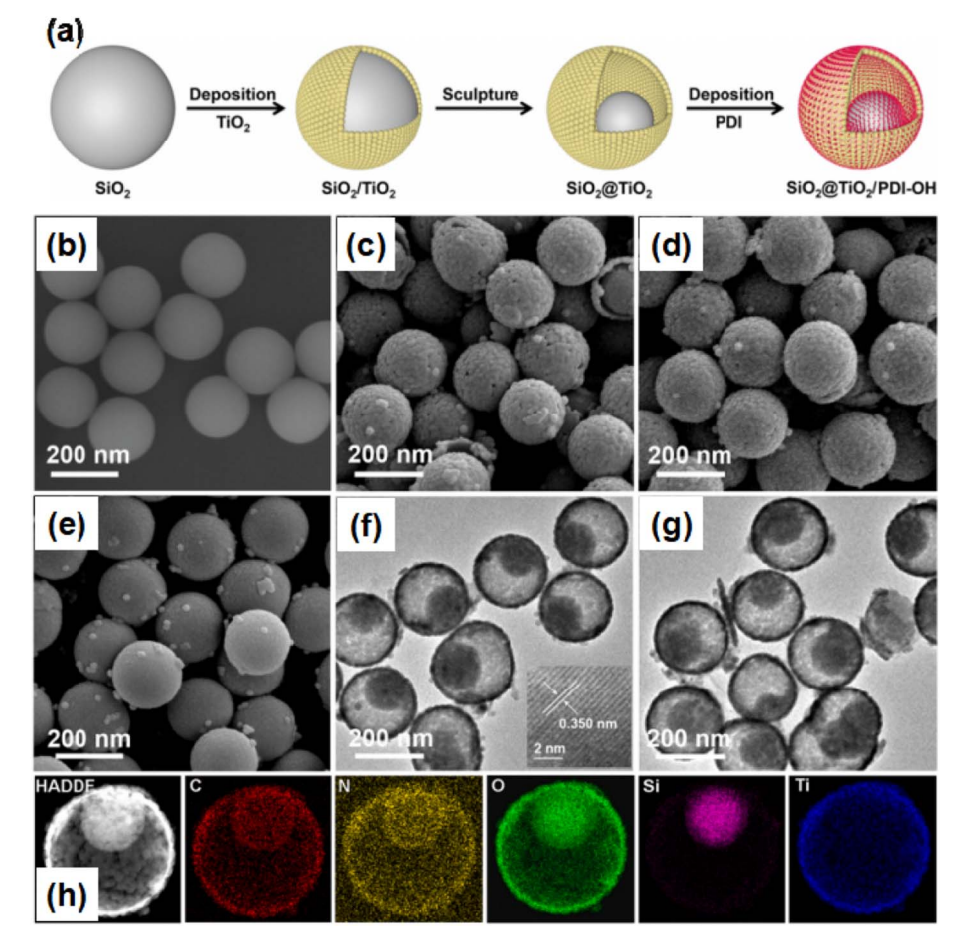


Fig. 7 (a) Schematic diagram of the preparation of $SiO_2@TiO_2/PDIs$. SEM images of (b) SiO_2 nanospheres, (c) $SiO_2@TiO_2$ before sculpturing, (d) $SiO_2@TiO_2$ after sculpturing and (e) $SiO_2@TiO_2/PDIs$. TEM images of (f) $SiO_2@TiO_2$ (inset: HRTEM of TiO_2) and (g) $SiO_2@TiO_2/PDIs$. (h) HADDF-TEM and EDS mapping images of $SiO_2@TiO_2/PDIs$. Reprinted with permission.³⁹ Copyright 2022, Elsevier.

spectrum absorption (λ > 700 nm), reduced the recombination of photo-generated carriers, and enhanced the production of reactive oxygen species. Consequently, the Sn₃O₄/PDI heterojunction demonstrated excellent bactericidal activity under an illumination wavelength of greater than 700 nm.

Ag₃PO₄ is a widely used metal oxide photocatalyst, which is known for its strong oxidation ability in environmental purification. However, its wide application is limited due to its poor photostability and low photoactivity. Thus, to address these challenges, Wang *et al.*⁵⁴ developed a Z-scheme Ag₃PO₄/PDI heterojunction photocatalyst using a two-step self-assembly method. The Ag₃PO₄/PDI Z-scheme photocatalyst showed superior photoactivity and enhanced photostability compared to pure Ag₃PO₄ and PDIs. This improvement can be attributed to the formation of a Z-scheme heterojunction at the Ag₃PO₄-PDI interface, which facilitates efficient carrier separation. XPS characterization, free radical trapping experiments, and theoretical simulation further confirmed the formation of a built-in electric field as the intrinsic driving force behind the Z-scheme mechanism.

3.2.5 Heterojunction between PDIs and metal sulfides. Among the various heterojunction systems, the combination of

PDIs with metal sulfides has attracted significant attention. Metal sulfides have suitable band structures that meet the thermodynamic requirements of water splitting. Compared to other semiconductors, metal sulfides have a deeper valence band, and therefore a better light response. For instance, Liu et al. 13 used a one-step hydrothermal method to create a 3D ZIS/ PDIIM heterojunction for photocatalytic H₂ evolution (Fig. 9a). Ultrathin ZnIn₂S₄ nanosheets (ZIS) with a thickness of 3.27 nm were tightly grown on the surface of PDI microrods functionalized with an imidazole group (PDIsIM) (Fig. 9b-e). The presence of the PDI template effectively dispersed the ultrathin ZIS nanosheets, preventing their self-aggregation and facilitating the exposure of their active sites. The maximum H2 evolution rate of ZIS/PDIM was approximately 13.04 mmol $g^{-1} h^{-1}$, which was 2.64-, 14.02- and 26.61-times higher than that of ZIS, PDIsIM, and PDIs, respectively. The excellent photocatalytic performance of ZIS/PDIM was attributed to its optimized morphology, increased exposure of active sites, photothermal effects, and enhanced separation of photo-generated charges. In another study, Zhang et al.56 constructed a CdS/PDI Z-scheme heterojunction for highly active O2 evolution. The uniform distribution of CdS on the surface of PDIs ensured close contact

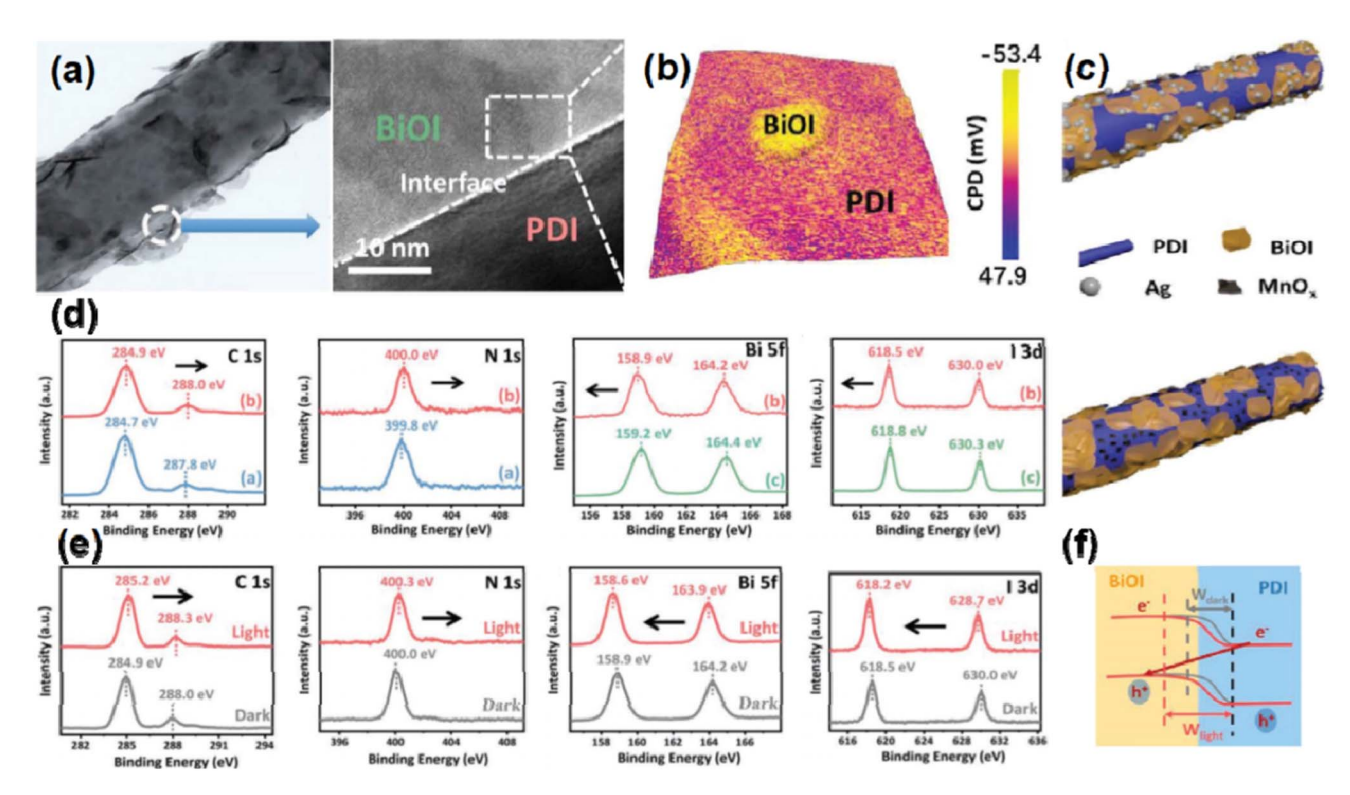


Fig. 8 (a) TEM and (b) HRTEM images of the sharp heterointerface in PDI/BiOI heterojunction. (c) Schematic diagram of Ag-deposited and MnOx-deposited PDI/BiOI heterojunction. (d and e) High-resolution XPS for C 1s, N 1s, Bi 5f, and I 3d of PDI/BiOI heterojunction in the dark or under 500 nm irradiation. (f) Z-scheme carrier transportation in PDI/BiOI heterojunction. Reprinted with permission. (a) Copyright 2021, Wiley.

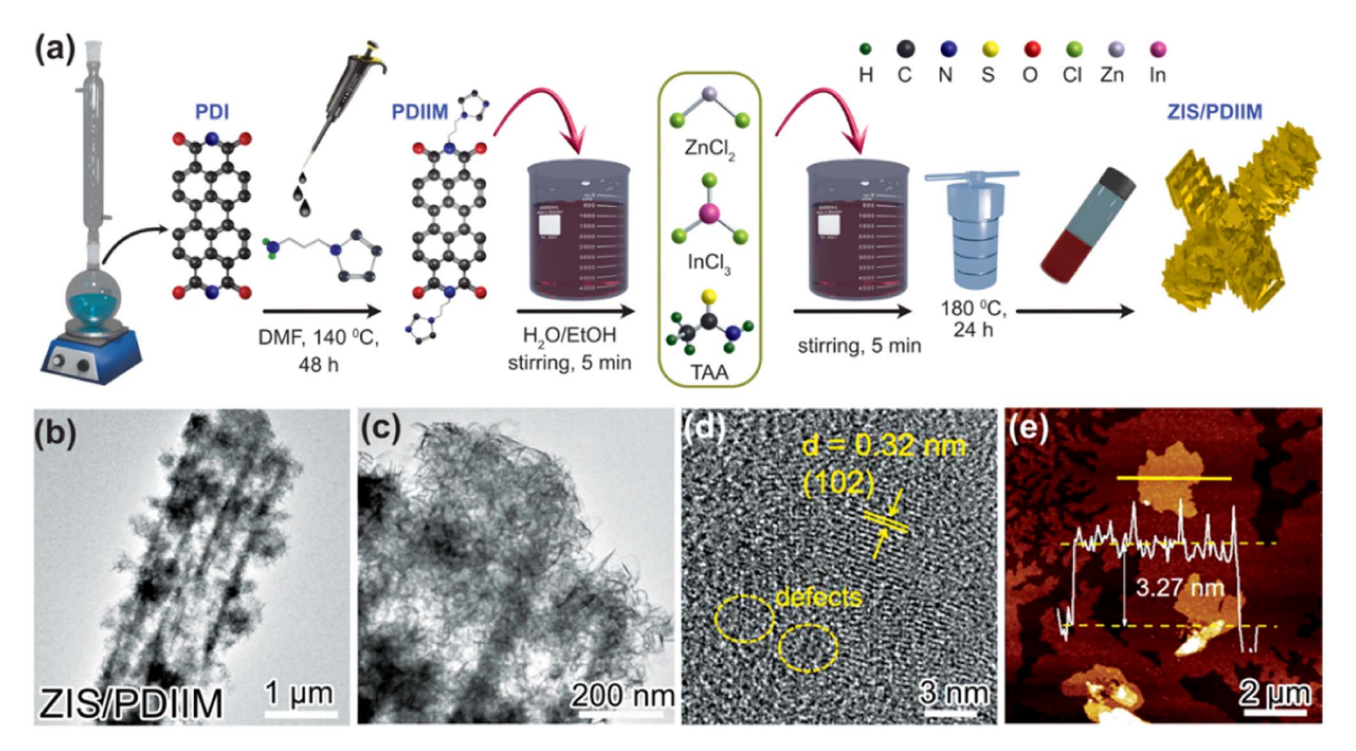


Fig. 9 (a) Synthesis diagram of the ZIS/PDIIM heterojunction. (b-d) HRTEM images of ZIS/PDIIM. (e) AFM image of ZIS/PDIIM. Reprinted with permission.¹³

between the two materials. The O₂ evolution rate of the CdS/PDI composites was two-fold of that of single PDIs under visible light. Density functional theory (DFT) calculations revealed that the rate-determining step in the photocatalytic water oxidation reaction involved the formation of the 'OOH intermediate state. The Z-scheme electron transfer pathway significantly improved the separation efficiency of photo-generated carriers, facilitating the strong reduction of photoelectrons on the conduction band of CdS and the oxidation of holes on the valence band of PDIs, thereby improving the photocatalytic O2 evolution activity.

The Ag₂S semiconductor exhibits excellent light absorption capabilities at wavelengths from the ultraviolet to near-infrared regions due to its narrow bandgap.57 Furthermore, its high reduction potential and chemical stability contribute to its improved photocatalytic performance. Hence, developing an efficient Ag₂S/PDI heterojunction is significant in the pursuit of effective photocatalysis. Zhu's group⁵⁸ successfully synthesized a novel p-Ag₂S/PDI heterojunction with full-spectrum responsiveness. In this composite system, the Ag₂S quantum dots played a dual role of enhancing the organized π - π stacking degree of PDIs, thereby boosting the migration of photogenerated electrons, and enhancing the light absorption of Ag₂S/PDIs. Consequently, the heterojunction exhibited a significantly improved performance in the ultraviolet, visible light, and full spectral regions. The phenol degradation rate and O2 evolution rate were 5.13- and 1.79-times higher, respectively, compared to the pure PDIs.

CuS, as a p-type semiconductor with a narrow bandgap and excellent light absorption, has been widely studied in photochemistry. Notably, CuS exhibits excellent stability and high reduction potential. Therefore, the hybridization of PDIs with CuS is an interesting approach to enhance their photocatalytic capabilities. In this regard, Hu et al. 59 synthesized a PDI/CuS pn heterojunction using a two-step self-assembly strategy. The PDI/CuS heterojunction exhibited the highest photocatalytic degradation activity for tetracycline, with degradation apparent rate constants that were 5.27- and 2.68-times higher than that of CuS and PDIs, respectively. The enhanced photocatalytic activity can be primarily attributed to the synergistic effects of the π – π stacking and p–n junctions, accelerating the separation of photo-generated charges. In addition, the light absorption of PDIs/CuS was significantly enhanced in the range of 200-800 nm, extending even into the near-infrared region. This extended light absorption range substantially contributed to its enhanced photocatalytic performance.

PDI/organic semiconductor heterojunctions

Despite the maturity of research and application of inorganic semiconductors in photocatalysis, their further development faces several challenges, including their limited reserves, high cost, biotoxicity, and photochemical stability, particularly metal sulfides. In contrast, organic materials composed of C, H, N, and O elements have unique advantages and appeal because of their abundant raw materials, low cost, and convenient synthesis routes. Organic semiconductors also have flexible and

adjustable band structures, higher carrier affinity, diverse morphologies, and broad spectral absorption. Organic semiconductors can be classified into three categories based on their properties, i.e., carbon nitride, organic framework compounds, and other self-assembled supramolecular materials. In this section, we introduce the research progress on PDI/inorganic semiconductor heterojunction systems in detail.

3.3.1 Heterojunction between PDIs and carbon nitride. The graphite-like carbon nitride (g-C₃N₄) photocatalyst, which was first reported by Wang et al.,60 has attracted increasing attention for applications in environmental pollutant removal and renewable energy production. This is due to its low cost, ease of preparation and surface functionalization, suitable electronic and band structures, and stable physical and chemical properties. However, despite the remarkable progress, the photocatalytic performance of g-C₃N₄ is still far from satisfying actual production needs, with issues such as easy recombination of photo-generated carriers, limited light absorption capacity, and the need for improved oxidation potential still existing. Therefore, it is of great significance to explore novel g-C₃N₄-based materials with strong light absorption, high carrier separation, and strong redox potentials for environmental pollution remediation and renewable energy generation. One of the most promising approaches to enhance the photocatalytic performance and promote the industrial application of g-C₃N₄ is the design of metal-free heterojunctions with PDIs. In this section, we provide an overview of the recent research progress on g-C₃N₄/PDI heterojunction photocatalysts in various photoredox reactions. The discussion includes their design strategies, carrier transport mechanisms, interface representation, and related aspects.

The construction of g-C₃N₄/PDI heterojunctions primarily involves growth by recrystallization, layer-by-layer selfassembly, and chemical bonding techniques. For example, Wang et al.61 achieved an all-organic g-C₃N₄/PDI heterojunction via the in situ recrystallization of PDIs on the surface of g-C₃N₄ (Fig. 10a). The crystal structures with strong intermolecular interactions significantly influenced the photocatalytic properties of the g-C₃N₄/PDI heterojunction, leading to enhanced light absorption and effective separation of photo-generated charges. In another study, Zhu's group⁶² prepared a one-dimensional/ two-dimensional g-C₃N₄/PDI heterojunction with a wide spectral response (254-700 nm) by introducing self-assembled PDI nanowires onto the surface of g-C3N4 nanosheets through in situ recrystallization. The π - π conjugated bonds in the g-C₃N₄/PDI system accelerated the transport of photo-generated carriers, while the cross-band structure between g-C₃N₄ and PDIs, together with the Z-scheme carrier pathway, enabled the spatial separation of the redox reaction sites. Therefore, the heterojunction achieved excellent photocatalytic degradation performance for phenol.

Furthermore, Li et al.63 prepared an all-organic S-scheme PDI/PCN heterojunction by in situ recrystallization on the surface of porous g-C₃N₄ (PCN) (Fig. 10b). The layered porous photocatalyst design improves the mass transfer performance, enhances the light absorption, and increases the specific surface area. In addition, the S-scheme heterojunction formed

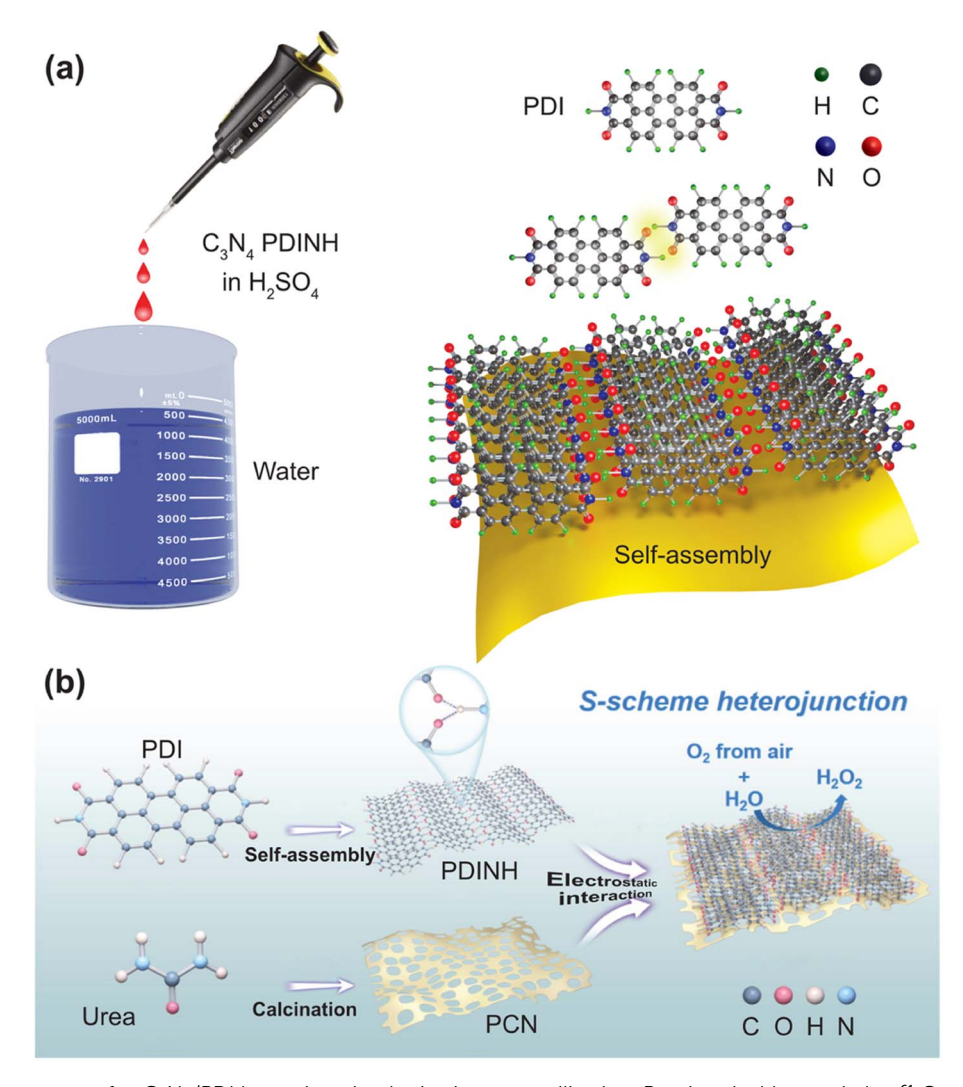


Fig. 10 (a) Synthesis strategy of $g-C_3N_4$ /PDI heterojunction by *in situ* recrystallization. Reprinted with permission. Copyright 2019, Wiley. (b) Synthesis strategy of S-scheme $g-C_3N_4$ /PDI heterojunction using *in situ* recrystallization. Reprinted with permission. Copyright 2023, Elsevier.

by PDIs and PCN showed suitable energy band alignment, enabling the separation and migration of photo-generated carriers. Consequently, the heterojunction demonstrated excellent photocatalytic performance for H_2O_2 production.

Layer-by-layer self-assembly is one of the most effective strategies to form PDI/g-C₃N₄ heterojunctions, involving the electrostatic interaction between PDIs and g-C₃N₄. In a study by Liu *et al.*, 64 a g-C₃N₄/PDI heterojunction was successfully prepared through *in situ* electrostatic assembly. The spatial arrangement of the g-C₃N₄/PDI structure exhibited excellent light absorption performance and facilitated the rapid separation and migration of photo-generated carriers, greatly improving the solar energy utilization for the enhanced photocatalytic degradation of phenol. Similarly, Zhu's group 65 obtained O-CN/PDI heterojunctions by combining positively charged oxygen-doped g-C₃N₄ (O-CN) with negatively charged PDIs. The π - π interaction between the self-assembled PDIs and O-CN facilitated electron delocalization, promoting electron migration. The incorporation of self-assembled PDIs extended

the visible light response range of O-CN and increased the production of photo-generated carriers. Furthermore, the crossband structure between O-CN and self-assembled PDIs generated a built-in electric field, which promoted the separation of interface charges. Additionally, the O-CN/PDI heterojunction exhibited enhanced photocatalytic activity in disinfection, degradation, and oxygen evolution due to the accumulation of active substances (h+, O2- and 1O2), which improved the oxidation ability of O-CN/PDIs. However, it should be noted that recrystallization growth and layer-by-layer self-assembly mainly rely on weak intermolecular interactions for assembly. These weak forces not only hinder the charge transfer between the PDIs and g-C₃N₄ interfaces, potentially leading to recombination centers for photo-generated electrons and holes, but also result in the formation of an unstable interface between PDIs and g-C₃N, which can lead to their separation.

Among the various strategies to construct g-C₃N₄/PDI heterojunctions, covalent bonding through amide bonds is the most commonly used and extensively studied approach. The

heterojunction interface formed by covalent bonding is the strongest, providing fast paths for the transfer of photogenerated charges between interfaces. For instance, Zhao et al.66 synthesized a g-C₃N₄/PDI heterojunction through acylation reactions, resulting in higher photocatalytic activity for the degradation of phenol in the presence of persulfate compared to PDIs and g-C₃N₄ alone. Guo et al.⁶⁷ achieved a Z-scheme g-C₃N₄/PDI heterojunction through the imidization reaction between perylene tetracarboxylic dianhydride (PTCDA) and g-C₃N₄ in an aqueous solution (Fig. 11a and c). Various test results revealed that PTCDA and g-C₃N₄ were surface hybridized through an O=C-N-C=O covalent bond in the PDI/g-C₃N₄ heterojunction. Notably, with an increase in the content of PTCDA, the color of g-C₃N₄/PDIs gradually turned red (Fig. 11b), and the PDI/g-C₃N₄ heterojunction with 1 wt% PTCDA exhibited the optimal photocatalytic degradation and mineralization capabilities under visible light. Xing et al.68 used a fine condensation strategy to create a covalently bonded direct Zscheme PDI/g-C₃N₄ heterojunction with close interface contact and high charge transfer efficiency (Fig. 11d). This design facilitated the spatial separation of photo-generated carriers through a Z-scheme transfer path, resulting in the PDI/g-C₃N₄ heterojunction displaying an excellent amine oxidation rate of 20.63 mmol g⁻¹ h⁻¹ and selectivity for the photocatalytic oxidative coupling of amines and imines.

Furthermore, in addition to its ability to form covalent bonds with g-C₃N₄ to form a heterojunction, the conjugated PTCDA with strong electron-donating enabled hole enrichment. Thus, Hu et al.69 created a well-ordered highly crystalline g-C3N4 nanoarray (CNA) with a tip e⁻ agglomeration effect, which was further tailored by grafting conjugated PTCDA. The resulting D-A regulated PDI/CNA materials effectively achieved the spatial separation of redox centers, where the perylene diimide molecule and the pyridine N atom around the alkali metal in the cavity acted as the reduction center, while the heptazine unit acted as the oxidation center. This well-designed structure effectively promoted the collection of visible light and the rapid separation and directional transfer of charges, while inhibiting the recombination of photo-generated carriers, resulting in a significant increase in the photocatalytic yield of H_2O_2 .

The role of PDIs in the PDI/g-C₃N₄ heterojunction was twofold, i.e., it provided an aromatic plane to interact with the triazine rings of g-C₃N₄, strengthening the π - π interactions, changed the plane structure of the layered g-C₃N₄, inducing plane distortion, and enhanced polarization in the material, resulting in a piezoelectric response. Hence, a unique g-C₃N₄/ PDI-g-C₃N₄ homojunction was fabricated via a facile thermal condensation method.70 This homojunction induced enhanced polarization and π - π interactions, promoting the piezocatalytic property and facilitating charge transfer, resulting in an

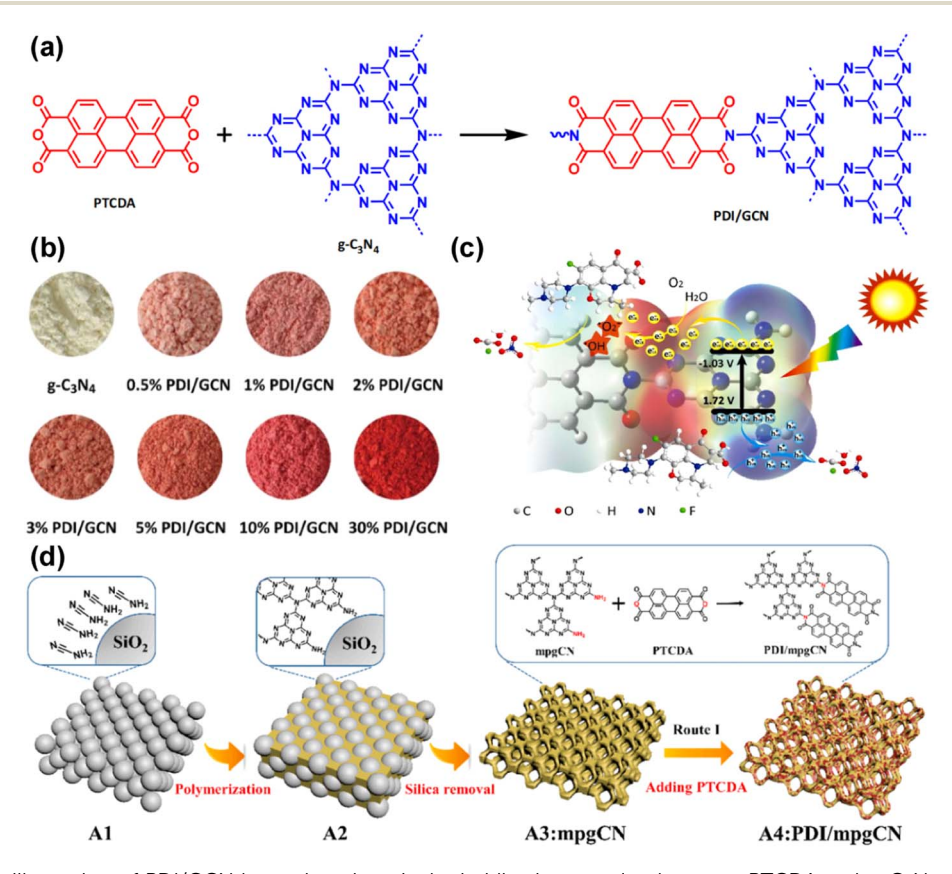


Fig. 11 (a) Schematic illustration of PDI/GCN heterojunction via the imidization reaction between PTCDA and $g-C_3N_4$. (b) Photographs of g-C₃N₄ and various PDI/GCN heterojunctions. (c) Schematic illustration of the mechanism of photocatalytic degradation of LEV over the 1% PDI/ GCN heterojunction. Reprinted with permission.⁷¹ Copyright 2019, the American Chemical Society. (d) Schematic illustration of the synthesis of PDI/mpgCN heterojunction. Reprinted with permission. 68 Copyright 2021, Elsevier.

excellent piezo-photocatalytic ATZ degradation performance compared to piezocatalysis and photocatalysis alone. The effective interfacial charge transfer enabled by covalent bonding significantly enhanced the photocatalytic activity of the PDI/g-C_3N_4 heterojunction. These findings open up new avenues for the development of PDI/g-C_3N_4 heterojunctions for renewable energy production and pollutant degradation.

The use of powder photocatalysts in commercial applications is limited due to their susceptibility to blowing away in the air and difficult recycling. Therefore, it is crucial to fix powder photocatalysts on a carrier material such as foam and film. Although many studies successfully obtained g-C₃N₄/PDI heterojunctions through the reaction of PTCDA and g-C₃N₄ under N₂ protection, their preparation process is time-consuming and it is difficult to prepare photocatalysts in membrane form, which limits their further use. Therefore, developing new methods for preparing g-C₃N₄/PDI heterojunctions in membrane form is critical. One approach is the modification of PDIs during the formation of g-C₃N₄ by selecting suitable g-C₃N₄ precursors with rich NH₂ groups and N₂ calcination atmosphere (Fig. 12a).72 In this method, the precursor turns into a liquid phase during the condensation process and transforms into g-C₃N₄/PDIs under calcination, enabling the fabrication of g-C₃N₄/PDI films by coating the precursor on SiO₂ films. These films showed desirable properties such as good flexibility, high tensile stress, and good thermal stability as a substrate during the calcination process. The resulting g ${\rm C_3N_4/PDI}$ membrane showed efficient phenol A removal within 30 min under visible light irradiation in the presence of PMS. Aerogels also serve as attractive support materials because of their large specific surface area and ease of recycling. For example, Lu *et al.*⁷³ prepared macroporous PDI/g- ${\rm C_3N_4/GO}$ aerogels *via* a hydrothermal method followed by freeze-drying (Fig. 12b and c). These ultra-light three-dimensional aerogels have strong visible light absorption, excellent charge transport properties, and a large specific surface area. They demonstrate excellent photocatalytic activity for NO at the ppb level under visible light irradiation.

In addition to binary g- C_3N_4 /PDI heterojunctions, there have been efforts to design and construct multi-component heterojunctions to further improve the photocatalytic activity of PDIs. These ternary heterojunctions combine wide bandgap semiconductors, narrow bandgap semiconductors, and carbon or metal materials, leveraging the synergistic effects of all components. Thus, these designs effectively enhance the overall photocatalytic performance of PDIs.

For instance, Zhu's group⁷⁴ developed an all-polymer g-C₃N₄/rGO/PDI Z-scheme heterojunction *via* a facile multi-step manufacturing route. As illustrated in Fig. 13a, the process involved coating the surface of PDI nanorods with rGO *via* a wet chemical reduction process to obtain RGO/PDIs. Subsequently, this material was loaded on g-C₃N₄ nanosheets using a solvent evaporation-deposition method. Heat treatment resulted in the successful formation of the g-C₃N₄/rGO/PDI heterojunction.

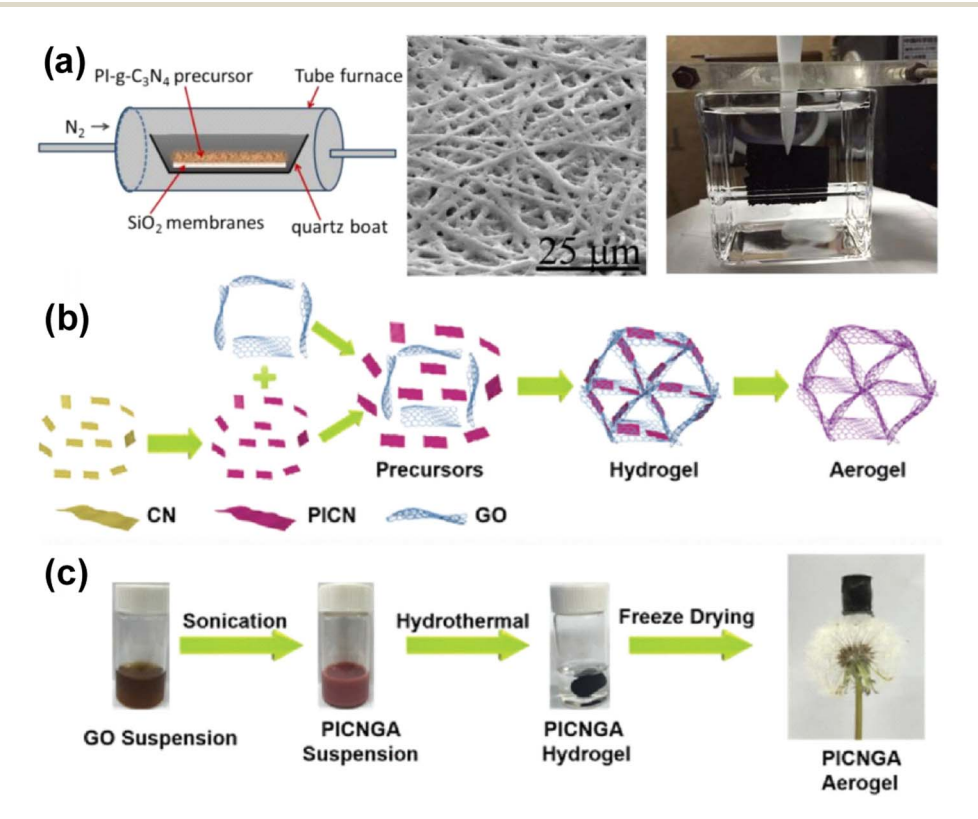


Fig. 12 (a) Illustration of calcination process, SEM images, and optical image of PDI-g-C₃N₄ membrane. Reprinted with permission.⁷² Copyright 201, Elsevier. (b) Schematic illustration of the synthesis of the PICNGA composite aerogel. (c) Photographs of the fabrication of the aerogel. Reprinted with permission.⁷³ Copyright 2018, Wiley.

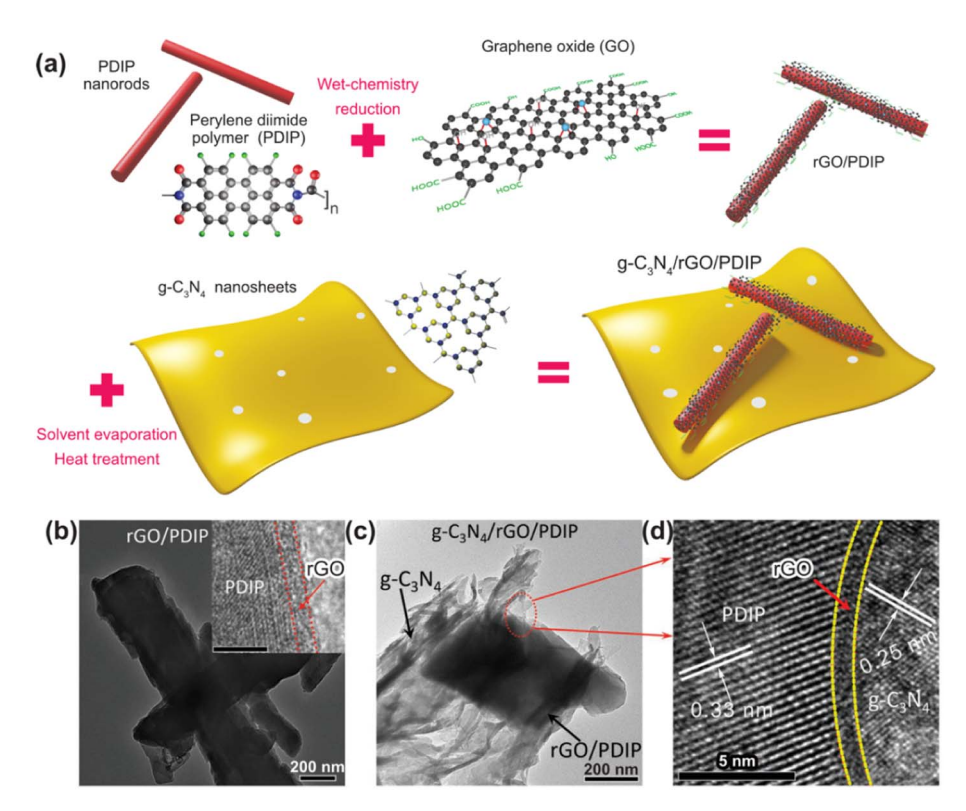


Fig. 13 (a) Schematic of the preparation of $g-C_3N_4/rGO/PDIs$. (b) TEM image (HRTEM image inset) of rGO/PDIs. (c) TEM image and (d) corresponding HRTEM image of g-C₃N₄/rGO/PDIs. Reprinted with permission.⁷⁴ Copyright 2019, Wiley.

The TEM results revealed the layered assembly of rGO and g-C₃N₄ on the surface of the PDI nanorods (Fig. 13c and d). The time profiles of transient absorption spectroscopy (TAS) demonstrated that the average lifetime of the trapped holes in g-C₃N₄/rGO/PDI was prolonged, while the lifetime of trapped electrons was shortened compared to pure PDIs. This finding supports the inhibited recombination of photo-generated electron-hole pairs. This phenomenon also fully confirms the formation of the Z-scheme charge transfer path between g-C₃N₄ and PDIs through the rGO layer. Based on these observations, the g-C₃N₄/rGO/PDI heterojunction achieved high efficiency and stable performance in photocatalytic overall water splitting, surpassing many reported photocatalysts based on g-C₃N₄.

Similarly, Yang et al.75 prepared a Z-scheme g-C₃N₄/rGO/PDI heterojunction. This heterojunction exhibited superior photocatalytic activity in removing NO and generating H₂O₂ under visible light irradiation. These studies offer new examples of advanced, stable, and cost-effective g-C₃N₄/PDI-based heterojunction photocatalysts for environmental pollution harness and renewable energy production.

3.3.2 Heterojunction between PDIs and metal-organic frameworks. Metal-organic frameworks (MOFs) are porous coordination polymers composed of organic connectors and inorganic metal clusters or ion nodes. They have attracted significant attention due to their uniform and adjustable pore structure, high specific surface area, and high density of unsaturated metal sites, making them suitable for solar-driven photocatalytic applications. However, similar to other semiconductors, MOFs are limited by their low photocatalytic quantum efficiency, which is mainly due to the poor separation efficiency of photo-generated charges. Accordingly, one promising approach to address this challenge is coupling MOFs with PDIs to construct MOF/PDI heterojunctions, promoting the separation of photo-generated charges.76,77 Moreover, the differences in interface potentials generate a built-in electric field, enabling effective spatial separation between the photoinduced electrons and holes, while suppressing their recombination.

For example, Chen et al.78 synthesized a supramolecular composite of MIL-53 (Fe)/PDIs using the solvothermal method. This composite exhibited a remarkable photocatalytic performance, degrading 94.08% of tetracycline within 30 min, which was 4-times higher than PDIs alone and 33-times higher than MIL-53 (Fe) alone. In the heterojunction, PDI nanofibers were dispersed and immobilized in MIL-53 (Fe) through covalent bonds, forming interconnected structures. Based on the band structure of PDIs and MIL-53 (Fe), a Z-scheme heterojunction was proposed, contributing to excellent tetracycline removal ability. Alternatively, the coupling of self-assembled PDIs with MOF materials, especially Cr-based MOFs, to obtain selfassembled PDI/MOF heterojunctions remains largely unexplored. Additionally, the internal electron transfer mechanism in these composite materials and the synergistic effect of photocatalytic PS activation are still unclear.

Thus, to address these gaps, Ji et al.79 developed a new Zscheme PDI/MIL-101(Cr) heterojunction via a one-pot method,

which was employed for persulfate (PS) activation under visible light. The PS/PM-7 (PDIs: MIL-101 (Cr) = 9:7, w/w, 0.5 g L^{-1}) system achieved the rapid degradation of iohexol, with a reaction rate 8.8-times higher than that of the PDI/PS/Vis system. The Z-scheme PM heterojunction possessed high charge transfer efficiency, with electrons injected from the CB of MIL-101 (Cr) to the VB of SA-PDIs. PS acted as a photo-generated electron acceptor, promoting carrier migration and the generation of reactive oxygen species, and thus accelerating the oxidation of iohexol. Among the various reported MOF materials, MIL-125 (Ti)-NH₂ (MTi) has attracted increasing attention due to its excellent chemical stability and water stability. The MTi amino functional groups served as molecular linkers to connect the PDIs. Liang et al.80 prepared a PDI/MTi heterojunction with Lewis acid-base pair structures through a simple acid-catalyzed approach. The amino group in MTi acted as a nano scaffold, binding to PDIs through ammonolysis reactions. The synergistic effect of the micropolarization field, multiple active sites, and C-N bonding interface enhanced the photocatalytic activity for killing Staphylococcus aureus and reducing Cr(vi).

3.3.3 Heterojunction between PDIs and other selfassembled supramolecular materials. Metal phthalocyanine (MPc), as an organic semiconductor, is a planar conjugated macrocyclic molecule with a suitable HOMO energy level that is slightly lower than the CB bottom of PDIs, making it suitable for Z-scheme band alignment. Among the various MPcs, zinc phthalocyanine (ZnPc) is widely used in photocatalysis. Sun et al.81 successfully designed and synthesized ultrathin phosphate-regulated ZnPc/PDI supramolecular Z-scheme heterojunctions for CO2 photoreduction under wide visible light. The improved charge separation efficiency, caused by the Zscheme heterojunction, significantly contributed to the enhancement in photocatalytic performance. Notably, the introduced phosphoric acid groups improved the uniform dispersion of ZnPc on PDI nanosheets by forming hydrogen bonds at the interface. Additionally, these groups acted as hole traps, accelerating the charge transfer and spatial separation. The ZnPc/PDI heterojunction exhibited significantly improved photocatalytic activity, showing about 6.5-times higher CO₂ photoreduction efficiency than that of the pure PDIs. The stronger SPS response of all the ZnPc-modified PDI samples, especially the 2ZnPc/PDI samples, confirmed the significant enhancement in the separation of photo-generated charges. However, the ZnPc/PDI heterojunction assembled through hydrogen bonding interactions may limit the transport of photo-generated carriers. Therefore, further research is needed to synthesize MPc/PDI heterojunctions with close interfaces and sufficient active sites to obtain high-performance photocatalysts.

For instance, Zhi *et al.*⁸² created an imide-based 2D covalent organic polymer, CoPcPDA-CMP, by integrating CoPc and PDI moieties, which were further exfoliated into CoPcPDA-CMP nanosheets. The successful formation of the six-membered imide ring was confirmed by FTIR. In the CoPcPDA-CMP NS photocatalytic system, the CoPc and PDI groups achieved CO₂ reduction and H₂O oxidation semi-reactions, respectively,

completing the entire CO_2 reduction reaction through Z-scheme charge transfer. Furthermore, combined with the excellent light absorption ability, charge separation efficiency, and electronic conductivity of CoPcPDA-CMP nanosheets, it exhibited an outstanding CO_2 photoreduction performance, competing with the most advanced visible-light-driven organic photocatalysts.

Polyaniline (PANI) is a non-toxic conductive polymer.83 Its molecular structure consists of aniline (-NH-) and quinone imine (=N-) groups, representing the reduced and oxidized forms of PANI, respectively. Polyaniline has a high reduction potential and narrow bandgap, making it responsive to visible light. Conversely, PDIs have a strong oxidation potential and low reduction potential. Thus, the energy band alignment between PANI and PDIs is favorable for the formation of Zscheme or S-scheme heterojunctions. Constructing a PDI/ PANI heterojunction in either the Z-scheme or S-scheme configuration not only addresses the challenge of the limited charge separation ability of PDIs but also expands their applicability by mitigating the constraints imposed by their low reduction potential. For instance, Dai et al.84 successfully constructed a three-dimensional Z-scheme PANI/PDI heterojunction, which demonstrated the effective degradation of tetracycline (TC) under visible light irradiation. This can be attributed to the establishment of a large delocalized π -electron conjugation system and energy-matched heterojunction between PANI and PDIs. The active species ('O₂-, h⁺, and H₂O₂) react with TC, leading to hydroxylation, dealkylation, aromatization and ring-opening processes, ultimately resulting in complete mineralization.

Porphyrin molecules, characterized by porphyrin rings and various substituents (carboxyl, hydroxyl, and sulfonic acid), have attracted considerable interest in photocatalysis due to their wide absorption spectra covering the entire solar spectrum.85 The HOMO energy level of porphyrin molecules closely matches the CB of PDIs, and their similar conjugated macrocycle structure facilitates size-matched interfaces through π - π interaction. This means that porphyrins can be used to build heterojunctions with PDIs, which are responsive to the full spectrum of sunlight. For example, Jing's group35 creatively designed a Z-scheme T-TCPP/PDI heterojunction by selecting tetra(4-carboxylphenyl)porphyrin (TCPP) as a reduction photocatalyst, PDIs as an oxidation photocatalyst, and TiO2 (T) as an energy platform for electron transfer. In the T-TCPP/PDI heterojunction system, the introduction of TCPP enhanced the charge separation, while the coupled TiO2 facilitated the extraction of photo-generated electrons accumulated on the CB of TCPP, thus enhancing the Z-scheme charge transfer between TCPP and PDIs. Based on the dominant role of the heterojunction, the optimized T-TCPP/PDIs showed a 10-times increase in CO production over pure PDIs and retained its excellent photostability. Zhu's group12 also successfully developed a TPPS/PDI heterojunction using TPPS (tetra(4sulfonatophenyl)porphyrin) and PDIs as an electron donor and electron acceptor, respectively, through π - π stacking interactions. In this case, there was no TiO2 as an energy platform for electron transfer, and the electron transfer in the TPPS/ PDI heterojunction was driven by the built-in electric field,

primarily through the type II mechanism. The donor-acceptor (D-A) interface with high charge separation between TPPS and PDIs significantly enhanced the charge separation and extended the excited state lifetime compared to the individual components, leading to excellent photocatalytic H₂ evolution.

3.4 PDI/metal heterojunction

Depositing precious metals on semiconductor photocatalysts is one of the methods commonly employed to improve their performance. Generally, precious metals are deposited as nanoparticles (NPs) on the photocatalyst surface, utilizing either the surface plasmon effect at the contact interface or the formation of a Schottky barrier to improve their performance. When metal particles absorb incident light, the photocatalyst system experiences the excitation of localized surface plasmon resonances, increasing the rate at which the semiconductor generates electron and hole pairs. Due to the lower work function of the semiconductor compared to the metal NPs, a Schottky barrier is formed between the metal and n-type semiconductor, causing the excited electrons in the semiconductor to transfer to the metal surface. Metal NPs act as an electron capture agent, further promoting the separation of photo-generated carriers. For instance, Wei et al.86 developed Pd@PDI/P25 and PDI/Pd@P25 systems using Pd quantum dots. These photocatalysts exhibited a core-shell structure, with Pd quantum dots located on the inner and outer surfaces of the shell, respectively, which showed excellent catalytic activity in phenol degradation and hydrogen evolution experiments. The electron transfer mechanism is as follows: a photon gets

absorbed, inducing the generation of an exciton in PDIs and the electron shuttles to the CB, and then transfers to the Pd quantum dots. The accumulation of hot electrons in Pd quantum dots enhances the Pd plasma oscillation effect, resulting in energy transfer and holes entering the PDIs. This process generates an increased number of PDI radical anions, enhancing the reduction ability of PDIs.

Despite being expensive and rare, gold (Au) remains an effective co-catalyst in photocatalysts due to its high activity. Miao et al.11 prepared a PDI@AuNP photocatalyst, which exhibited a 1.7-times larger degradation rate of phenol than that of PDI nanowires (Fig. 14a-c). The surface plasmon resonance effect of AuNPs and the resonance energy transfer effect between PDIs and AuNPs improved the visible light utilization and carrier separation efficiency of the heterojunction, thereby improving the photocatalytic activity.

The low reduction potential of platinum (Pt) also makes it suitable for coupling with PDIs to improve their photocatalytic activity. Additionally, the Schottky barrier between Pt and PDIs accelerates the transfer of photo-generated electrons from PDIs to Pt. Liu et al.87 successfully prepared a Pt quantum dot/PDI heterojunction using a simple chemical reduction method. This heterojunction exhibited an excellent photocatalytic performance for the degradation of phenol under visible light irradiation. The optimal 1 wt% Pt QD/PDI composite demonstrated a 6.2-fold improvement in activity compared to pure PDI nanorods for the degradation of phenol. The formation of a Schottky barrier between Pt quantum dots and PDI nanorods accelerated the migration and separation of photo-generated

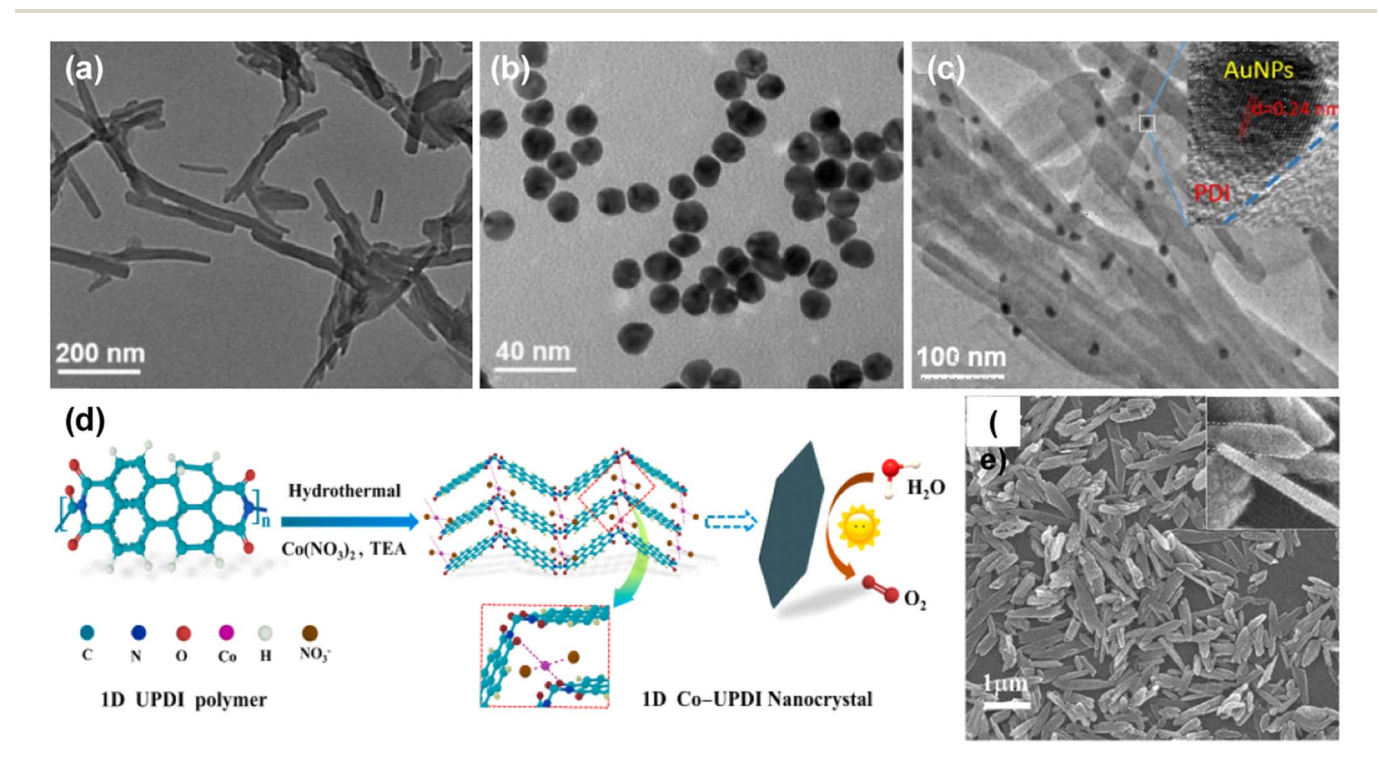


Fig. 14 TEM images of (a) self-assembled PDIs, (b) AuNPs, and (c) PDIs@AuNPs. Reprinted with permission. Copyright 2021, Elsevier. (d) Schematic illustration of the synthesis of CoPcPDA-CMP NSs. (e) TEM image of CoPcPDA-CMP NSs. Reprinted with permission.⁸² Copyright 2022, Wiley.

carriers. The Pt quantum dots effectively captured and shifted the photo-generated electrons, leading to the rapid transfer and efficient separation of photo-generated carriers, ultimately enhancing the photocatalytic performance.

However, although precious metals can significantly improve the photocatalytic performance of PDIs, their high cost and limited availability restrict their widespread industrial use. In this case, non-precious metals offer promising alternatives due to their abundant reserves, cost-effectiveness, and potential for large-scale applications. Therefore, exploring PDI/non precious metal heterojunctions holds great research value and necessity.

For example, Zeng $et~al.^{ss}$ addressed the poor water solubility and easy aggregation of PDIs, which limit their application in homogeneous catalytic reactions, by synthesizing organic polymer Zn-PDI photocatalysts. The interplay between metal-PDI coordination and π - π stacking of the organized PDI arrays in Zn-PDIs facilitated consecutive photo-induced electron transfer. These synergistic effects between the PDI array and Zn sites further enhanced the photocatalytic activity of Zn-PDIs for the basic oxidation of benzyl alcohol and amines.

Inspired by the advantage of minimal spatial dimension of nanocrystals, Zhong *et al.*⁸⁹ successfully synthesized large-scale 1D nanocrystals of cobalt perylene diimide polymer (Co-PDIs NRs). When Fe(NO₃)₃ was used as an electron acceptor, Co-PDI NRs exhibited the highest photocatalytic oxygen evolution. This excellent performance was attributed to the efficient electron–hole separation and the *in situ* generation of α -FeOOH as a co-catalyst.

Building on the integration of 1D nanocrystals, strong built-in electric fields, and the functional properties of cobalt, Cao *et al.*90 further synthesized 1D nanocrystals of cobalt-intercalated urea perylene imide polymer composite (Co-UPDI NRs) (Fig. 14d and e). The optimal oxygen production rate of Co-UPDI NRs reached 7992.3 μ mol h⁻¹ g⁻¹, which was approximately 13-times higher than that of UPDIs (580.7 μ mol h⁻¹ g⁻¹). The experimental results indicated that the superior oxygen production performance of Co-UPDI NRs resulted from their improved photoelectric conversion efficiency and the *in situ* formation of CoOOH as a co-catalyst.

Heterogeneous photocatalytic reactions predominantly occur at the surface. Therefore, maximizing the exposure of active sites on the surface of catalysts is crucial for enhancing the reaction efficiency. The utilization of atoms can be improved by reducing the size of metal nanoparticles and increasing their dispersion on the semiconductor surface. Particularly, employing monatomic metals allows for maximum atom utilization efficiency and the generation of abundant active sites for surface catalytic reactions.

For instance, Shen and co-workers used a simple two-step immersion calcination method to introduce Co single atoms and ultra-small CoOx clusters in polymer diacetylene PDIs (Fig. 15a and b). The obtained Co/PDI photocatalyst showed excellent activity for water oxidation under visible light irradiation, achieving an oxygen evolution rate of 5.53 mmol $h^{-1} \, g^{-1} \, (\lambda > 420 \, \text{nm})$. The AQY for oxygen evolution was 8.17% at 450 nm and 0.77% at longer visible wavelengths (Fig. 15c). This

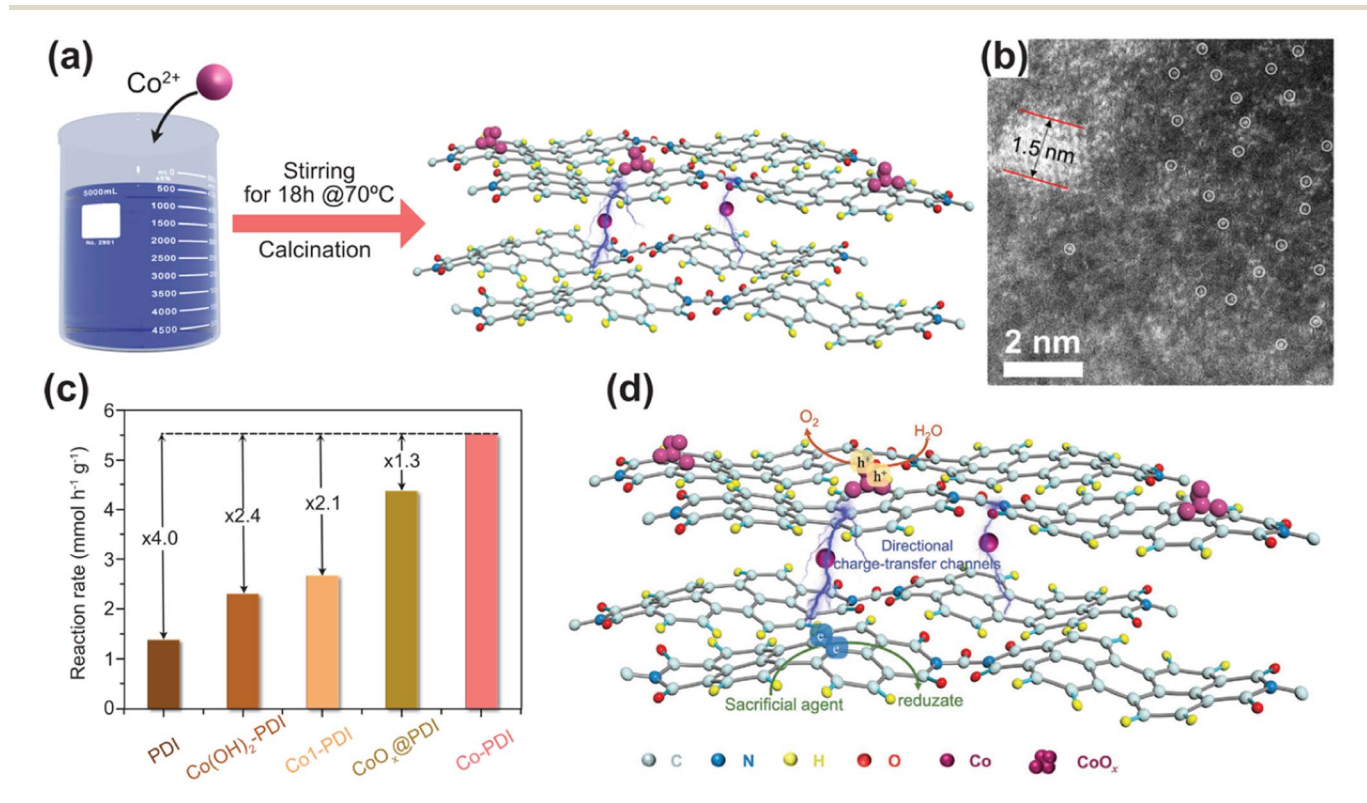


Fig. 15 (a) Schematic illustration of the process for the preparation of Co-PDIs. (b) HAADF-STEM image of Co-PDIs. (c) Photocatalytic oxygen evolution rates of PDIs, Co(OH)₂-PDIs, Co1-PDIs, CoOx@PDIs, and Co-PDIs under visible light (λ > 420 nm). (d) Illustration of the charge-transfer process in Co-PDIs upon light irradiation. Reprinted with permission.⁹¹ Copyright 2022, Wiley.

indicates that Co/PDIs is an outstanding photocatalyst for oxygen evolution. The theoretical calculations and experimental results revealed that the Co single atom acts as an electronic mediator, connecting adjacent PDI layers to establish a direct channel for rapid charge transfer. Simultaneously, the ultrasmall CoOx clusters acted as hole collectors and reaction sites, accelerating the oxygen evolution reaction kinetics (Fig. 15d). This synergistic effect significantly boosted the photocatalytic performance of oxygen evolution.

In another study, Zhu's group92 created a PDI photocatalyst modified with dual co-catalysts, Co₃O₄ and Pt, for photocatalytic water oxidation. Notably, this photocatalyst exhibited a high O₂ yield of 24.4 mmol g⁻¹ h⁻¹ under visible light, with an AQY of 6.9% under 420 nm monochromatic light. The rational design of the dual co-catalysts generated an electric field, providing an anisotropic driving force for photogenerated holes towards Co₃O₄ and photogenerated electrons towards Pt, synergistically improving the space charge separation efficiency for water oxidation.

PDIs/carbon material heterojunctions

Carbon-based materials such as carbon nanotubes, fullerenes, graphene and carbon quantum dots (CQDs) have remarkable chemical stability, high conductivity and large external specific surface area. Introducing carbon in semiconductors derived from carbon-based materials offers several benefits, including extending their absorption spectral range and reducing the recombination of photo-generated charges.93 Among the various carbon materials, CQDs stand out due to their simple preparation, high yield, low toxicity, and cost-effective precursors.94 Furthermore, CQDs exhibit broadened light absorption characteristics, excellent electronic conductivity, and upconversion effects.95

For instance, Liu et al.96 successfully prepared carbon quantum dot-doped perylene diimides (PDIs/CQDs) using a one-step acidification polymerization method. The apparent rate constant of the photocatalytic degradation of naproxen over PDIs/CQDs was 3.50-times higher than that of the original PDIs.

To improve the applicability of PDI/CQD materials, the authors further developed PDI/CQD cellulose acetate membranes, which demonstrated excellent stability and efficiency under different water conditions. Graphene quantum dots (GQDs), another type of CQDs, can function as both electron donors and acceptors, enabling the efficient regulation of the transfer of photo-generated charges. GQDs have excellent conductivity, non-toxicity, and quantum confinement effects, and thus they are widely used to enhance the photocatalytic performance of PDIs. For example, Zhu's group97 successfully prepared GQD/ PDI composites through electrostatic interactions. The photocatalytic activity of GQDs/PDIs was evaluated by studying the degradation of phenol and hydrogen production under visible light. When the mass fraction of GQDs in PDIs reached 14%, the phenol degradation rate of GODs/PDIs was 4.73-times higher than that of pure PDIs, and the hydrogen production rate $(1.60 \text{ mmol g}^{-1} \text{ h}^{-1})$ was 1.88-times higher than that of pure PDIs. The improved photocatalytic redox activity of GQDs/PDIs was attributed to the formation of long-range electron delocalization through the π - π interactions between GODs and PDIs. Additionally, the quantum confinement effect of GQDs facilitated the transfer of electrons from GQDs to PDIs, resulting in a more negative CB position for PDIs, further enhancing their reduction ability. Besides GQDs, the 3D graphene structure has attracted significant attention in photocatalysis due to its large surface area, strong adsorption capacity, and simple preparation process. Furthermore, the excellent conductivity of reduced 3D graphene promotes the migration of photo-generated carriers, while its 3D porous structure enhances the adsorption and enrichment capabilities, providing more reaction sites. Notably, supporting PDIs on 3D graphene significantly enhances the utilization efficiency of photo-generated charges and sunlight, thereby demonstrating an excellent photocatalytic performance. Recently, Zhu's group98 developed a PDI-anchored graphene 3D structure through π - π interactions. The photoelectric degradation rate of MB over PDIs/rGO was nearly double that of pure PDIs or rGO under the same conditions. This enhancement in photodegradation ability can be attributed to two main factors, as follows: (1) the π - π stacking interaction

Table 1 Summary of the different types of PDI-based heterojunctions with different electron transfer paths

Heterojunction	Conduction band (V)	Valence Band (V)	Bandgap (eV)	Туре	Ref.
PDIs/Bi ₅ O ₇ I-OVs	-0.20/-0.25	1.54/2.56	1.74/2.81	I	126
PDIs/TPPS	-0.72/-1.26	0.84/0.10	1.56/1.36	II	12
PDIs/Ag ₂ S	-0.34/-0.44	1.39/1.37	1.73/1.81	II	56
PDIs/g-C ₃ N ₄	-0.19/-1.06	1.47/1.28	1.66/2.34	II	66
PDIs/BiOI	-0.38/0.89	2.61/1.39	1.72/1.77	Z	14
PDIs/BN	-0.92/-0.72	0.88/2.98	1.80/3.70	Z	143
PDIs/MIL-53(Fe)	-0.33/-0.26	1.23/2.41	1.68/2.67	Z	78
PDIs/BiOCl	-0.45/-0.41	1.27/2.10	1.72/2.55	Z	28
PDIs/MIL-101(Cr)	-0.16/0.62	1.54/2.92	1.70/2.30	Z	79
PDIs/Ag ₃ PO ₄	-0.34/0.27	1.46/2.7	1.70/2.43	Z	54
PDIs/CdS	-0.39/-1.02	1.58/1.42	1.97/2.44	Z	56
PDIs/g-C ₃ N ₄	-0.28/-1.26	1.52/1.32	1.79/2.58	Z	62
PDIIM/ZIS	-0.22/-0.66	1.77/1.70	1.99/2.36	S	13
PDIs/COFs	-0.27/-0.95	1.48/1.20	1.75/2.15	S	106
$PDIs/TiO_2$	0.98/-0.57	2.74/2.6	1.74/3.20	S	110

enables carrier delocalization along the π - π stacking direction and (2) the large surface of 3D PDIs/rGO not only improves the adsorption capacity but also provides more reaction sites and multi-dimensional channels.

Based on the above discussion, it is known that most incorporated semiconductors with suitable energy band structures can form heterojunctions with PDIs. However, the different redox potentials of the semiconductors usually lead to different electron transfer channels when forming heterojunctions with PDIs. Therefore, we summarize the different types of PDI-based heterojunctions with different electron transfer paths in Table 1, which will provide some reference for the construction of efficient PDI-based heterostructures.

4. Applications of PDI-based heterojunctions

PDIs-based photocatalysts have been attracting attention due to their potential in applications such as energy storage, energy conversion, and environmental protection. In this section, we provide a concise overview of their applications in photocatalytic water splitting, pollutants degradation, and other photocatalytic reactions.

4.1 Applications in photocatalytic water splitting

Photocatalytic hydrogen production. The use of fossil energy has undoubtedly brought convenience to humans but has also resulted in a serious energy crisis and environmental pollution. Thus, to address this challenge, the development of hydrogen (H₂) energy has emerged as a promising solution given its abundant reserves, high energy density, and no pollution to the environment. Among the various methods for the generation of hydrogen, photocatalytic water splitting, which converts solar energy into H₂ energy, 99 is currently regarded as highly promising. In this process, achieving a lower potential of the CB than that of H₂O (0 eV vs. NHE) is crucial. Accordingly, PDI-based photocatalysts, with a CB position of about -0.36 eV vs. NHE, have been extensively investigated for photocatalytic H₂ production. ¹⁸ To highlight and compare their performance, we summarized the H2 production activity of various PDI-based photocatalysts in Table 2.

However, pure PDIs faces challenges in producing $\rm H_2$ due to their high recombination rate of photo-generated charges, low reduction potential, and unsuitable surface properties for $\rm H_2$ production. Nevertheless, by modifying the energy band structure, electronic structure, functional groups, and other surface properties, significant improvements can be achieved in $\rm H_2$ production performance. For example, Hua and co-workers successfully obtained phosphoric acid-substituted PDIs, which showed an excellent $\rm H_2$ production rate of 11.7 mmol g $^{-1}$ h $^{-1}$ and an AQY of 2.96% at 550 nm. Through the substitution of terminal groups with strong electron-withdrawing acceptor groups, the separation of photoinduced carriers was enhanced and the spectral response range was extended, thus increasing the photocatalytic $\rm H_2$ production activity. To broaden the absorption spectrum and enhance the separation of

photoinduced charges, Ding et al. 100 employed a strategy involving the formation of coordination bonds between zirconium(iv) metal cations and organic supramolecular system based on PDIs. A series of PDI supramolecular photocatalysts (P-PMPDIs) doped with different Zr^{IV} cations through phosphonate/Zr^{IV} coordination bonds was successfully synthesized. Among them, P-PMPDIs-Zr (Zr^{IV} : P-PMPDIs = 0.25:1) showed the highest activity in the photocatalytic hydrogen evolution reaction, with a rate of 50.46 mmol g⁻¹ h⁻¹, excellent AQY (11.7%) at 630 nm, and remarkable stability. It is worth noting that doping other types of metal ions in PMPDIs can also enhance the photocatalytic H2 production performance. The doping of Zr significantly improved the built-in electric field and the separation efficiency of photo-generated charges in PMPDIs. Additionally, it endowed PMPDIs with a high CB potential by regulating the band structure, thus enhancing its photocatalytic H₂ production performance.

In addition to metal doping, non-metallic element doping can also contribute to improving the photocatalytic $\rm H_2$ production of PDIs. Xu *et al.*¹⁰¹ successfully created three heteroatom-doped cyclic PDI photocatalysts (N-APDIs, S-APDIs, and Se-APDIs). The heteroatom-cyclized PDIs showed superior $\rm H_2$ evolution rates compared to PDIs under visible light. Among the three photocatalysts, N-APDIs had the highest $\rm H_2$ production rate (61.49 mmol g⁻¹ h⁻¹) with an AQY of 5.90% under 420 nm monochromatic light. The improved photocatalytic $\rm H_2$ production activity of N-APDIs can be attributed to the enhanced molecular dipole, which generates a strong built-in electric field, thus boosting the separation and migration of photo-generated charges. Furthermore, the doping of ring heteroatoms can serve as favorable active sites to promote hydrogen production activity.

Researchers widely acknowledge that increasing the number of active centers is a fundamental approach to improve the photocatalytic activity of H₂ production. 102 Therefore, constructing PDIs with rich morphological characteristics and active sites is a viable strategy to improve the H2 production efficiency. In particular, ultrathin nanosheets offer the advantage of exposing a large number of active sites, while shortening the distance for photo-generated charges to migrate to the surface of the photocatalyst and inhibiting bulk recombination.103 Zhu and co-workers104 proposed the concept of ultrathin PDI nanosheets with a thickness of about 0.8 nm. Due to the space effect and strong hydrogen bonding of phthalic acid, phthalic acid-substituted PDIs (PDIs-phthalic) mainly assembled on the hydrogen bond plane, thereby inhibiting π - π stacking self-assembly and resulting in ultrathin nanosheets. PDIs-phthalic showed a hydrogen production rate of 1.1 mmol h^{-1} g⁻¹ under visible light, which was 9.2-times and 4.8-times that of PDIs-isophthalic and PDIs-terephthalic, respectively. The excellent photocatalytic H₂ production of PDIs-phthalic is attributed to its ultrathin structure, which shortened the travel distance of photo-generated charges.

Despite its potential, the photocatalytic performance of PDIs is still hindered by the slow movement of photo-generated charges due to the high symmetry of its chemical structure. Thus, to address this issue, the construction of a built-in electric

Table 2 Summary of the photocatalytic activity of PDI-based photocatalysts toward H₂ evolution reaction

Photocatalyst	Co-catalyst	Light source	Light intensities	Measurement conditions	Rate of H_2 evolution (mmol $g^{-1} h^{-1}$)	Apparent quantum efficiency	Ref.
TATF-COF/PUP	3 wt% Pt	350 W Xe lamp ($\lambda > 420 \text{ nm}$)	Not available	5 mg photocatalyst; 100 mL 0.1 M ascorbic acid aqueous solution	94.5	19.7% at 420 nm	106
P-PMPDIs-Zr	3 wt% Pt	300 W Xe lamp ($\lambda > 400 \text{ nm}$)	$100~\mathrm{mW~cm}^{-2}$	50 mg photocatalyst, 50 mL aqueous solution (5 g ascorbic acid)	50.46	11.7% at 630 nm	100
P-PMPDIs	3 wt% Pt	300 W Xe lamp ($\lambda > 400 \text{ nm}$)	Not available	50 mg photocatalyst, 50 mL aqueous solution (5 g ascorbic acid)	11.7	2.96% at 550 nm	18
PDIs-phthalic	3 wt% Pt	300 W Xe lamp ($\lambda > 420 \text{ nm}$)	$23.0 \mathrm{\ mW\ cm}^{-2}$	25 mg photocatalyst, 200 mM ascorbic acid solution	1.1	Not available	104
$\mathrm{Zn_{0.7}Cd_{0.3}S/PDIs}$	Not available	Not available	Not available	10 mg photocatalyst, 100 mL aqueous solution (0.35 M Na ₂ S, 0.25 M Na ₂ SO ₃)	5.166	22% at 420 nm	107
ZIS/PDIsIM	Not available	300 W Xe lamp ($\lambda > 320 \text{ nm}$)	$0.6~\mathrm{W~cm}^{-2}$	10 mg photocatalyst, 100 mL aqueous solution (0.35 M Na ₂ S, 0.25 M Na ₂ SO ₃)	13.04	Not available	13
g - $C_3N_4/PDIs$	1 wt% Pt	300 W Xe lamp ($\lambda > 420 \text{ nm}$)	Not available	10 mg photocatalyst, 100 mL aqueous solution (0.2 M ascorbic acid)	1.6	Not available	62
g - $C_3N_4/Pt/PDIs$	Not available	400 W Xe lamp ($\lambda > 420 \text{ nm}$)	$20~\mathrm{mW~cm}^{-2}$	25 mg photocatalyst, 100 mL 10 vol% TEOA aqueous solution	0.015	0.31% at 420 nm	108
N-APDIs	7.7 wt% Pt	500 W Xe lamp ($\lambda > 420 \text{ nm}$)	Not available	20 mg photocatalyst, 50 mL aqueous solution (5 g ascorbic acid)	61.49	5.9% at 420 nm	101
$\mathrm{PDIs}/\mathrm{TiO}_2$	1 wt% Pt	300 W Xe lamp ($\lambda > 365 \text{ nm}$)	$100~\mathrm{mW~cm}^{-2}$	100 mg photocatalyst, 100 mL 20 vol% methanol aqueous solution	1.2	70.69% at 365 nm	34
TPPS/PDIs	Not available	300 W Xe lamp ($\lambda > 365 \text{ nm}$)	$550~\mathrm{mW~cm}^{-2}$	0.1 mg photocatalyst, 100 mL 10 vol% TEOA aqueous solution	30.36	2.53% at 400 nm	12
GQDs/PDIs	3 wt% Pt	500 W Xe lamp ($\lambda > 420 \text{ nm}$)	Not available	25 mg photocatalyst,100 mL 0.3 M ascorbic acid aqueous solution	1.6	0.5% at 420 nm	97
CN-P	3 wt% Pt	450 nm LED light source	Not available	5 mg photocatalyst, 100 mL 20 vol% TEOA aqueous solution	17.7	5.8% at 450 nm	109
PTA	4.6 wt% Pt	300 W Xe lamp ($\lambda > 420 \text{ nm}$)	$530~\mathrm{mW~cm}^{-2}$	7 mg photocatalyst, 0.2 M ascorbic acid solution	118.9	13.5% at 420 nm	105
$\mathrm{Zn_{0.5}Cd_{0.5}S/PDIs}$	Not available	Solar simulator (AM1.5)	$100~\mathrm{mW~cm}^{-2}$	50 mg photocatalyst, 80 mL aqueous solution (0.35 M Na ₂ S, 0.25 M Na ₂ SO ₃)	1.32	Not available	52
${ m TiO_2/PDIs}$	$5 \text{ mg H}_2\text{PtCl}_6 \cdot 6\text{H}_2\text{O}$	300 W Xe lamp	Not available	50 mg photocatalyst, 10 vol% TEOA aqueous solution	9.77	Not available	110

field in PDI-based photocatalysts has emerged as an effective strategy to drive the rapid separation of photo-generated charges and guide their migration towards the active sites, thus enhancing the solar energy conversion efficiency. For example, Zhu's group¹⁰⁵ developed single-molecule layer supramolecular perylene tetracarboxylic acid (PTA) nanosheets with a thickness of approximately 1.5 nanometers, serving as a photocatalyst for H₂ evolution (Fig. 16a-c). By optimizing the kinetics, thermodynamics, and surface reaction conditions, the obtained PTA nanosheets showed good photocatalytic H2 production activity, reaching an H2 production rate of 118.9 mmol h^{-1} g^{-1} and a quantum yield of 13.5% at 420 nm (Fig. 16d and e). The enhancement in the reduction potential and generation of a built-in electric field in the PTA nanosheets promoted the separation and migration of photo-generated charges, supporting their excellent H2 production activity (Fig. 16f and g). The photo-deposition experiment further

confirmed the orientation of IEF and its impact on the anisotropic separation of photo-generated carriers (Fig. 16h). Notably, the hydrogen production rate of the PTA photocatalyst is the highest among PDI-based photocatalysts. This work provides a valuable reference for future efforts in efficient molecular structure design engineering.

The construction of a PDI heterojunction offers a dual advantage by enhancing the separation efficiency of charges, while preserving the strong redox ability of the photocatalysts, thereby achieving efficient photocatalytic H₂ production. For instance, Zhu's group¹² constructed a TPPS/PDI heterojunction with porphyrin (TPPS) as the electron donor and PDIs as the electron acceptor. The heterojunction exhibited a surface potential of 70.16 mV, indicating the generation of a strong internal electric field. At the interface, the electric field from PDIs to TPPS promoted the transfer of photo-generated electrons from TPPS to PDIs, resulting in the significant separation

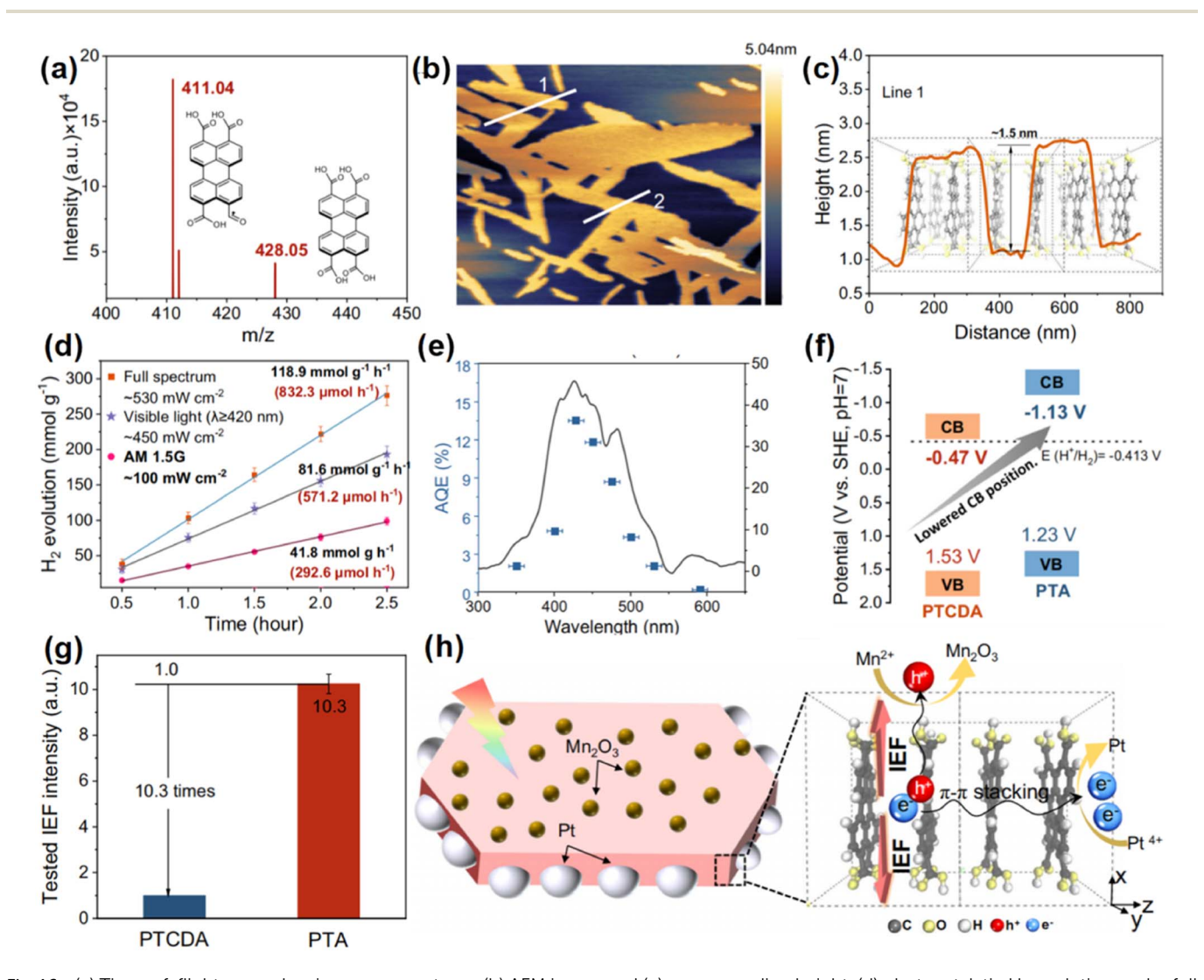


Fig. 16 (a) Time-of-flight secondary ion mass spectrum, (b) AFM image and (c) corresponding height, (d) photocatalytic H_2 evolution under full spectrum and (e) wavelength-dependent AQE for photocatalytic HER over PTA and the surface photovoltage of PTA. (f) Band structures of PTCDA and PTA measured experimentally. (g) Tested IEF intensity and (h) schematic illustration of Pt and Mn_2O_3 photo-deposition on PTA under visible light ($\lambda \ge 420$ nm). Reprinted with permission.¹⁰⁵ Copyright 2022, Nature.

of photo-generated carriers. This heterojunction reached an $\rm H_2$ production rate of 30.36 mmol h⁻¹ g⁻¹. This study offers valuable insights into the preparation of PDI-based heterojunctions with high photocatalytic hydrogen production ability. In another study, Li et al. 106 manufactured an S-scheme conjugated COF/perylene diimide urea polymer (PUP) all-organic heterojunction via the in situ coupling of a two-dimensional triazinebased imine-linked COF with PUP. The COF/PUP heterojunction exhibited an optimal photocatalytic H2 evolution rate (94.5 mmol h⁻¹ g⁻¹) and an exceptionally high AQY of up to 19.7% at 420 nm.

4.1.2 Photocatalytic O_2 production. The photocatalytic O_2 production reaction, involving a four-electron process, is considered the rate-determining step in overall water-splitting reactions due to its high energy barrier and slow kinetics.111 Typically, the addition of sacrificial agents is required in the water-splitting process to facilitate the reaction. These sacrificial agents react with the holes, replacing the four-electron process of water splitting to produce O2, while allowing the VB electrons of PDIs to participate in the reduction reaction. However, due to cost considerations, the reliance on sacrificial agents significantly limits the application of PDIs in water splitting to H₂. Therefore, the development of PDI photocatalysts with high O2 production ability is crucial for achieving H2 production through water splitting. Significant progress has been made in the development of PDI-based photocatalysts for photocatalytic O2 production. This section provides a brief summary of the latest advancements in PDI-based photocatalysts for O2 generation, which are also summarized in Table 3.

Compared to other all-organic photocatalysts, PDIs stand out due to their wide visible light absorption range and deep oxidation potential, making them highly promising materials for photocatalytic O2 production. Zhu's group demonstrated that pure, unmodified PDIs nanoassemblies could serve as photocatalysts for O₂ production under visible light, opening new possibilities for the development of PDIs in photocatalytic O_2 production. However, the photocatalytic O_2 evolution activity of these PDI nanoassemblies remains low (only 2.6 μmol h⁻¹ g^{-1}) due to the easy recombination of photo-generated charges. Thus, to enhance the photocatalytic O₂ production activity of PDIs, Zhu's group²⁶ further prepared one-dimensional supramolecular organic nanofibers composed of carboxyl-substituted PDI molecules through H-type π - π stacking and hydrogen bonding self-assembly. These nanofibers achieved effective photocatalytic O2 production without the need for metal cocatalysts. The π - π stacking structure significantly decreased the bandgap of PDIs, resulting in lower VB and CB energy levels. The deeper VB position represents the stronger oxidizing ability of the holes in the photocatalytic reaction. Compared to pure PDIs, the O₂ evolution rate of PDI nanofibers is about 19.8-times higher. This improvement can be attributed to the introduction of terminal carboxyl groups, which enhances the internal electric field in the supramolecular nanofibers and deepens the VB, thereby improving the efficiency of photoinduced carrier migration and separation. These findings further advance the development of PDIs in photocatalytic O2 production. Clearly, the built-in electric field plays a crucial role in achieving high

efficiency in carrier extraction, separation, and migration, as well as high O2 activity. Numerous studies have focused on enhancing the built-in electric field to achieve the efficient photocatalytic O2 production of PDIs. For example, Zhu's group²⁴ constructed a highly crystalline photocatalyst (urea-PDIs). The original PDI molecule possesses a small dipole moment due to its symmetrical structure. However, the introduction of the negative carbonyl increases the dipole moment. The high crystallinity and large molecular dipoles contribute to the establishment of an internal electric field, resulting in improved charge separation and transport efficiency of urea-PDIs (Fig. 17a-d). With the strongest built-in electric field, urea-PDIs exhibited the highest O₂ evolution rate (3223.9 μmol $g^{-1} h^{-1}$) under visible light without a co-catalyst (Fig. 17e). In another study, Liu et al. 112 prepared linear conjugated polymer oxamide-PDI photocatalysts through precise structural design and molecular packing control. The high crystallinity and large internal dipole moment of oxamide-PDIs generated a large built-in electric field, enabling efficient carrier migration and separation. Consequently, oxamide-PDIs achieved a fullspectrum O₂ evolution rate of 5110.25 μmol g⁻¹ h⁻¹ and could operate continuously for more than 30 h, with a cumulative O_2 production of 111.7 mmol g^{-1} .

Heterojunctions offer an important approach to constructing a powerful internal electric field, enabling efficient photocatalytic O2 production by spatially isolating redox sites. For instance, Zhang et al.56 created a CdS/PDI Z-scheme heterojunction, where the Fermi level of CdS is higher than that of PDIs, leading to electron transfer from CdS to PDIs. This results in the formation of abundant holes on the surface of CdS and a large number of electrons on the surface of PDIs, establishing a strong internal electric field from CdS to PDIs. This internal electric field results in band bending and additional potential energy for photogenerated electrons in the space charge region. The photo-generated electrons of PDIs are excited from the VB to CB, and then recombine with the holes in the VB of CdS, which is facilitated through the internal electric field. This leads to the separation of electrons and holes in the VB of PDIs from the CB of CdS. The construction of this Z-type heterojunction effectively improves the transport efficiency of photo-generated carriers, while retaining the strong redox ability of both semiconductors. The average O2 production activity of 15% CdS/ PDIs was measured to be 1392.29 μ mol g⁻¹ h⁻¹. Another approach to promote the photocatalytic O2 production performance of PDIs by constructing a strong built-in electric field was demonstrated by Yang and co-workers.58 They designed a p-Ag₂S/n-PDI heterojunction with a photocatalytic O₂ production rate of about 34.6256 µmol g⁻¹ h⁻¹ under full-spectrum irradiation. The excellent photocatalytic O2 production of p-Ag2S/n-PDIs is attributed to the enhanced light absorption, strong oxidation ability, and excellent carrier separation caused by the built-in electric field between Ag₂S and PDIs.

The remarkable aspect of the research discussed above is that it was conducted without using O₂ production co-catalysts. However, the introduction of co-catalysts has become an attractive strategy due to their ability to extract and capture photo-generated charges, provide additional redox active sites,

Published on 05 January 2024. Downloaded by Technische Universitat Chemnitz on 1/27/2024 1:17:51 PM.

 Table 3
 Summary of the photocatalytic activity of PDI-based photocatalysts toward O2 evolution reaction

Photocatalyst	Co-catalyst	Light source	Light intensities	Measurement conditions	Rate of O_2 evolution (μ mol $g^{-1} h^{-1}$)	Apparent quantum efficiency	Ref.
Urea-PDIs	None	300 W Xe lamp ($\lambda > 420 \text{ nm}$)	$383~\mathrm{mW~cm}^{-2}$	25 mg photocatalyst; 0.1 g La_2O_3 ; 100 mL of 0.05 M AoMO_2 acmedis solution	3223.9	3.86% at 450 nm	24
$Co-PDIs/Fe(OH)_3$	None	300 W Xe lamp ($\lambda > 420 \text{ nm}$)	$1.5~\mathrm{mW~cm}^{-2}$	1 mg photocatalyst, 100 mL of 3 mM	27 000	1.16% at 500 nm	88
PDIs-NH	None	300 W Xe lamp ($\lambda > 420 \text{ nm}$)	$385~\mathrm{mW~cm}^{-2}$	re(tNO ₃)3 aqueous solution 15 mg photocatalyst; 0.1 g La ₂ O ₃ ; 20 mM AoNO, aqueous solution	40 600	2.96% at 550 nm	22
Co-PDIs	None	300 W Xe lamp ($\lambda > 420 \text{ nm}$)	$1.5~\mathrm{mW~cm}^{-2}$	1 mg photocatalyst; 100 mL of 3 mM	5530	Not available	89
Co-UPDIs	None	300 W Xe lamp ($\lambda > 420 \text{ nm}$)	Not available	10 mg photocatalyst, 100 mL of 5.0 mM	580	4.39% at 450 nm	06
Fe(OH) ₃ @Ni-PDIs NHs	None	300 W Xe lamp ($\lambda > 420 \text{ nm}$)	Not available	1 mg photocatalyst; 100 mL of 3.0 mM Fe(NO.). aqueous solution	22 000	Not available	114
CdS/PDIs	None	300 W Xe lamp ($\lambda > 420 \text{ nm}$)	Not available	50 mg photocatalyst; 0.1 g La ₂ O ₃ ; 100 mL	1392.29	Not available	26
$ m p ext{-}Ag_2S/n ext{-}PDIs$	None	500 W Xe lamp	Not available	50 mg photocatalyst, 100 mL of 0.01 M	34.62	Not available	26
Bu-PDIs	None	300 W Xe lamp ($\lambda > 420 \text{ nm}$)	Not available	Agno ₃ aqueous solution 20 mg photocatalyst, 100 mg La ₂ O ₃ , 100 mg AgNO 75 mL of deignized unter	2345	2.77% at 420 nm	115
Oxamide-PDIs	None	300 W Xe lamp ($\lambda > 300 \text{ nm}$)	$783~\mathrm{mW~cm}^{-2}$	25 mg photocatalyst; 0.1 g La ₂ O ₃ ; 100 mL of 0.01 M AnnO amenous solution	5110	2.77% at 420 nm	116
PDIs	None	300 W Xe lamp ($\lambda > 300 \text{ nm}$)	Not available	25 mg photocatalyst; 0.1 g La ₂ O ₃ ; 100 mL	2524.88	2.77% at 420 nm	17
PDIs/Co ₃ O ₄ /Pt	None	300 W Xe lamp (\(\lambda > 300 \text{ nm} \)	$438~\mathrm{mW~cm}^{-2}$	of 0.01 M AgNO ₃ adjuctors solution 15 mg photocatalyst, 100 mL of 20 mM AgNO ₃ solution	24 400	6.9% at 420 nm	117

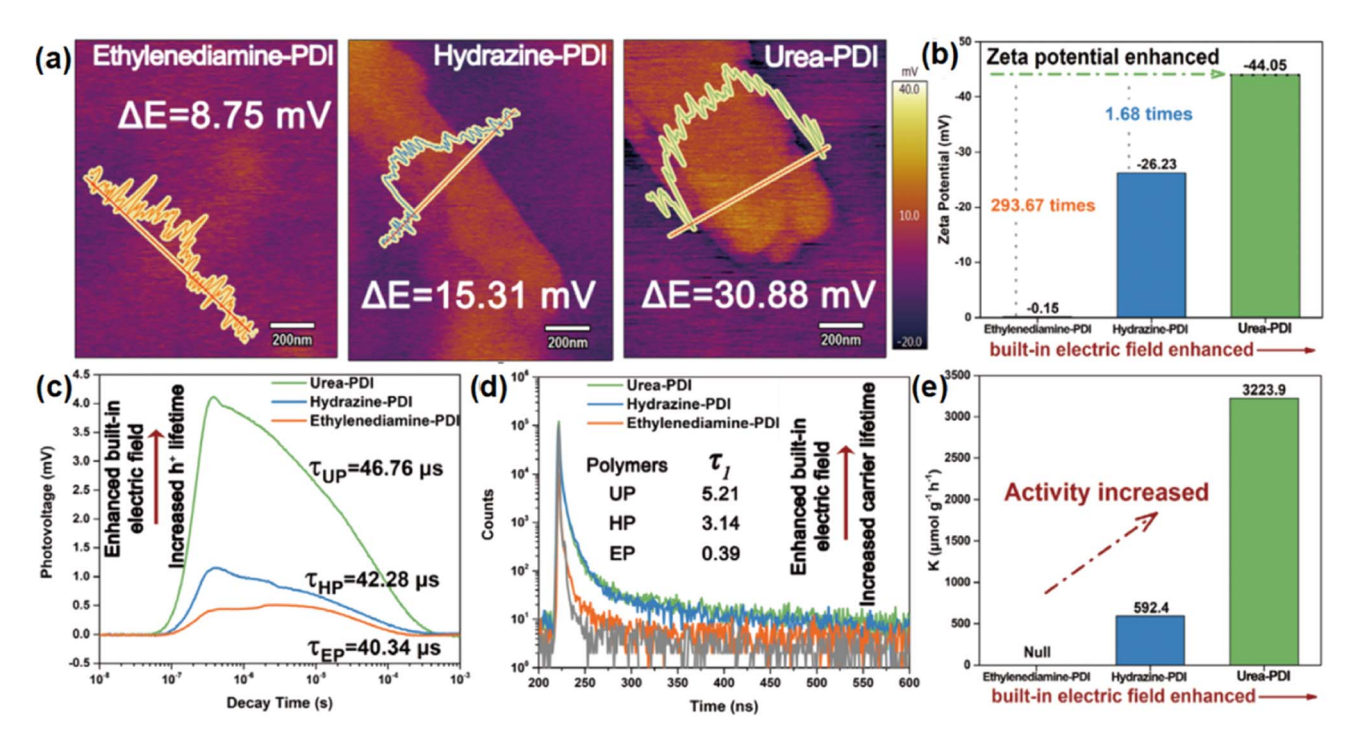


Fig. 17 (a) Surface potential of different polymers detected with KPFM. (b) Zeta potential of different polymers. (c) Lifetime of photo-generated holes detected by transient SPV. (d) Transient fluorescence spectrum of the polymers. (e) Increased photocatalytic oxygen evolution with enhanced built-in electric field. Reprinted with permission.²² Copyright 2022, Wiley

and lower the reaction potential and activation energy of surface O₂ precipitation. ¹¹³ Consequently, significant efforts have been devoted to developing efficient semiconductor/co-catalyst composite materials, including PDIs, to enhance their performance for photocatalytic O2 production. For example, Shen and co-workers91 developed Co and CoOx cluster co-catalystmodified PDIs (Co-PDIs) via an impregnation-calcination method. The O2 evolution rate of Co-PDIs under visible light reached 5.53 mmol $h^{-1} g^{-1}$, which was about three-times higher than that of PDIs. The Co atom established a charge transport channel between the PDIs layers, while the CoOx cluster acted as a hole collector, accumulating a large number of holes on the surface of PDIs. The synergistic effect between them accelerated the charge transfer process in Co-PDIs, thereby enhancing the photocatalytic oxidation ability for water. In the O2 evolution reaction on the photocatalyst surface, many efficient non-noble metal hydroxides (M = Fe, Co, Ni, etc.) have been developed. However, currently, there are few reports on combining cocatalysts with the crystal engineering design of PDIs to construct simple, low-cost and efficient photocatalytic systems for water oxidation. Addressing this gap, Zhong et al.89 synthesized one-dimensional nanocrystals (NCs) of Co-PDI polymer. These NCs showed high photocatalytic O2 evolution activity, reaching an optimal value of 27 000 μmol g⁻¹ h⁻¹ under visible light using Fe (NO₃)₃ as the electron acceptor. The excellent photocatalytic O2 production activity of NCs is attributed to the synergistic effect between one-dimensional nanocrystals and in situ-generated α-FeOOH, resulting in wide light absorption, fast charge separation, and reduced charge recombination. Zhu's group²² also prepared a Co(OH)₂-loaded crystalline PDI

photocatalyst, which displayed a strong built-in electric field induced by its high crystallinity, thereby greatly accelerating the separation and transfer of photogenerated charges. In the absence of a co-catalyst, PDIs exhibited an excellent photocatalytic O_2 production rate of up to 14.2 mmol $g^{-1} h^{-1}$. Alternatively, when Co(OH)2 was loaded on PDIs as a co-catalyst using the impregnation method, PDIs demonstrated a breakthrough in photocatalytic O2 production from water under visible light, with an oxygen evolution rate of 40.6 mmol g⁻¹ h⁻¹ and apparent quantum efficiency of 10.4% at 400 nm. Notably, the O2 production rate of this PDI photocatalyst is currently the highest among PDI-based photocatalysts. This work emphasizes not only the significant enhancement in the photocatalytic activity of PDIs through the construction of an internal electric field but also highlights the importance of designing appropriate co-catalysts for improving the O2 production performance of PDIs.

4.1.3 Photocatalytic overall water splitting. Thus far, there is limited research focused on the photocatalytic overall water splitting using PDI-based photocatalysts. Most studies have primarily investigated either the H2 evolution half-reaction or the O₂ evolution half-reaction, often requiring the addition of sacrificial agents during the process. However, obtaining H2 in this way is inefficient and economically unfavorable due to the high consumption of these agents. Therefore, the development of sacrificial agent-free photocatalysts for overall water splitting is of great significance.

Artificial Z-scheme photocatalysts, inspired by natural photosynthesis processes, offer significant potential for achieving highly efficient photocatalytic overall water splitting. 120

By combining the highly-efficient photocatalytic O2 evolution performance of 1D Co-PDIs/Fe³⁺ and the highly-efficient photocatalytic H2 evolution performance of Ru/SrTiO3:Rh, a traditional Z-scheme photocatalyst system was constructed. In this system, Ru/SrTiO₃:Rh acts as the photocatalyst for H₂ evolution, while 1D Co-PDIs/Fe³⁺ serves as the photocatalyst for O₂ evolution in the presence of 1.0 mM Fe³⁺/1.0 mM Fe²⁺ as a redox mediator (Fig. 18a).89 Under visible light, the simultaneous evolution of H₂ $(\sim 4.0 \text{ }\mu\text{mol } \text{h}^{-1})$ and O_2 $(\sim 2.0 \text{ }\mu\text{mol } \text{h}^{-1})$ with a stoichiometric ratio 2:1 was realized. However, this traditional Z-scheme photocatalyst has some drawbacks. For instance, photo-generated electrons and holes with strong redox ability are susceptible to consumption by shuttle redox ion pairs. The application of traditional Z-scheme photocatalysts is also limited by factors such as the light shielding effect, feasibility limitation of solution systems, and pH sensitivity of solutions. Furthermore, most redox media are prone to inactivation, resulting in a decrease in the reaction rate over time.

Compared to traditional Z-scheme photocatalysts, all solid-state Z-scheme photocatalysts offer several advantages. They eliminate the need for redox ion pairs, instead relying on excellent electron mediators, such as noble metals and other conductive materials (Fig. 18b). Generally, all solid-state Z-scheme photocatalysts are considered superior because they prevent the consumption of strong redox electron and hole pairs, enabling the better recovery of photocatalysts. Moreover, they significantly enhance the carrier transfer through the influence of electron mediators. For example, Zhu's group⁷⁴ successfully constructed an all-solid-state Z-scheme g-C₃N₄/rGO/PDI Z-type heterojunction for overall water splitting. This heterojunction has a large internal electric field and low resistance, facilitating

efficient charge separation and transport. During the reaction, the photo-generated electrons in the CB of PDIs transfer to the VB of g-C₃N₄ through the rGO interlayer, while the holes follow the opposite path. This arrangement preserves the strong redox ability of both semiconductors, enabling complete water splitting to generate H₂ and O₂. The H₂ and O₂ release rates reached 15.80 and 7.80 μ mol g⁻¹ h⁻¹, respectively, without the need for a sacrificial agent (Fig. 19). These rates surpass that of many reported g-C₃N₄-based photocatalysts. However, the construction process of all solid-state Z-scheme photocatalysts is complex, and the electron transfer media may introduce challenges such as shielding effects and high costs.

Compared to traditional Z-scheme and all-solid-state Zscheme heterojunction systems, direct Z-scheme photocatalysts offer several advantages given that they operate without the need for redox and charge carrier media, leading to inhibited reverse reactions and significantly reduced shielding effects (Fig. 18c). In addition, direct Z-scheme photocatalysts exhibit good corrosion resistance. For instance, Liu and coworkers¹²¹ reported the preparation of a direct Z-scheme PDI/ Zn_{0.8}Cd_{0.2}S heterojunction for photocatalytic overall water splitting. This heterojunction exhibited an H2 evolution rate of 71.98 μ mol g⁻¹ h⁻¹ and O₂ evolution rate of 32.44 μ mol g⁻¹ h⁻¹, with a stoichiometric ratio close to 2:1 for H2 and O2. Additionally, the heterojunction displayed excellent cycle stability. The construction of the PDIs/Zn_{0.8}Cd_{0.2}S heterojunction resulted in efficient charge separation and strong redox ability, resulting in significantly enhanced photocatalytic activity for overall water splitting.

The emerging S-scheme heterojunction, which consists of reducing and oxidizing photocatalysts, has gained significant

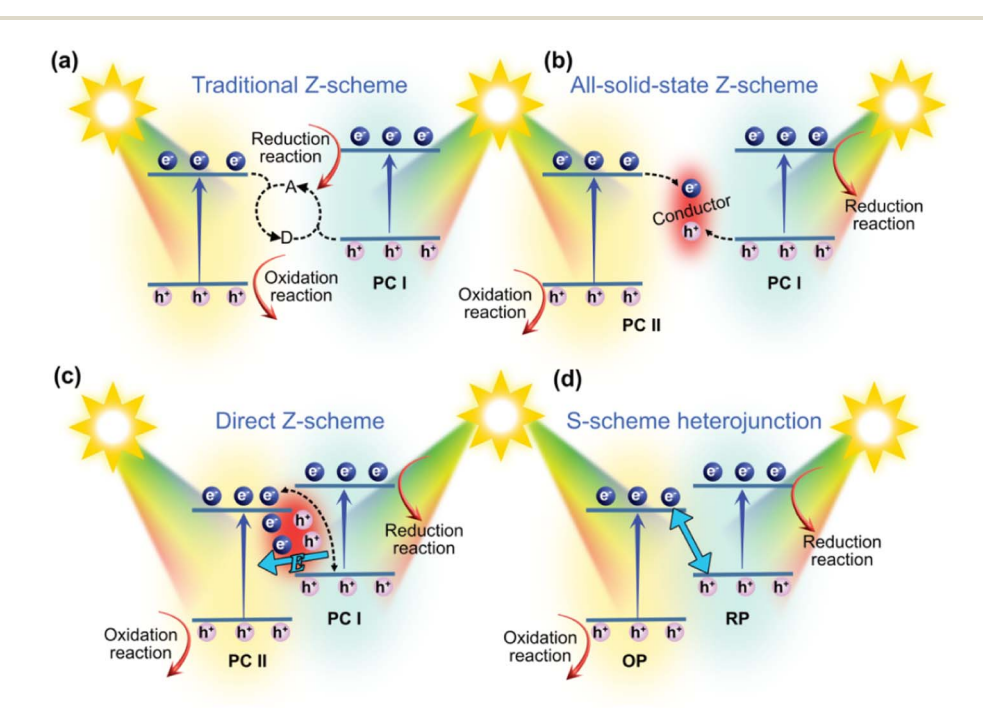


Fig. 18 (a) Schematic illustration of charge carrier transfer in traditional Z-scheme heterojunction, (b) all-solid-state Z-scheme heterojunction, (c) direct Z-scheme heterojunction, and (d) S-scheme heterojunction.

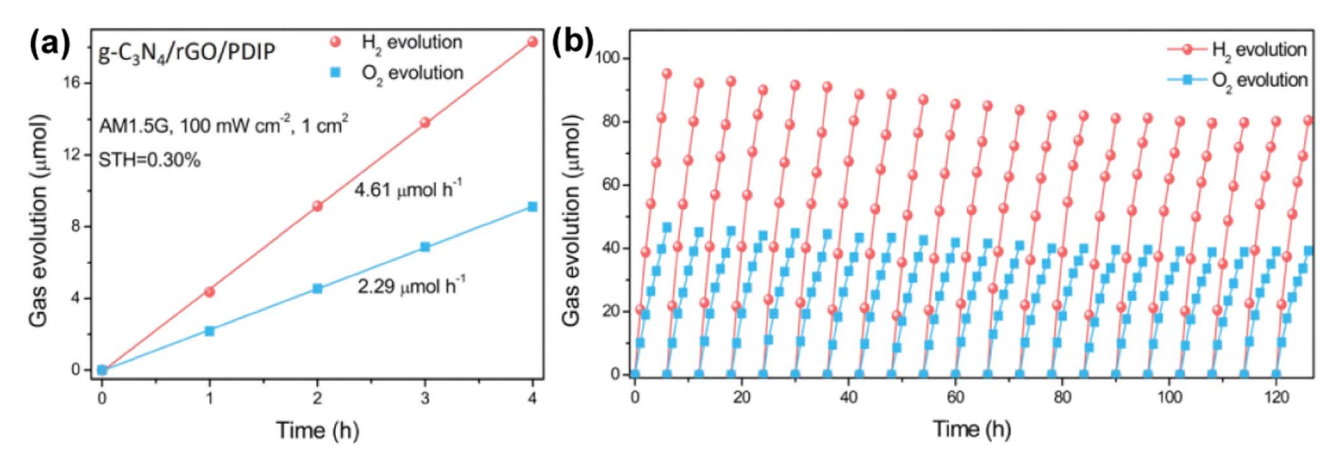


Fig. 19 (a) Photocatalytic overall water splitting and (b) repeated cycles under AM 1.5 G simulated sunlight of g-C₃N₄/rGO/PDIs. Reprinted with permission.74 Copyright 2021, Wiley

attention in photocatalytic overall water splitting due to its seemingly more suitable charge transfer mechanism (Fig. 18d). A notable example of photocatalytic overall water splitting is the TiO₂/PDI S-scheme heterojunction synthesized by Fang et al. 110 through a simple solvent compounding method. The PDI-TiO₂ heterojunction exhibited an H₂ evolution rate of 238 μmol g⁻¹ h^{-1} and O_2 evolution rate of 114.18 μ mol g^{-1} h^{-1} , with a stoichiometric ratio close to 2:1 for H2 and O2. The excellent photocatalytic performance of TiO2/PDIs can be attributed to the S-scheme charge transfer mechanism, which effectively suppresses the recombination of photo-generated charges and maximizes the absorption in the full solar spectrum, thereby greatly improving the H₂ evolution activity.

The above-mentioned studies on overall water splitting were realized in the presence of co-catalysts, which reflects that cocatalysts play an important role in the reaction of overall water splitting. In this case, although cocatalysts themselves usually do not have light absorption properties, coupling them with semiconductor materials can significantly improve their photocatalytic activity. The main functions of cocatalysts are as follows: (1) inhibiting the occurrence of reverse reactions, (2) inhibiting photo-corrosion and improving the stability of photocatalysts, (3) reducing the activation energy or overpotential of H2 and O2 generation reactions on semiconductor surfaces and providing reactive sites and (4) improving the separation efficiency of photogenerated electrons and holes at the interface of the main photocatalyst. Therefore, the reasonable design and construction of oxidation and reduction cocatalysts on the surface of the catalyst are very important for promoting the development of PDI-based photocatalysts for overall water splitting.

Applications in the degradation of pollutants

Photocatalysis technology has emerged as a crucial, economical, and effective approach to tackle environmental pollution issues. Leveraging the advantages of PDIs as photocatalysts, PDIs-based photocatalysts have been widely reported to effectively remove a variety of organic pollutants, including phenols, pesticides, and antibiotics. When a PDI-based heterojunction is

excited under illumination, the photo-generated electrons on the CB can reduce the dissolved O2 attached to the surface of the material to generate strong oxidizing free radicals of 'O2 and ¹O₂. Meanwhile, the photo-generated holes on the VB migrate to the surface of the material, resulting in the formation of strong oxidizing free radicals of 'OH and h⁺. These active free radicals engage in oxidation reactions with organic pollutants, leading to their degradation into non-toxic inorganic substances and low-toxic small molecules.

For instance, Miao et al.11 used the electrostatic adsorption method to synthesize a PDI@AuNP visible-light photocatalyst. The excitation of plasmon resonances resulted in energy transfer from AuNPs to PDIs, promoting the carrier separation and enhancing photocatalytic efficiency. Compared to PDI nanowires, the degradation rate of phenol by PDIs@AuNPs increased by 1.72 times. In another study, Chen et al. 122 investigated the degradation capability of PDI nanofibers using ofloxacin as a model pollutant and compared their photocatalytic activity under different water qualities. The results showed degradation rate constants of 0.334 \pm 0.195, 0.250 \pm $0.018,\,0.208\pm0.014$ and $0.224\pm0.009~{
m min}^{-1}$, for ofloxacin in ultrapure water, tap water, Pearl River water, and wastewater, respectively. Although the degradation performance slightly decreased in tap water, Pearl River water, and wastewater, the effective degradation of ofloxacin was still achieved, highlighting the applicability of PDI nanofibers in real environmental conditions.

Furthermore, Zhang et al.42 prepared PDI nanofibers and constructed a heterojunction with Bi₂WO₆ to evaluate the degradation performance of Bi₂WO₆/PDIs for phenol. The photocatalytic degradation process generated a large amount of superoxide radicals for the degradation of phenol. The apparent rate constant of Bi₂WO₆/PDIs was 7.65-times higher than that of Bi₂WO₆ alone and 1.75-times higher than that of self-assembled PDIs, demonstrating the significantly enhanced photocatalytic activity of the Bi₂WO₆/PDI heterojunction. In the study by Liu and co-workers,64 PDI/mpg-C3N4 composites were synthesized and employed for the degradation of bisphenol A (BPA). Among the tested samples, 20% PDIs/mpg-C₃N₄ had the highest visible

light catalytic activity, achieving a degradation efficiency of 90%. The degradation rate of BPA by 20% PDIs/mpg- C_3N_4 was 7.3-times and 3.4-times higher than that of mpg- C_3N_4 and self-assembled PDIs, respectively.

However, although the above-mentioned studies meaning-fully improved the degradation rate of PDI-based photocatalysts for pollutants, relatively few studies have been conducted on their mineralization rate. If the complete mineralization of organic pollutants into inorganic substances can be achieved, their toxicity will be completely eliminated. For example, the hp-PDI-NA photocatalyst reported by Zhu *et al.* ¹⁹ degraded 100% of phenol within 6 h, but its mineralization rate was only 16%. Zhu *et al.* ²⁶ also reported that the degradation rate of phenol by nano-PDI reached 60% within 12 h, but its mineralization rate was only 20%. Obviously, it is still very challenging to achieve a high mineralization rate of PDI-based photocatalysts for the degradation of pollutants.

Significant advancements have been achieved in the degradation of organic pollutants using PDI-based heterojunctions. To highlight and compare their performance for degrading various pollutants, in this section, we summarize the latest significant progress in the photocatalytic degradation of organic contaminants by PDI-based heterojunctions, as presented in Table 4. However, the low efficiency of photo-generated carrier migration and the rapid recombination of electron–hole pairs remain challenges that impede the widespread application of PDI-based photocatalysts in pollutant degradation.

The combination of photocatalysis and the persulfate (PS) advanced oxidation process is considered one of the most efficient, low energy consumption, and environmentally friendly methods for activating PS and removing persistent organic pollutants.123 This coupling effect between photocatalysts and PS serves multiple purposes, i.e., it inhibits the recombination of photo-generated carriers, accelerates their separation, and generates multiple active free radicals (including SO_4 , 1O_2 , O2'-, h⁺, and 'OH⁻) to achieve the oxidative degradation and mineralization of organic pollutants. However, photocatalysts still face certain limitations in the photocatalysis-coupled PS systems, including low solar energy utilization efficiency, easy recombination of photo-generated carriers, low matching between energy band structure and PS activation energy, limited exposure of active sites, and insufficient stability. These shortcomings contribute to the weak coupling effect between PS and the photocatalyst, consequently hampering the wider application of photocatalysis coupled with the advanced oxidation process of PS in the treatment of pollutants.

PDI-based heterojunction photocatalysts possess various advantages including affordability, rich chemical composition, broad light absorption range, precise molecular structure design, controllable energy band structure, high carrier mobility, and strong electron affinity. These properties make PDI-based heterojunctions highly promising for the photocatalytic activation and degradation of organic pollutants coupled with PS.

For instance, in the study conducted by Yang and coworkers, ¹²⁴ a novel PDI/PS/Vis system was constructed and evaluated for its photocatalytic performance using bisphenol A as the target pollutant. As shown in Fig. 20a, the minimal

Table 4 Summary of the	he photocatalytic activi	Table 4 Summary of the photocatalytic activity of PDI-based photocatalysts toward phenol degradation	d phenol degradation				
Photocatalyst	The amount of catalyst	Light source	Light intensity	Targeted pollutant	The amount of targeted pollutant	Degradation rate constant k	Ref.
Bi, WO ₆ /PDIs	25 mg	500 W Xe lamp ($\lambda > 420 \text{ nm}$)	28 mW cm^{-2}	Phenol	50 mL, 5 mg ⁻¹	$0.357 \ h^{-1}$	42
Bi ₅ O ₇ I-OVs/PDIs	25 mg	300 W Xe lamp $(\lambda > 420 \text{ nm})$	Not available	Phenol	$25 \text{ mL}, 7 \text{ mg L}^{-1}$	$0.593 \ \mathrm{h^{-1}}$	126
PDIs/BiOCl	20 mg	300 W Xe lamp $(\lambda > 420 \text{ nm})$	Not available	Phenol	$20 \text{ mL}, 5 \text{ mg}^{-1}$	0.013 min^{-1}	28
BiOCl/PDIs	25 mg	300 W Xe lamp $(\lambda > 420 \text{ nm})$	69.7 mW cm^{-2}	Phenol	$50 \text{ mL}, 5 \text{ mg}^{-1}$	$0.22 \; \mathrm{h}^{-1}$	47
Pt QDs/PDIs	25 mg	500 W Xe lamp $(\lambda > 420 \text{ nm})$	Not available	Phenol	$50 \text{ mL}, 5 \text{ mg}^{-1}$	0.015 min^{-1}	87
PTCDI/P25	25 mg	300 W Xe lamp $(\lambda > 420 \text{ nm})$	Not available	Phenol	$50 \text{ mL}, 5 \text{ mg L}^{-1}$	$0.08 \; \mathrm{h^{-1}}$	37
${ m TiO_2/PDIH}$	25 mg	300 W Xe lamp $(\lambda > 420 \text{ nm})$	Not available	Phenol	$50 \text{ mL}, 5 \text{ mg L}^{-1}$	$0.09 \; \mathrm{h^{-1}}$	38
$p-Ag_2S/n-PDIs$	25 mg	500 W Xe lamp $(\lambda > 420 \text{ nm})$	Not available	Phenol	$50 \text{ mL}, 5 \text{ mg L}^{-1}$	1.55 min^{-1}	28
PTCDI-C60	25 mg	300 W Xe lamp ($\lambda > 420 \text{ nm}$)	35 mW cm^{-2}	Phenol	$50 \text{ mL}, 5 \text{ mg L}^{-1}$	$0.216~{ m h}^{-1}$	127
PDIs/rGO	Not available	300 W Xe lamp $(\lambda > 300 \text{ nm})$	$35 \mathrm{\ mW \ cm^{-2}}$	Phenol	Dynamic system	$0.66 \; \mathrm{h^{-1}}$	127
GQDs/PDIs	25 mg	300 W Xe lamp $(\lambda > 420 \text{ nm})$	Not available	Phenol	$50 \text{ mL}, 5 \text{ mg L}^{-1}$	$0.018~{ m h}^{-1}$	26
${ m TiO_2}$ @CI-PDIs-BSA	50 mg	300 W Xe lamp ($\lambda > 420 \text{ nm}$)	Not available	Phenol	$50 \mathrm{\ mL}, 10 \mathrm{\ mg \ L}^{-1}$	$0.3068~{ m min}^{-1}$	14
hp-PDIs-NA	25 mg	300 W Xe lamp ($\lambda > 420 \text{ nm}$)	Not available	Phenol	$50 \text{ mL}, 10 \text{ mg L}^{-1}$	$0.51 \; h^{-1}$	19

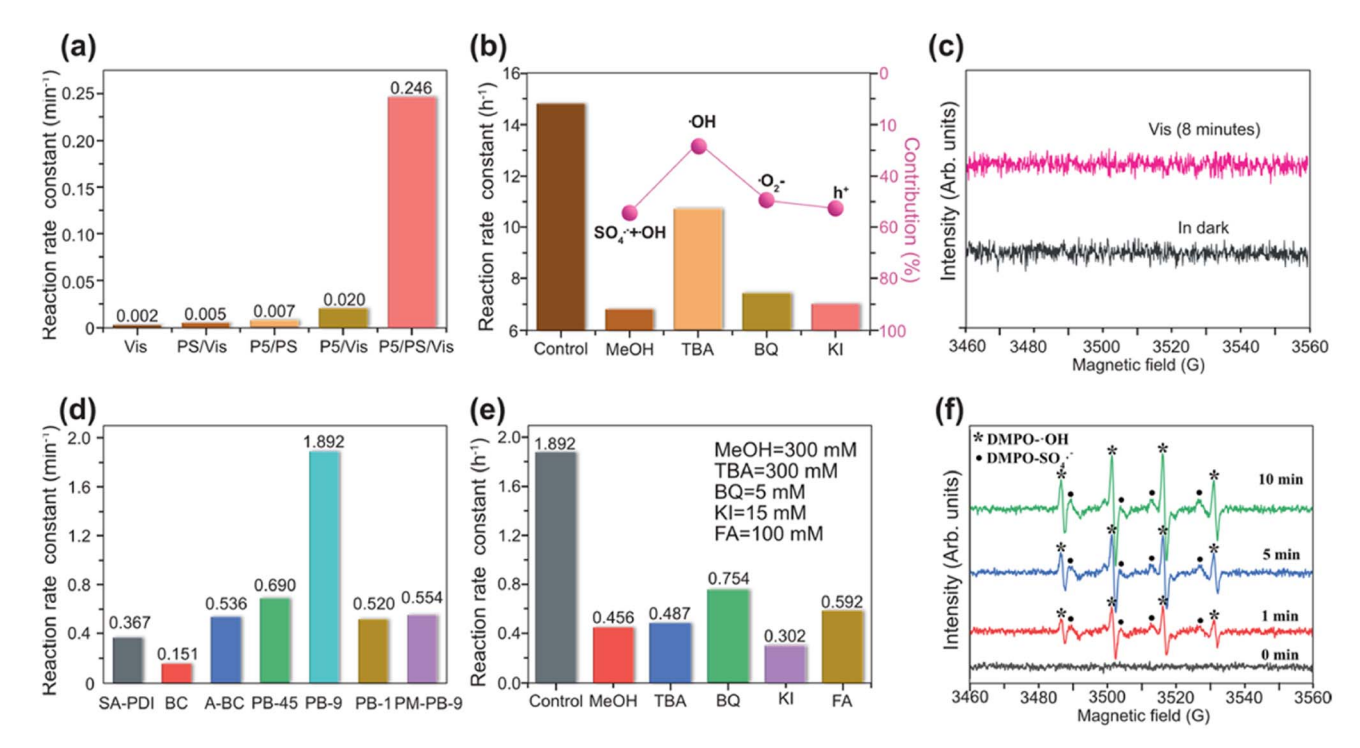


Fig. 20 (a) Reaction rate constant for the degradation of photocatalytic bisphenol A. (b) Reaction rate constants for the degradation of bisphenol A with different sacrificial agents. (c) EPR signal spectra. Reprinted with permission. 125 Copyright 2021, Elsevier. (d) Reaction rate constant of photocatalytic IOH degradation. (e) Reaction rate constants of IOH degradation with different sacrificial agents. (f) EPR signal spectra. Reprinted with permission. 126 Copyright 2021, Elsevier.

degradation of bisphenol A was observed under visible light or PS/visible light alone. However, both PS and PDIs (P5) individually achieved approximately 28.8% BPA degradation within 15 min. P5 under visible light irradiation achieved 50% bisphenol A degradation. Nevertheless, the degradation rate was still too slow, possibly due to the low concentration of free radicals due to electron and hole recombination. After adding PS, bisphenol A was completely degraded within 15 min in the PDI/PS/Vis system. Notably, the reaction rate constants of the PDI/PS/Vis system were 123, 49.2, 35.1- and 12.3-times higher than that of the Vis system, PS/Vis system, PDI/PS system, and PDI/Vis system, respectively. These results show that the photocatalytic coupling with the PS system significantly improves the photodegradation efficiency.

To understand the intermediate products and their toxicity during pollutant degradation, high-performance liquid chromatography-mass spectrometry and DFT calculations were employed. These analyses revealed the generation of 12 types of intermediate products during the degradation process. Additionally, the toxicity of each intermediate was predicted using the ecological structure-activity relationship (ECOSAR) program. The findings indicated that BPA has high biological toxicity, while the intermediate products from the degradation of bisphenol A in the PDI/PS/Vis system initially increased, and subsequently decreased, ultimately generating non-toxic ringopening products. These insights are crucial for assessing the environmental impact of the pollutant degradation process.

However, the removal rate of pollutants by the PDI/PS/Vis system still remained relatively low, which is mainly due to the predominant role of superoxide radicals ('O2-) rather than hydroxyl radicals ('OH) in the degradation process (Fig. 20b and c). The 'OH species is more effective in degrading persistent organic pollutants due to its high oxidation potential (\sim 2.8 V). Thus, to improve the efficiency of PDI/PS/Vis systems, a new approach involves constructing PDI-based materials capable of generating 'OH more easily. In this regard, Yang et al. 125 developed a novel binary photocatalyst consisting of biochar loaded with PDIs (PDIs/BC). As shown in Fig. 20d, both BC and PDIs individually exhibit good degradation activity towards iohexol. However, when BC and PDIs were combined, their degradation activity was significantly enhanced. Through free radical capture experiments, it was evident that the active free radicals involved in IOH degradation are h⁺, 'OH, ¹O₂, 'O₂⁻ and SO₄, with 'OH playing a primary role in the IOH degradation process (Fig. 20e and f). The enhanced performance of BC/PDIs for the degradation of iohexol can be attributed not only to the introduction of BC, which enhances the utilization efficiency of photo-generated carriers, but also because it changes the free radical generation pathway, resulting in increased 'OH production.

Although PDI-based photocatalysts have primarily been applied to liquid-phase pollutants, there are still limited reports on the degradation of gas-phase pollutants, which warrants further exploration.

4.3 Applications in other photocatalytic reactions

4.3.1 Photocatalytic N_2 fixation. Ammonia (NH₃) is an essential compound widely used in various fields such as agriculture, industry, and pharmaceuticals, serving as a vital green energy carrier and basic chemical. At present, the industrial synthesis of NH₃ relies on the energy-intensive Haber Bosch reaction, which generates significant CO2 emissions. Therefore, it is urgent to develop a low-energy, cost-effective, and environmentally friendly process to continuously convert atmospheric nitrogen (N2) into NH3. In this case, photocatalytic N2 fixation, often regarded as the "holy grail" reaction, 128 offers a promising solution due to its economic viability, sustainability, safety, and simple operation, emerging as the most attractive technology for the synthesis of NH3. However, N2 molecules have extremely strong nonpolar N≡N triple bonds, presenting a significant challenge for efficient photocatalytic N2 fixation. Furthermore, current photocatalysts still suffer from slow charge transfer, resulting in unsatisfactory activity for N2 fixation. Therefore, the development of highly efficient photocatalysts for N2 fixation is crucial.

PDIs, which are known for their good chemical stability, simple preparation, high abundance, and low cost, hold great potential for photocatalytic N_2 fixation. It is in the study conducted by Yang and coworkers, In the study conducted by Yang and coworkers, In the designed a novel BOPDI photocatalytic N_2 fixation process. They designed a novel BOPDI photocatalyst, which incorporated polar bridged electron donor-acceptor units (D-A). The introduction of the D-A structure in BOPDIs led to an asymmetrical spatial configuration, effectively increasing the molecular dipole moment and enhancing the internal electric field. The strong internal electric field improved the separation and transfer efficiency of photogenerated carriers, thereby enhancing the photocatalytic activity performance.

Remarkably, without the need for sacrificial agents or cocatalysts, the BOPDI photocatalyst achieved an NH_3 production rate of 74.0 μ mol g⁻¹ h⁻¹, which was 11-times higher than that of the original PDIs. The AQY of NH_3 over BOPDIs under 450 nm monochromatic light was measured to be 1.29%. The photocatalytic mechanism of N_2 fixation by BOPDIs was attributed to the strong internal electric field, which facilitated electron migration to the embedded units. Meanwhile, the photoinduced holes remained on the benzene ring and perylene units, forming long-lived intermediate states. These electrons were capable of activating N_2 to generate NH_3 , while the remaining holes participated in the activation of H_2O to produce O_2 . Notably, this work marked the first application of PDI composite materials in photocatalytic N_2 fixation for NH_3 synthesis.

4.3.2 Photocatalytic H_2O_2 production. Hydrogen peroxide (H_2O_2) has been widely recognized as a green oxidant, and thus employed in sterilization and industrial wastewater treatment. It is also considered an excellent energy carrier. However, the conventional industrial method for producing H_2O_2 , the anthraquinone oxidation method, presents challenges such as complex processes, high energy consumption, and generation of toxic by-products. Hence, it is necessary to develop alternative methods that are safe, energy-efficient, and environmentally friendly for H_2O_2 production. In recent years, photocatalytic technology has received significant attention for H_2O_2 production due its availability to address these requirements and

facilitate H_2O_2 production in a safe, low-energy, and sustainable manner. 69,131

An example of these advancements is the creation of an MIL-125-PDI heterojunction for H₂O₂ production by Yamashita and co-workers.76 The H2O2 production rates for MIL-125-NH2 and the PDA precursor were measured to be 1111 and 1511 μ M g⁻¹ h⁻¹, respectively. However, the physical mixture of MIL-125-NH₂ and PDA showed an unsatisfactory H_2O_2 yield (1022 μ M g⁻¹ h⁻¹). In contrast, the MIL-125-PDI heterojunction demonstrated a significantly higher H₂O₂ production rate of 4800 μM $g^{-1} h^{-1}$, surpassing that of MIL-125-NH₂ by a factor of 4.3. The AQY value for H₂O₂ production decreased with an increase in the wavelength of the incident light. This result is consistent with the optical properties of MIL-125-PDIs, highlighting the crucial role of light absorption ability in the photocatalytic activity of H2O2 production. To elucidate the mechanism of H₂O₂ production by MIL-125-NH₂ and MIL-125-PDIs, a capture experiment of active species was conducted. In the case of MIL-125-NH₂, the photoreduction of O₂ to H₂O₂ requires a two-step single-electron process. In the case of MIL-125-PDIs, besides the original two-step single electron process (constituting 19% of the mechanism), a dominant one-step double electron O₂ reduction process (making up 81%) occurs, leading to the formation of H2O2. This work demonstrates that PDIs still retain photocatalytic activity for H2O2 production; however, their performance remains very low. This is a research prospect for the development of PDI-based photocatalysts aimed to promote the practical application of PDIs in H₂O₂ production.

4.3.3 Photocatalytic CO₂ reduction. The burning of fossil fuels is a major contributor to the release of large amounts of CO_2 into the atmosphere as a result of human activities, leading to severe adverse effects on the climate and environment. Thus, to address these issues and mitigate environmental and energy-related challenges, the conversion of excessive CO_2 into high-value-added fuels has emerged as a promising approach. Among the various methods, photocatalytic CO_2 reduction stands out due to its environmentally friendly nature and mild reaction conditions. ¹³²

Photocatalytic CO_2 reduction holds great potential given that it can yield a diverse range of products. However, the stable chemical structure of CO_2 molecules poses a significant challenge, given that their reduction at room temperature is extremely difficult. This difficulty further adds to the complexity of achieving efficient photocatalytic CO_2 reduction.

Hu and co-workers ¹³³ introduced a novel approach by anchoring PDI photosensitizers on mesoporous nanocrystalline zirconia (ZrO₂) through salicylic acid groups. The resulting ZrO₂|PDI composite, together with Re(bpy) (CO)₃Cl and TEOA as a sacrificial electron donor in DMF, exhibited remarkable photocatalytic CO₂ reduction under 100 mW cm $^{-2}$ LED white light illumination. The measured turnover number (TON) of CO₂ to CO catalysis achieved by ZrO₂|PDIs was comparable to previously reported photosensitive CO₂ catalysis TON values. The strong anchoring of salicylic acid on the surface of ZrO₂ and efficient electron transfer at low catalyst concentrations make ZrO₂|PDIs a promising candidate for CO₂ photoreduction applications.

However, the photocatalytic activity of pure PDIs for CO₂ reduction is largely affected by their near-zero CB bottom level, resulting in low thermodynamic-energy photoexcited electrons.134 Thus, to address this limitation, the construction of PDI-based heterojunctions enables the precise adjustment of the energy band structure of PDIs and promotes photogenerated charge separation, thereby improving their photocatalytic performance in CO₂ conversion using H₂O as an electron donor. Metal phthalocyanines (MPcs), as planar conjugated macrocyclic molecules, have suitable HOMO energy levels, which are slightly lower than the CB bottom of PDIs, making them compatible with Z-scheme band alignment. Jing's group81 extensively investigated MPcs in CO2 photoreduction. For example, they developed an ultrathin phosphate-modulated zinc phthalocyanine (ZnPc)/PDI supermolecule Z-scheme heterojunction. Surprisingly, the optimized ZnPc/PDI heterojunction showed CO2 photocatalytic reduction activity of about 30-times higher than that of the original PDIs. This excellent photocatalytic performance can be mainly attributed to the closely interconnected Z-type heterojunction, which greatly enhances the charge transfer and separation, as well as the negative field formed by the modified phosphate anions on PDIs, facilitating the capture of photo-generated holes.

In another study, to achieve efficient CO2 photoreduction with pure water as an electron donor, Jiang et al.82 designed an imide-based 2D covalent organic polymer, CoPcPDA-CMP, by polyimidization reaction of tetraaminophthalocyanatocobalt(II) (CoTAPc) and PTCDA. The resulting nanosheets, CoPcPDA-CMP NSs, demonstrated exceptional light absorption, charge separation efficiency, and electronic conductivity. When employed for efficient CO₂ photoreduction under visible light, using H₂O as a sacrificial agent, they achieved a CO yield of 14.27 μ mol g⁻¹ h⁻¹ and CO selectivity as high as 92%. These results establish CoPcPDA-CMP NSs as competitive with state-of-the-art organic photocatalysts for overall CO₂ photoreduction reactions. Spectral experiments confirmed the photoexcited electron transfer process in the CoPcPDA-CMP NSs, validating the Z-type photocatalytic mechanism. This work contributes to the advancement of highly active organic photocatalyst design and synthesis for CO2 conversion.

Photosynthetic biological hybridization systems, as emerging technology, offer a promising platform for the synthesis of high-value-added chemicals from ${\rm CO_2}$ by leveraging the excellent light collection ability of semiconductors and the synthesis capabilities of biological cells or enzymes. However, although organic semiconductor-bacteria biohybrid photosynthetic systems have demonstrated excellent performances, the use of inorganic semiconductors faces challenges due to the difficulties in adjusting their optical properties and concerns regarding the toxicity and phototoxicity of heavy metals. Thus, to overcome these issues, the use of organic semiconductors presents an effective solution.

Taking advantage of the excellent solar capture ability of π -conjugated molecules, the biocompatibility and hole/electron separation efficiency of the p-n PFP/PDI heterojunction, and the enhanced electron transfer from PFP/PDIs to *M. thermoacetica*, Wang *et al.*¹³⁵ constructed a non-photosynthetic bacteria-

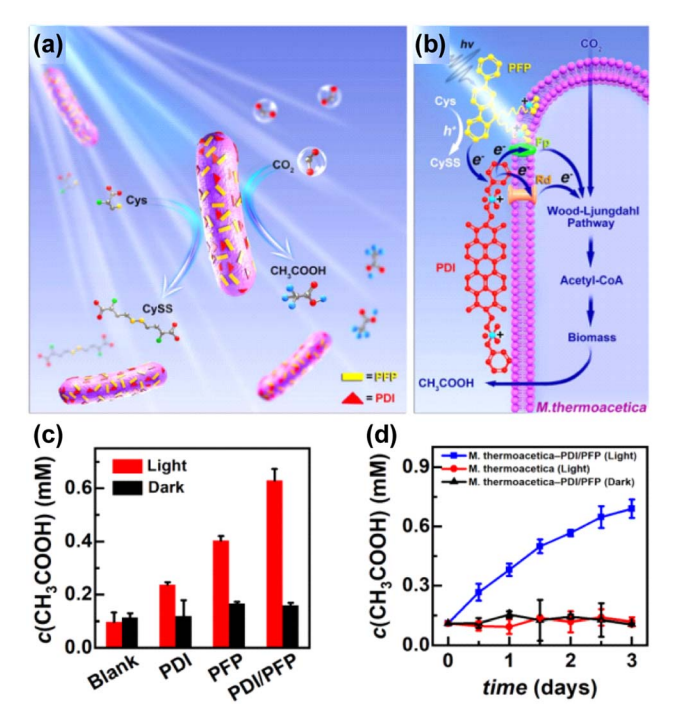


Fig. 21 (a) Photosynthetic production of acetic acid. (b) The produced acetic acid amount of PDIs/PFP/*M. thermoacetica* in an alternating light–dark cycle of 3 days. (c) Photosynthetic production of acetic acid by conjugated molecules/*M. thermoacetica* under light and deletional controls. (d) The produced acetic acid amount of PDI/PFP/*M. thermoacetica* in an alternating light-dark cycle of 12 hours each. Reprinted with permission.¹³⁵ Copyright 2020, Wiley.

based photosynthetic biohybrid system for CO₂ photoreduction (Fig. 21a and b). Under light irradiation, the PDI/PFP/*M. thermoacetica* system exhibited the significant production of acetic acid, surpassing the yields achieved by the PDI/*M thermoacetica* and PFP/*M. thermoacetica* systems. Importantly, the system demonstrated no significant attenuation in performance over a period of three days (Fig. 21c and d). This innovative approach holds great promise for efficient CO₂ photoreduction in photosynthetic biological hybridization systems, offering improved sustainability and chemical synthesis capabilities.

4.3.4 Photocatalytic conversion of organic molecules. The synthesis of 3,4-dihydroisoquinoline (DHIQ), a crucial intermediate in the production of morpholine and isoquinoline alkanes, traditionally involves the dehydrogenation of 1,2,3,4-tetrahydroisoquinoline (THIQ). However, this conventional method relies on high valence metal oxidants, which contradict the principles of green chemistry and do not allow the recovery of the catalyst. Thus, in recent years, heterogeneous photocatalytic dehydrogenation has emerged as an attractive approach for the sustainable and environmentally friendly synthesis of high-value-added organic compounds. In this context, as a highly stable n-type semiconductor material, PDIs have strong photocatalytic oxidation capabilities, making them promising candidates for efficient DHIQ synthesis by the photocatalytic oxidization of THIQ.

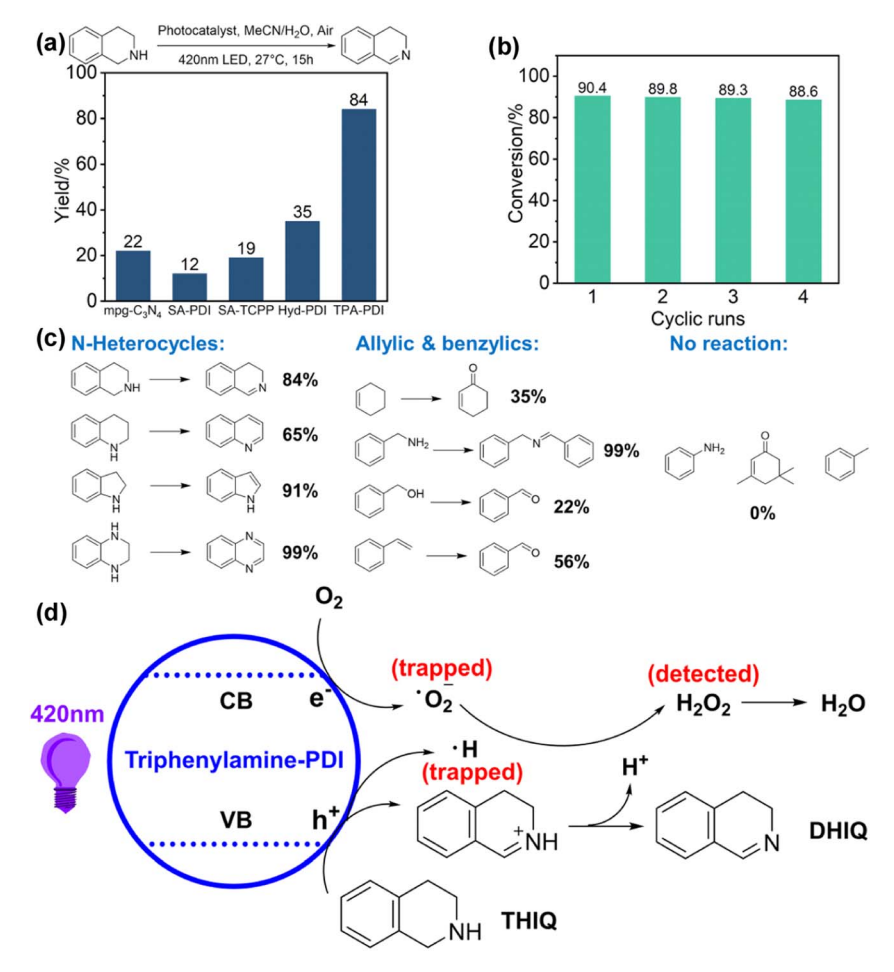


Fig. 22 (a) Photocatalytic selective oxidation of 1,2,3,4-tetrahydroisoquinoline to 3,4-dihydroisoquinoline over different photocatalysts. (b) Continuous catalytic runs for the oxidation of 1,2,3,4-tetrahydroisoquinoline to 3,4-dihydroisoquinoline over triphenylamine-PDIs. (c) Substrate scope. (d) Proposed reaction mechanism for the photocatalytic oxidation of THIQ to DHIQ. Reprinted with permission. ¹³⁶ Copyright 2022, Wiley.

group136 Zhu's developed an ultrathin porous triphenylamine-diimide (PDI) photocatalyst with photooxidation abilities for the oxidation reaction of THIQ to DHIQ. After 15 h of illumination, the conversion rate of triphenylamine-PDIs reached 90%, with a selectivity of 92% and 84% yield (Fig. 22a). Remarkably, even after four catalytic cycles, the triphenylamine-PDI photocatalyst showed a minimal decrease in performance, demonstrating its structural stability due to its covalent linkage (Fig. 22b). Notably, the yields of other nheterocyclic substrates also exceeded 90% (Fig. 22c). The high photocatalytic activity of triphenylamine-PDIs is attributed to the electron donor-acceptor structure formed by triphenylamine and PDIs, which enhances the driving force for the efficient generation and separation of photo-generated charges. The high crystallinity of triphenylamine-PDIs facilitates the rapid transfer of photo-generated charges. Based on free radical trapping experiments, the photocatalytic mechanism was elucidated, as shown in Fig. 22d. Under illumination, the photogenerated electrons on CB reacted with adsorbed O2 to generate 'O2⁻, while the photo-generated holes on the VB are involved in THIQ oxidation reactions. This work provides feasible options

and promising prospects for advancing photocatalytic selective oxidation technology.

Imines play a crucial role as intermediates in various industries, such as dyes, pharmaceuticals, and fine chemicals. The photocatalytic synthesis of imines using PDIs offers a green and sustainable approach. Despite the highly positive VB potential of PDIs, which suggests that photo-generated holes can serve as strong oxidants for the synthesis of imines, the intrinsic defects caused by non-covalent systems lead to inefficient carrier transport in PDI photocatalysts, resulting in a poor photocatalytic performance.

Thus, to overcome these limitations, Li *et al.*⁶⁸ developed a covalent bond PDI/mesoporous g-C₃N₄ (mpgCN) Z-scheme heterojunction for the photocatalytic oxidative coupling of amines. The optimal PDI/mpgCN heterojunction achieved a conversion efficiency as high as 99%, which was 8.1-times, 2.4-times, and 11.4-times higher than that of the CN, mpgCN, and PDIs samples, respectively. Additionally, the selectivity of *n*-benzyl benzylamine reached 99%. The outstanding photocatalytic activity of PDIs/mpgCN was attributed to the maximum separation and transfer of interfacial charges facilitated by covalent bonding.

Based on free radical capture experiments and previous reports, the authors proposed a possible photocatalytic oxidative coupling process of benzyl amine over PDIs/mpgCN. According to the Z-scheme electron transfer pathway, the photo-generated electrons accumulated on the CB of mpgCN reduce O₂ to O₂. under illumination. Simultaneously, PDIs is oxidized by photo-generated holes, forming PDIs * as an intermediate. Subsequently, PDIs*+ reacts with benzylamine to generate PhCH2NH2*+. Subsequently, PhCH2NH2*+ is further converted into PhCH=NH, which couples with another benzylamine molecule to form the n-benzylethyl benzylamine product. However, the photocatalytic performance of PDI-based photocatalysts is not high. Thus, to address these challenges, it is necessary to develop PDI photocatalyst materials with strong driving force for photo-generated charge separation and photocatalytic oxidation ability, which can effectively function in aqueous solution.

5. **Outlooks**

All-organic n-type PDI materials, as semiconductors, are emerging as the next generation of visible-light-driven "star" photocatalysts in energy and environmental applications. These materials possess an attractive band structure, high molar extinction coefficient, abundant element resources, excellent photothermal stability, and convenient synthesis routes. Thus, to further enhance their photocatalytic activity, the current research on PDI-based photocatalysts is focused on regulating their intrinsic structure.

The strategies aimed at improving the photocatalytic performance of PDI photocatalysts include molecular structure design, enhancing their crystallinity, and controlling their morphology. To date, considerable progress has been made in optimizing these factors in intrinsic PDI materials, resulting in improved photocatalytic activity. Additionally, the construction of PDI heterojunctions has emerged as another strategy for enhancing the photocatalytic performance of PDI-based photocatalysts.

However, despite the rapid development of PDI-based photocatalysts in addressing environmental pollution and renewable energy production, several significant limitations and challenges persist. Thus, considering these issues, we propose the following research directions.

5.1 Improving the charge separation and migration efficiency

Although highly active PDI photocatalysts have been reported, their separation and migration efficiency of photo-generated charges still needs to be improved. In this case, surface defects offer an effective way to manipulate their charge transport behavior, band structure, and surface catalytic reactions, 137 thus greatly improving their photocatalytic performance. The precise engineering of surface defects can improve the charge separation efficiency and facilitate the construction of stable heterojunctions with other semiconductors, changing the interface interaction from electrostatic adsorption to chemical bridging.138 However, limited research has been conducted on the impact of surface defect modifications on the photocatalytic activity of PDIs. Therefore, investigating PDI-based heterojunction photocatalysts formed by combining the surface defect-modified PDIs with other semiconductors holds important research significance in constructing PDI-based heterojunctions with highly efficient contact interfaces and improved photocatalytic activity.

5.2 Exploiting crystal facets for enhanced photocatalysis

Different crystal facets with distinct geometric and electronic structures results in diverse physical and chemical properties, such as surface energy, defect formation ability, and affinity for foreign elements. 139 The photocatalytic activity of PDIs is highly dependent on their crystal facets, but there are few reports exploring the different crystal facets of PDIs. Therefore, the preparation of PDIs with specific exposed crystal facets and their integration into heterojunctions with other semiconductors will play a crucial role in constructing well-defined interfaces and improving their photocatalytic activity.

5.3 Exploring diverse PDI nanostructures

Morphology plays a vital role in photocatalytic performance. Certain photocatalysts with unique morphologies have advantages such as large specific surface area, low photo-generated charge recombination, and high light energy utilization. Although PDI nanostructures, such as nanosheets, nanowires, and nanorods, have been extensively investigated, the further exploration of PDI nanostructures with high specific surface areas and high exposed active sites is needed. Examples include quantum dots, hollow tubes, and hollow spheres. Additionally, the multiple construction and stacking modes between PDI heterojunctions and other semiconductors significantly impact the interface characteristics, thus improving the photocatalytic performance of PDI-based heterojunctions.

5.4 Investigating isotype heterojunctions of PDIs

Iso-type heterojunctions between different phases of identical substances, characterized by staggered bandgaps, exhibit higher stability, close contact, and natural compatibility compared to hetero-type heterojunctions. Notably, excellent photocatalytic performance has been observed in various isotype heterojunctions such as rutile/anatase TiO2, 140 monoclinic/ tetragonal BiVO4, 141 and iso-type heptazine-/triazine-g-C3N4.142 Although different phases, compositions, and structures have been prepared, no reports have explored PDI iso-type heterojunction photocatalysts. Thus, investigating PDI iso-type heterojunctions will become a significant research direction for PDI heterojunction studies in the future.

5.5 Elucidating charge transfer routes and photocatalytic mechanisms

The transfer routes of photo-generated charges and the underlying photocatalytic mechanism in different types of PDI-based heterojunctions require further clarification. For instance, PDI/ g- C_3N_4 heterojunctions prepared through different methods or applied in different fields exhibit significantly different transfer routes, such as type II or Z-scheme heterojunctions. Thus, understanding why these differences arise in the same PDI-based heterojunction is essential. Accordingly, advanced characterization methods such as *in situ* irradiated XPS, radical trapping, fs-TAS, operando Kelvin probe force microscopy, nanoelectrochemistry, and DFT calculations should be employed and further developed to unravel these complexities.

5.6 Enhancing interface stability in PDI-based heterojunctions

The interface stability of PDI-based heterojunctions is a critical factor to consider. These heterojunctions are assembled by combining PDIs with semiconductors through electrostatic interactions, non-covalent bonds, covalent bonds, chemical or physical adsorption, and more. However, during long-term photocatalytic reactions, the interaction between the semiconductors may gradually weaken, compromising the transfer of photo-generated charges at the interface and reducing the photocatalytic activity. Therefore, further research is required to enhance the interface interaction in PDI-based heterojunctions, ensuring their long-term stability and suitability for practical applications.

5.7 Photocatalytic reaction performed without sacrificial agents

Water oxidation is a complex process with high energy consumption and slow kinetics, which is characterized by a high thermodynamic energy barrier, multi-electron, multiproton transfer, and oxygen-oxygen bond formation. Therefore, in addition to reports on the photocatalytic degradation of pollutants, antibacterial activity, etc., most performance tests of PDI-based photocatalysts have been conducted in the presence of a sacrificial agent, such as H₂ production, O₂ production, N₂ fixation, and CO2 reduction. However, sacrificial agents are relatively expensive, which is unrealistic in the production process, and it also has a great impact on the research of catalytic mechanisms. Therefore, it is of great significance to realize and explore photocatalytic reactions without adding sacrificial agents. In addition, by adding low-value chemicals to capture photogenerated holes, realizing their high value and improving their photocatalytic efficiency are also important directions for future research on PDI-based catalysts.

Conflicts of interest

The authors declare that they have no known competing financial interests or personal relationships that could have appeared to influence the work reported in this paper.

Acknowledgements

This study was supported by the National Natural Science Foundation of China (22308223, U1703351, 52073179), the High-level Talents launching Project (RCZK202328), Tianshan

Talent Support Program for Xin Jia, and the Program of Introducing Talents of Discipline to Universities (D20018). We thank Albert Rodriguez Sheremet and Elizaveta Dogadina for helping create some visualizations.

References

- 1 G. Liao, Y. Gong, L. Zhang, H. Gao, G. Yang and B. Fang, Energy Environ. Sci., 2019, 12, 2080–2147.
- 2 Y. K. Zhu, J. Z. Li, J. M. Cao, C. X. Lv, G. Q. Huang, G. L. Zhang, Y. Xu, S. C. Zhang, P. P. Meng, T. R. Zhan and D. J. Yang, *APL Mater.*, 2020, 8, 041108.
- 3 Y. Zhu, Y. Zhuang, L. Wang, H. Tang, X. Meng and X. She, *Chin. J. Catal.*, 2022, **43**, 2558–2568.
- 4 L. Zhang, S. Hou, T. Wang, S. Liu, X. Gao, C. Wang and G. Wang, *Small*, 2022, **18**, 2202252.
- 5 X. Li, J. Yu, M. Jaroniec and X. Chen, *Chem. Rev.*, 2019, **119**, 3962–4179.
- 6 H. Li, R. Li, G. Liu, M. Zhai and J. Yu, *Adv. Mater.*, 2023, e2301307.
- 7 Y. Li, X. Zhang and D. Liu, J. Photochem. Photobiol., C, 2021, 48, 100436.
- 8 L. Yang, Y. Fu, F. Sun, M. Deng, C. Zhang, N. Li, D. Hao, Q. Wang and G. Zhuang, *J. Colloid Interface Sci.*, 2023, **639**, 472–483.
- 9 D. Liu, J. Wang, X. Bai, R. Zong and Y. Zhu, *Adv. Mater.*, 2016, **28**, 7284–7290.
- 10 Z. Zhang, J. Liu, P.-Y. Gu, R. Ji, L. Jin, S. Zhou, J. He, D. Chen, Q. Xu and J. Lu, Sep. Purif. Technol., 2022, 287, 120539.
- 11 H. Miao, J. Yang, Y. Wei, W. Li and Y. Zhu, *Appl. Catal., B*, 2018, 239, 61–67.
- 12 J. Yang, J. Jing, W. Li and Y. Zhu, Adv. Sci., 2022, 9, 2201134.
- 13 L. Liu, Y. Wu, R. Song, Y. Zhang, Y. Ma, J. Wan, M. Zhang, H. Cui, H. Yang, X. Chen and J. Wang, *J. Colloid Interface Sci.*, 2022, **628**, 701–711.
- 14 H. Ben, Y. Liu, X. Liu, X. Liu, C. Ling, C. Liang and L. Zhang, *Adv. Funct. Mater.*, 2021, **31**, 2102315.
- 15 H. Wang, L. Zhao, X. Liu, J. Xu, W. Hou, J. Wang, E. He, R. Zhang and H. Zhang, *Dyes Pigm.*, 2017, 137, 322–328.
- W. Zhou, G. Liu, B. Yang, Q. Ji, W. Xiang, H. He, Z. Xu, C. Qi,
 S. Li, S. Yang and C. Xu, Sci. Total Environ., 2021, 780,
 146483.
- 17 J. Zhang, Z. Wang, J. Shi, W. Zhu, L. Yang, Y. Wang and Z. Zou, *Adv. Funct. Mater.*, 2022, **32**, 2205895.
- 18 K. Kong, S. Zhang, Y. Chu, Y. Hu, F. Yu, H. Ye, H. Ding and J. Hua, *Chem. Commun.*, 2019, 55, 8090–8093.
- 19 Y. Sun, D. Wang and Y. Zhu, *Chem. Eng. J.*, 2022, **438**, 135667.
- 20 Z. Zhang, Y. Zhu, X. Chen, H. Zhang and J. Wang, *Adv. Mater.*, 2019, **31**, 1806626.
- 21 J. Jing, J. Yang, W. Li, Z. Wu and Y. Zhu, *Adv. Mater.*, 2022, 34, 2106807.
- 22 Y. Sheng, W. Li, L. Xu and Y. Zhu, *Adv. Mater.*, 2022, 34, 2102354
- 23 Y. Zhang, D. Wang, W. Liu, Y. Lou, Y. Zhang, Y. Dong, J. Xu,C. Pan and Y. Zhu, *Appl. Catal.*, B, 2022, 300, 120762.

- 24 Z. Zhang, X. Chen, H. Zhang, W. Liu, W. Zhu and Y. Zhu, Adv. Mater., 2020, 32, 1907746.
- 25 H. Zhang, X. Chen, Z. Zhang, K. Yu, W. Zhu and Y. Zhu, *Appl. Catal.*, *B*, 2021, **287**, 119957.
- 26 J. Wang, W. Shi, D. Liu, Z. Zhang, Y. Zhu and D. Wang, Appl. Catal., B, 2017, 202, 289–297.
- 27 G. Liao, C. Li, S.-Y. Liu, B. Fang and H. Yang, *Phys. Rep.*, 2022, **983**, 1–4.
- 28 X. Gao, K. Gao, X. Li, Y. Shang and F. Fu, *Catal. Sci. Technol.*, 2020, 10, 372–381.
- 29 M. Deng, J. Guo, X. Ma, Y. Fu, H. Du, D. Hao and Q. Wang, *Sep. Purif. Technol.*, 2023, **326**, 124786.
- 30 W. Wu, Z. Zhang, L. Sun, R. Wei, L. Gao, X. Pan, J. Zhang, J. Yu and G. Xiao, Sep. Purif. Technol., 2023, 311, 123230.
- 31 J. Hsu, L. W. Wei, C. Chen and H. Wang, *J. Cleaner Prod.*, 2022, 380, 134918.
- 32 X. Bai, L. Guo, T. Jia, D. Hao, C. Wang, H. Li and R. Zong, *J. Hazard. Mater.*, 2022, **435**, 128992.
- 33 Y. Zhu, J. Li, C. Dong, J. Ren, Y. Huang, D. Zhao, R. Cai, D. Wei, X. Yang, C. Lv, W. Theis, Y. Bu, W. Han, S. Shen and D. Yang, *Appl. Catal.*, B, 2019, 255, 117764.
- 34 X. Li, X. Ly, Q. Zhang, B. Huang, P. Wang, X. Qin, X. Zhang and Y. Dai, *J. Colloid Interface Sci.*, 2018, 525, 136–142.
- 35 Y. Wang, Z. Zhao, R. Sun, J. Bian, Z. Zhang and L. Jing, *Nanoscale*, 2022, **14**, 8041–8049.
- 36 L. Liu, M. Yue, J. Lu, J. Hu, Y. Liang and W. Cui, Appl. Surf. Sci., 2018, 456, 645–656.
- 37 W. Wei, D. Liu, Z. Wei and Y. Zhu, *ACS Catal.*, 2017, 7, 652–663
- 38 W. Wei and Y. Zhu, Small, 2019, 15, 1903933.
- 39 Q. Liu, S. Cao, Q. Sun, C. Xing, W. Gao, X. Lu, X. Li, G. Yang, S. Yu and Y. Chen, *J. Hazard. Mater.*, 2022, 436, 129321.
- 40 X. Jin, L. Ye, H. Xie and G. Chen, *Coord. Chem. Rev.*, 2017, 349, 84–101.
- 41 B. Li, S. Chen, D. Huang, M. Cheng, C. Du, C. Feng, Y. Yang, L. Lei, Y. Chen, W. Xue and R. Deng, *J. Phys. Chem. C*, 2021, 125, 18693–18707.
- 42 K. Zhang, J. Wang, W. Jiang, W. Yao, H. Yang and Y. Zhu, *Appl. Catal.*, *B*, 2018, 232, 175–181.
- 43 J. Han, Y. Deng, N. Li, D. Chen, Q. Xu, H. Li, J. He and J. Lu, J. Colloid Interface Sci., 2021, 582, 1021–1032.
- 44 X. Zhang, L. Shi, L. Yao and L. Cui, *Mater. Res. Bull.*, 2022, **146**, 111589.
- 45 H. Wang, Y. Zhou, J. Wang, A. Li and P. Corvini, *Chem. Eng. J.*, 2022, 433, 133622.
- 46 Y. Guan, J. Wu, Q. Liu, H. Wang, G. Liu, P. He and X. Qi, *Energy Fuels*, 2021, 35, 11415–11426.
- 47 Q. Ji, Z. Xu, W. Xiang, Y. Wu, X. Cheng, C. Xu, C. Qi, H. He, J. Hu, S. Yang, S. Li and L. Zhang, *Chemosphere*, 2020, 253, 126751.
- 48 J. Dasgupta, J. Sikder, S. Chakraborty, U. Adhikari, V. P. B. Reddy, A. Mondal and S. Curcio, ACS Sustain. Chem. Eng., 2017, 5, 6817–6826.
- 49 X. Yang, Y. Li, G. Y. Chen, H. R. Liu, L. Li Yuan, L. Yang and D. Liu, ACS Appl. Nano Mater., 2022, 5, 9829–9839.
- 50 Y. Xu, X. Zhu, H. Yan, P. Wang, M. Song, C. Ma, Z. Chen, J. Chu, X. Liu and Z. Lu, *Chin. J. Catal.*, 2022, 43, 1111–1122.

- 51 D. Liu, Y. Li, X. Zhang, L. Yang and X. Luo, *Chemcatchem*, 2022, 14, e202200087.
- 52 T. Sun, J. Song, J. Jia, X. Li and X. Sun, *Nano Energy*, 2016, 26, 83–89.
- 53 M. Duan, L. Jiang, B. Shao, C. Feng, H. Yu, H. Guo, H. Chen and W. Tang, *Appl. Catal.*, *B*, 2021, **297**, 120439.
- 54 T. Cai, W. Zeng, Y. Liu, L. Wang, W. Dong, H. Chen and X. Xia, *Appl. Catal.*, *B*, 2020, **263**, 118327.
- 55 R. Yang, G. Song, L. Wang, Z. Yang, J. Zhang, X. Zhang, S. Wang, L. Ding, N. Ren, A. Wang and X. Yu, *Small*, 2021, 17, 2102744.
- 56 (a) J. Zhang, D. Yang, J. Shi, Z. Wang, W. Zhu, Y. Wang and Z. Chen, *J. Mater. Chem. A*, 2022, 10, 14513–14528; (b) J. Yang, H. Miao, W. Li, H. Li and Y. Zhu, *J. Mater. Chem. A*, 2019, 7, 6482–6490.
- 57 J. Wang, S. Lin, N. Tian, T. Ma, Y. Zhang and H. Huang, *Adv. Funct. Mater.*, 2021, **31**, 2008008.
- 58 J. Yang, H. Miao, W. Li, H. Li and Y. Zhu, *J. Mater. Chem. A*, 2019, 7, 6482–6490.
- 59 L. Yan, W. Wang, Q. Zhao, Z. Zhu, B. Liu and C. Hu, J. Colloid Interface Sci., 2022, 606, 898–911.
- 60 X. Wang, K. Maeda, A. Thomas, K. Takanabe, G. Xin, J. M. Carlsson, K. Domen and M. Antonietti, *Nat. Mater.*, 2009, 8, 76–80.
- 61 L. Wang, X. Zhang, X. Yu, F. Gao, Z. Shen, X. Zhang, S. Ge, J. Liu, Z. Gu and C. Chen, *Adv. Mater.*, 2019, 31, 1901965.
- 62 H. Miao, J. Yang, Y. Sheng, W. Li and Y. Zhu, Sol. RRL, 2021, 5, 2000453.
- 63 X. Li, D. Chen, N. Li, Q. Xu, H. Li and J. Lu, *J. Colloid Interface Sci.*, 2023, **633**, 691–702.
- 64 J. Liu, R. Wang, B. Wang, M. Zheng, R. Yang, X. Zhu, Y. Song, M. Cheng, H. Xu and H. Li, *Appl. Surf. Sci.*, 2022, 605, 154625.
- 65 Q. Gao, J. Xu, Z. Wang and Y. Zhu, Appl. Catal., B, 2020, 271, 118933.
- 66 J. Zhang, X. Zhao, Y. Wang, Y. Gong, D. Cao and M. Qiao, Appl. Catal., B, 2018, 237, 976.
- 67 X. Wang, J. Q. Meng, X. Yang, A. Hu, Y. Yang and Y. Guo, *ACS Appl. Mater. Interfaces*, 2019, 11, 588–602.
- 68 C. Xing, G. Yu, T. Chen, S. Liu, Q. Sun, Q. Liu, Y. Hu, H. Liu and X. Li, *Appl. Catal., B*, 2021, **298**, 120534.
- 69 J. Hu, C. Chen, H. Yang, F. Yang, J. Qu, X. Yang, W. Sun, L. Dai and C. Li, Appl. Catal., B, 2022, 317, 121723.
- 70 R. Tang, D. Gong, Y. Zhou, Y. Deng, C. Feng, S. Xiong, Y. Huang, G. Peng and L. Li, *Appl. Catal.*, B, 2022, 303, 120929.
- 71 X. Wang, J. Meng, X. Yang, A. Hu, Y. Yang and Y. Guo, *ACS Appl. Mater. Interfaces*, 2019, **11**, 588–602.
- 72 Y. Wang, H. Wang, J. Li and X. Zhao, *Appl. Catal., B*, 2020, 278, 118981.
- 73 J. Hu, D. Chen, N. Li, Q. Xu, H. Li, J. He and J. Lu, *Small*, 2018, 14, 1800416.
- 74 X. Chen, J. Wang, Y. Chai, Z. Zhang and Y. Zhu, *Adv. Mater.*, 2021, 33, 2007479.
- 75 L. Yang, P. Wang, J. Yin, C. Wang, G. Dong, Y. Wang and W. Ho, *Appl. Catal.*, *B*, 2019, **250**, 42–51.

- 76 X. Chen, Y. Kondo, S. Li, Y. Kuwahara, K. Mori, D. Zhang, C. Louis and H. Yamashita, *J. Mater. Chem. A*, 2021, 9, 26371–26380.
- 77 Z. You, Z. Wang, K. Tian and X. Yao, *J. Environ. Chem. Eng.*, 2023, **11**, 110159.
- 78 H. Chen, W. Zeng, Y. Liu, W. Dong, T. Cai, L. Tang, J. Li and W. Li, *ACS Appl. Mater. Interfaces*, 2021, **13**, 16364–16373.
- 79 Q. Ji, X. Cheng, X. Kong, D. Sun, Y. Wu, Z. Xu, Y. Liu, X. Duan, H. He, S. Li, L. Zhang and S. Yang, *Chem. Eng. J.*, 2022, 435, 134947.
- 80 S. Wang, Y. Xia, G. Yan, M. Chen, X. Wang, L. Wu and R. Liang, Appl. Catal., B, 2022, 317, 121798.
- 81 R. Sun, Y. Wang, Z. Zhang, Y. Qu, Z. Li, B. Li, H. Wu, X. Hua, S. Zhang, F. Zhang and L. Jing, *Chem. Eng. J.*, 2021, 426, 121798.
- 82 Q. Zhi, J. Zhou, W. Liu, L. Gong, W. Liu, H. Liu, K. Wang and J. Jiang, *Small*, 2022, **18**, 2201314.
- 83 O. S. Ekande and M. Kumar, *J. Environ. Chem. Eng.*, 2021, 9, 105725.
- 84 W. Dai, L. Jiang, J. Wang, Y. Pu, Y. Zhu, Y. Wang and B. Xiao, *Chem. Eng. J.*, 2020, **397**, 125476.
- 85 V. N. Gopalakrishnan, J. Becerra, E. F. Pena, M. Sakar, F. Beland and T. Do, *Green Chem.*, 2021, 23, 8332–8360.
- 86 W. Wei, Z. Wei, D. Liu and Y. Zhu, *Appl. Catal.*, *B*, 2018, **230**, 49–57.
- 87 D. Liu, L. Chen, W. Chen, M. Qin and S. Wei, *Dalton Trans.*, 2021, **50**, 4008–4016.
- 88 L. Zeng, T. Liu, C. He, D. Shi, F. Zhang and C. Duan, *J. Am. Chem. Soc.*, 2016, **138**, 3958–3961.
- 89 Z. Zhong, R. Li, W. Lin, X. Xu, X. Tian, X. Li, X. Chen and L. Kang, *Appl. Catal.*, *B*, 2020, **260**, 118135.
- 90 A. Cao, R. Li, X. Xu, W. Huang, Y. He, J. Li, M. Sun, X. Chen and L. Kang, *Appl. Catal.*, B, 2022, 309, 121293.
- 91 Z. Lin, Y. Wang, Z. Peng, Y. Huang, F. Meng, J. Chen, C. Dong, Q. Zhang, R. Wang, D. Zhao, J. Chen, L. Gu and S. Shen, *Adv. Energy Mater.*, 2022, **12**, 2200716.
- 92 W. Li, Z. Wei, Y. Sheng, J. Xu, Y. Ren, J. Jing, J. Yang, J. Li and Y. Zhu, *ACS Energy Lett.*, 2023, **8**, 2652–2660.
- 93 A. Kumar, G. Sharma, M. Naushad, A. a. H. Al-Muhtaseb, A. Garcia-Penas, G. T. Mola, C. Si and F. J. Stadler, *Chem. Eng. J.*, 2020, 382, 122937.
- 94 S. Sharma, V. Dutta, P. Singh, P. Raizada, A. Rahmani-Sani, A. Hosseini-Bandegharaei and V. K. Thakur, *J. Cleaner Prod.*, 2019, 228, 755–769.
- 95 C. Cheng, Q. Liang, M. Yan, Z. Liu, Q. He, T. Wu, S. Luo, Y. Pan, C. Zhao and Y. Liu, J. Hazard. Mater., 2022, 424, 127721.
- 96 Z. Fang, Y. Liu, P. Chen, D. Li, H. Liu, Z. Xiao, Y. Zheng, Z. Lin, J. Luo, W. Lv and G. Liu, *Chem. Eng. J.*, 2023, 451, 138571.
- 97 J. Yang, H. Miao, J. Jing, Y. Zhu and W. Choi, *Appl. Catal., B*, 2021, 281, 119547.
- 98 Y. Sheng, H. Miao, J. Jing, W. Yao and Y. Zhu, *Appl. Catal., B*, 2020, 272, 118897.
- 99 Y. Zhu, C. Lv, Z. Yin, J. Ren, X. Yang, C. Dong, H. Liu, R. Cai, Y. Huang, W. Theis, S. Shen and D. Yang, *Angew. Chem., Int. Ed.*, 2020, 59, 868–873.

- 100 H. Ding, Z. Wang, K. Kong, S. Feng, L. Xu, H. Ye, W. Wu, X. Gong and J. Hua, J. Mater. Chem. A, 2021, 9, 7675–7683.
- 101 H. Xu, Z. Wang, S. Feng, X. Liu, X. Gong and J. Hua, Int. J. Hydrogen Energy, 2023, 48, 8071–8081.
- 102 B. Yang, J. Han, Q. Zhang, G. Liao, W. Cheng, G. Ge, J. Liu, X. Yang, R. Wang and X. Jia, *Carbon*, 2023, 202, 348–357.
- 103 (a) B. Yang, J. Zhao, W. Yang, X. Sun, R. Wang and X. Jia, *J. Colloid Interface Sci.*, 2021, 589, 179–186; (b) B. Yang, X. Li, Q. Zhang, X. Yang, J. Wan, G. Liao, J. Zhao, R. Wang, J. Liu, R. D. Rodriguez and X. Jia, *Appl. Catal.*, *B*, 2022, 314, 121521.
- 104 Y. Sheng, W. Li, Y. Zhu and L. Zhang, *Appl. Catal., B*, 2021, **298**, 120585.
- 105 Y. Guo, Q. Zhou, J. Nan, W. Shi, F. Cui and Y. Zhu, *Nat. Commun.*, 2022, **13**, 2067.
- 106 Z. Liang, R. Shen, P. Zhang, Y. Li, N. Li and X. Li, *Chin. J. Catal.*, 2022, **43**, 2581–2591.
- 107 J. Song, Y. Chen, D. Sun and X. Li, *Inorg. Chem. Commun.*, 2018, **92**, 27–34.
- 108 S. Chen, C. Wang, B. R. Bunes, Y. Li, C. Wang and L. Zang, *Appl. Catal.*, *A*, 2015, **498**, 63–68.
- 109 C. Ye, J. Li, H. Wu, X. Li, B. Chen, C. Tung and L. Wu, *ACS Appl. Mater. Interfaces*, 2018, **10**, 3515–3521.
- 110 L. Liu, J. Liu, S. Zong, Z. Huang, X. Feng, J. Zheng and Y. Fang, *Int. J. Hydrogen Energy*, 2022, 47, 39486–39498.
- 111 C. Ye, X. Wang, J. Li, Z. Li, X. Li, L. Zhang, B. Chen, C. Tung and L. Wu, *ACS Catal.*, 2016, **6**, 8336–8341.
- 112 D. Liu, X. Yang, P. Chen, X. Zhang, G. Chen, Q. Guo, H. Hou and Y. Li, *Adv. Mater.*, 2023, 35, 2300655.
- 113 H. Zhao, Q. Mao, L. Jian, Y. Dong and Y. Zhu, *Chin. J. Catal.*, 2022, **43**, 1774–1804.
- 114 Z. Zhong, X. Xu, A. Cao, W. You, Z. Tao and L. Kang, *J. Power Sources*, 2021, **489**, 229493.
- 115 S. Feng, Z. Wang, H. Xu, S. Li, X. Gong and J. Hua, *Polym. Chem.*, 2021, **12**, 7056–7064.
- 116 D. Liu, X. Yang, P. Chen, X. Zhang, G. Chen, Q. Guo, H. Hou and Y. Li, *Adv. Mater.*, 2023, 35, 2300655.
- 117 W. Li, Z. Wei, Y. Sheng, J. Xu, Y. Ren, J. Jing, J. Yang, J. Li and Y. Zhu, *ACS Energy Lett.*, 2023, **8**, 2652–2660.
- 118 Q. Xu, L. Zhang, J. Yu, S. Wageh, A. A. Al-Ghamdi and M. Jaroniec, *Mater. Today*, 2018, 21, 1042–1063.
- 119 Q. Xu, L. Zhang, B. Cheng, J. Fan and J. Yu, *Chem*, 2020, 6, 1543–1559.
- 120 Y. Yuan, D. Chen, S. Yang, L. Yang, J. Wang, D. Cao, W. Tu, Z. Yu and Z. Zou, *J. Mater. Chem. A*, 2017, 5, 21205–21213.
- 121 Z. Liu, X. Lin, Y. Chen, N. Song, Y. Hao, S. Jia, H. Sun, Y. Sun, Y. Yan, Y. Li and Y. Yan, J. Taiwan Inst. Chem. Eng., 2023, 143, 104693.
- 122 P. Chen, L. Blaney, G. Cagnetta, J. Huang, B. Wang, Y. Wang, S. Deng and G. Yu, *Environ. Sci. Technol.*, 2019, 53, 1564–1575.
- 123 G. Chen, Y. Yu, L. Liang, X. Duan, R. Li, X. Lu, B. Yan, N. Li and S. Wang, *J. Hazard. Mater.*, 2021, **408**, 124461.
- 124 Q. Ji, X. Cheng, Y. Wu, W. Xiang, H. He, Z. Xu, C. Xu, C. Qi, S. Li, L. Zhang and S. Yang, *Appl. Catal.*, B, 2021, 282, 119579.

- 125 Q. Ji, X. Cheng, D. Sun, Y. Wu, X. Kong, H. He, Z. Xu, C. Xu, C. Qi, Y. Liu, S. Li, L. Zhang, S. Yang and C. Sun, Chem. Eng. J., 2021, **414**, 128793.
- 126 X. Gao, K. Gao, F. Fu, C. Liang, Q. Li, J. Liu, L. Gao and Y. Zhu, Appl. Catal., B, 2020, 265, 118562.
- 127 Y. Wei, M. Ma, W. Li, J. Yang, H. Miao, Z. Zhang and Y. Zhu, Appl. Catal., B, 2018, 238, 302-308.
- 128 X. Gao, L. An, D. Qu, W. Jiang, Y. Chai, S. Sun, X. Liu and Z. Sun, Sci. Bull., 2019, 64, 918-925.
- 129 Q. Wang, J. Cao, P. Chen, S. Yang, C. Fu, F. Liu and S. Yin, Appl. Catal., A, 2023, 649, 118978.
- 130 S. Yang, X. Deng, P. Chen, G. Li, Q. Wang, Q. Wang and S. Yin, Chem. Eng. J., 2022, 441, 136084.
- 131 S. Feng, Y.-P. Zhang, H. Xu, X. Gong and J. Hua, J. Alloys Compd., 2023, 938, 168500.
- 132 J. Wang, R. Guo, Z. Bi, X. Chen, X. Hu and W. Pan, Nanoscale, 2022, 14, 11512-11528.
- 133 Z. Zhao, F. Niu, P. Li, H. Wang, Z. Zhang, G. J. Meyer and K. Hu, J. Am. Chem. Soc., 2022, 144, 7043-7047.

- 134 W. Fan, Q. Zhang and Y. Wang, Phys. Chem. Chem. Phys., 2013, 15, 2632-2649,
- 135 P. Gai, W. Yu, H. Zhao, R. Qi, F. Li, L. Liu, F. Lv and S. Wang, Angew. Chem., Int. Ed., 2020, 59, 7224-7229.
- 136 H. Zhang, K. Yu, Z. Wu and Y. Zhu, Ecomat, 2022, 4, e12215.
- 137 X. Sun, X. Zhang and Y. Xie, Matter, 2020, 2, 842-861.
- 138 S. Zhang, Y. Si, B. Li, L. Yang, W. Dai and S. Luo, Small, 2021, 17, 2004980.
- 139 R. Li, F. Zhang, D. Wang, J. Yang, M. Li, J. Zhu, X. Zhou, H. Han and C. Li, Nat. Commun., 2013, 4, 1432.
- 140 Y. Li and A. Selloni, ACS Catal., 2016, 6, 4769-4774.
- 141 X. Liang, P. Wang, F. Tong, X. Liu, C. Wang, M. Wang, Q. Zhang, Z. Wang, Y. Liu, Z. Zheng, Y. Dai and B. Huang, Adv. Funct. Mater., 2021, 31, 2008656.
- 142 S. Patnaik, B. P. Mishra and K. Parida, Catal. Sci. Technol., 2021, 11, 7505-7524.
- 143 X. Ji, X. Liu, Y. Guo and J. Zhang, Chem. Eng. J., 2021, 425, 131260.